Dynamics and Synchronization of Motifs of Neuronal Populations in the Presence of Delayed Interactions

TESI DOCTORAL

Leonardo Lyra Gollo

Director:
Prof. Claudio Mirasso

Presentada al Departament de Física
Universitat de les Illes Balears
2012

Dynamics and Synchronization of Motifs of Neuronal Populations in the Presence of Delayed Interactions

Leonardo Lyra Gollo
Tesi presentada al Departament de Física de la Universitat de les Illes Balears

PhD Thesis

Director: Prof. Claudio Mirasso

This document was typeset with LaTeX 2_ε

que aquesta tesi doctoral ha estat realitzada pel Sr. *Leonardo Lyra Gollo* sota la seva direcciò a l'Institut de Física Interdisciplinaria i Sistemas Complexos i, per a què consti, firma la present

Tesi doctoral presentada per Leonardo Lyra Gollo per optar al títol de Doctor, en el Programa de Física del Departament de Física de la Universitat de les Illes Balears, realitzada a l'IFISC sota la direcció de Claudio Mirasso, Catedràtic d'Universitat.

Vist i plau, Director de la tesi	Doctorant
Prof. Claudio Mirasso	Leonardo Lyra Gollo

Palma, 02 de juny de 2012

A Natália

Contents

Part I

Introduction

Chapter 1

Biological Overview

The purpose of this introductory chapter is twofold: to motivate, and to contextualize. The motivation aims at evidencing the importance of synchronization to brain functioning. Consciousness, cognition, behavior and perception require the interaction of multiple large groups of interconnected neurons, which are often segregated and distant. Fundamentally, the synchronous and precisely coordinated spiking activity is considered a middle-ground link between single-neuron activity to large-scale brain activity (Buzsáki and Draguhn, 2004). Afterwards, the contextualization is provided by the description of elementary characteristics, and relationships of the brain substrate, particularly emphasizing the structures involved in our results.

Section (1.1) is devoted to the identification of two essential principles of structural and functional organization of the neuronal dynamics: segregation and integration. We signalize that the former principle is a recognized aspect that is observed in the brain. The latter principle is presumably a prerequisite for the cognitive functions to emerge from the activity of segregated and specialized areas. To understand how the brain integrates neuronal activity of segregated and frequently distant areas constitutes a long-standing theoretical inquiry of neuroscience. The cornerstone of most models tackling this issue relies on the synchronization of neuronal activity.

Before we address the problem of synchronization between distant neuronal populations, this chapter contextualizes the field with respect to the established knowledge in biology. We provide a rather peripheral overview

that highlights only the most relevant components invoked in the following chapters. As our prime efforts, we attempt to offer:

- an intuitive view of the architectural structure of the nervous system (section 1.2);
- a comparative assessment of the existing experimental techniques to capture the brain dynamics (section 1.3);
- and a guide to understand the genesis of the neuronal dynamics (section 1.4).

1.1

Segregation and integration: Two organizational principles of the brain

The structure of the central nervous system is thought to be hierarchical (Maunsell and Van Essen, 1983; Zeki and Shipp, 1988; Felleman and Van Essen, 1991; Mesulam, 1998). According to this conceptualization, the sensory neurons and the periphery of the sensory systems comprise the bottom level of such hierarchy. On the other extreme, the deep cortical regions comprise the top level of the hierarchy. Under scrutiny, pervading all levels, cyto- and myeloarchitectural studies of the brain tissue indicate a segregated arrangement.

Different aspects of the brain organization reflect the segregation principle. The following sections (1.1.1, and 1.1.2) shall discuss some striking examples of segregation at the peripheral level, where a plethora of studies have acquired abundant knowledge.

The cortical level also presents a categorical segregation. However, at fine scale the cortical segregation gets lopsidedly fuzzier. Over a century ago, Campbell and Brodmann, the two contemporaries, mapped the human cerebral cortex with distinct segregation borders because they had used distinct criteria in their citoarchitectonic approach (Campbell, 1905; Brodmann, 1909). Currently, utilizing more sophisticated methods, several groups follow the same goal to characterize the human cortex (ffytche and Catani, 2005; Sporns, 2010).

Along the history, a multitude of clinical studies involving brain damage show that some brain functions depend on the integrity of specific brain areas (Kolb and Whishaw, 1990; Sporns, 2010). This represents another rich field supporting the principle of segregation in the brain.

Altogether, these approaches demonstrate the tendency of segregation of brain activity. The recognition of this fact leads straightforwardly to the necessity of an integration principle. Cognitive functions, like perception, attention, and memory, demand to assemble pieces of information that are coded at distant regions. Such integration is another organizational principle of the brain.

Owing to their fundamental importance, most brain functions are thought to rely on the interrelationship of segregation and integration. The coexistence of these two principles has been proposed to be the origin of neural complexity (Sporns, 2010). A remarkable attempt to quantitatively measure the complexity of a system also depends on the expression of both segregation and integration (Sporns, 2010). In a completely segregated system, the units are independent and there is only randomness. In a completely integrated system, all units behave identically and there is only regularity. Both extreme cases have no complexity. Therefore, complexity depends on the coexistence of order/disorder, random/regularity, and segregation/integration. This mixture distinctly prevails in the brain structure and its function.

1.1.1 Sensory input enters from specialized pathways

As the animals grew in size and complexity, certain cell types, the sensory neurons, adapted to extract the maximum information of the environment with respect to different aspects of the sensory stimulus. This specificity is a consequence of differences in physical and chemical structures of the neurons. There are great differences among the receptor neurons of the sensory systems. Even within a given sensory modality, there are different specializations of the receptor neurons. For example, the olfactory system has hundreds of different chemoreceptor neurons that respond optimally to different chemical compounds; the somatosensory system possesses several types of receptors (thermoreceptors, mechanoreceptors); etc.

1.1.2 Examples of receptive fields

From the periphery of the central nervous system to the higher levels, the sensory systems receive, process and transmit information. Irrespective of the sensory modalities, the pathway of the information flow is typically restricted by the receptive fields.

The receptive field of a neuron is the region of sensory space that elicit neuronal responses in the presence of a stimulus (Alonso and Chen, 2009). The receptive field is a neural mechanism utilized to decompose complex stimuli. This procedure of decomposing is undertaken early in the periphery, and it is typically maintained along several hierarchical levels. This strategy to process complex information is thought to provide a reliable way for the information to reach the intended sensory cortical area.

A considerable amount of the established knowledge about the receptive fields has been gathered in the peripheral areas. Independently of the sensory mode, the peripheral zones typically offer less challenging experimental barriers. To illustrate a little of the generality of the segregation principle, next we discuss some classical examples of receptive field in the peripheral areas of different sensory modalities.

Somatosensorial system. The somatosensory system responds to different sorts of stimulus: touch, vibration, body position, temperature or pain. The receptive fields in such system comprise a limited region of the skin or the internal organs where a stimulus can elicit a neuronal response. The size of the receptive fields vary both as a function of the stimulus, and the part of the body. The precision to detect changes of a somatosensorial stimulus decreases with the size of the receptive field. In humans, some areas have a very detailed somatosensorial resolution like the fingers, the lips, and the tongue; whereas other areas have poor resolution like the back, and the back of the legs. This resolution can be assessed by the two-point limen detection (Squire et al., 2003), a typical test to find the minimum detectable distance between two blunt probes. The areas with the smallest (largest) two-point limen represent the highest (lowest) resolution. Moreover, in addition to plentiful innervations of sensory neurons, superior resolution also demands a sufficient amount of cortical tissue to process the information. As reflected by the sensibility, both the distribution of innervations and the amount of cortical tissue are highly non-uniform. As the cortical homuncu-

lus have popularized (Kandel et al., 2000), large proportions of cortical tissue correspond to the processing of especial regions of the body.

Visual system. From the peripheral level to the deep cortical level, the concept of receptive field pervades our knowledge about the visual system. Following the flow direction of the neuronal activity elicited by the visual stimulus, neurons from any level show traces of the receptive fields: photoreceptors, retinal ganglion, lateral geniculate nucleus, primary visual cortex (striate), up to extrastriate cortical cells. In the first layer, the receptive field of a photoreceptor neuron corresponds to the region in which light alters the firing response of that cell. For the ganglion cells in the retina, the receptive field encompasses the sensitive areas of their afferent photoreceptors. Among these neurons, the ganglion cells at the fovea (center of the retina) have the smallest receptive field, providing the finest resolution. Rising the level along this flow direction, the receptive fields increase in size and specificity of the stimulus. Neurons may respond to objects and faces (Bruce et al., 1981; Desimone et al., 1984; Tsao and Livingstone, 2008), or even to a single person (Quiroga et al., 2005).

In the vision, the concept of receptive field has also been extended to capture a spatiotemporal feature of the stimulus. This generalization allows the characterization of direction selective responses from neurons in primary visual cortex (Alonso and Chen, 2009).

Auditory system. The neuronal receptive fields in the auditory system code at least two features of the stimuli: spatial and spectro-temporal information (Alonso and Chen, 2009). The response of neurons with the spatial receptive field depends on the position of the sound source (Knudsen and Konishi, 1978; Knudsen, 1982; Ashida and Carr, 2011). Such location can be precisely estimated by coincidence detection using the minute temporal disparity of arriving spikes from the sensory neurons of the two ears (Jeffress, 1948; Joris et al., 1998; Agmon-Snir et al., 1998), or by the recently proposed code by population spike rate (Vasilkov and Tikidji-Hamburyan, 2012). Neurons with the spectro-temporal receptive field respond preferentially to sound of a given frequency (Robles and Ruggero, 2001). The frequency decomposition of complex sounds takes place at the cochlea. The cochlea is a sensory organ in the auditory system that has a precise repre-

sentation of sound frequency: the base detects higher tones and the apex detects lower tones.

Olfactory system. The olfactory system depends on a chemical signaling that is rather complex and poorly understood. There are a multitude of families of olfactory receptor neurons, each type of neuron responding optimally to a certain odorant. Recently, an olfactory receptive field has been proposed to be mapped as a function of the molecular carbon chain length of the odorant (Mori et al., 1999; Wilson, 2001; Wilson and Stevenson, 2003; Alonso and Chen, 2009).

1.1.3 Intra- and cross-modal convergence: Picking up from fragments

The stimulus enters the brain through a myriad of relatively independent channels at the sensory systems. Each channel receives rather small data sets. Practically, the information of several of those small data sets must be collected to achieve any percept. This convergence is fundamental and ubiquitous within and among different sensory modalities.

Convergence occurs at many levels. It is, however, more prominent at higher levels, where the activity is most raveled and cannot be decomposed into distinct contributions from discrepant sources. Despite being a requirement, convergence alone does not guarantee integration.

1.1.4 The binding problem

Sensory, cognitive and motor processes involve essential interactions among large populations of neurons within different brain regions that must exchange information among themselves. The bind problem refers to how information from distinct populations is exchanged. A solid base to understand the neuronal pattern of activity representing the integration of coherent information is still needed (Roskies, 1999). It is still a general open question, which arises whenever information from distinct areas must be exchanged. The binding problem was originally stated as a theoretical problem when the experiments seemed to indicate that none of the localized parts of the brain could generate some aspects of mind's function like con-

sciousness or reason (von der Malsburg, 1981). Such studies raised hopes to fundamental question like: Will the solution of the binding problem resolve the mystery of consciousness?

The most popular hypothesis for the binding conundrum involves the temporal correlation of firing patterns. It states that features should be bound by the synchronization of spikes of distant neurons. This is called the binding by synchrony theory and its validity is still under debate.

1.2 An overview of the functional anatomy of the central nervous system

There are two main lines of thought to understand neuroanatomy proceeding from a simple state to a more complex state (Squire et al., 2003). Evolution is the first line; it is hard to overstate about the importance of evolution because it constitutes a prime foundation of biology. Embryology is the second line; in a much faster time scale, embryology studies the dynamics of development of embryos from a single cell to the fetus stage.

From the two complementary approaches we learn that all vertebrates share the same functional systems. This has profound implications on the way the research in those systems is typically undertaken. Such principles offer a solid foundation to tackle elaborated problems involving complex brains. The support of these pillars provides reasonable security to the successful approach: to solve a difficult problem beginning with a simple version and then increasing the level of complexity. The difficult problem in neuroscience consists of understanding the dynamics of a multitude of interconnected neurons and its manifold consequences. Despite the importance of this approach in complex systems, a straightforward extrapolation can occasionally be meaningless. A careful analysis is usually required because the interaction of non-linear elements can lead to unpredictable phenomenology, or can show counter-intuitive behavior (Anderson, 1972). Consciousness is a conspicuous example of behavior that emerge when increasing the complexity level of the system. To understand the emergence of consciousness constitutes a fundamental goal of neuroscience.

Another remarkable lesson gotten from the evolutionary and the embryologic approaches is that, in terms of cell biology, nerve cells are basically the same in all animals (Squire et al., 2003). The focus is thus directed to what changes most during evolution and embryogenesis: the arrangement of the network. The architecture of the nervous system is profoundly important!

1.2.1 *C. elegans*: An especial example

In spite of many efforts, the anatomical knowledge of the nervous system, studied for centuries, is still not well known, except very general principles. A very celebrated exception occurs with the *Caenorhabditis elegans*.

The *C. elegans* is a nematode of about one millimeter in length. This worm lives in temperate soil environments, but it is easily grown in the laboratory. It has become a model organism in molecular and developmental biology mainly because of its simplicity. All its somatic cells have been mapped; they are around a thousand cells. In addition, it was the first multicellular organism to have its genome entirely sequenced.

C. elegans was also the first and unique (by the date) organism to have the whole nervous system mapped. The wild type organisms are essentially invariant with respect to the number, and type of neurons and the synapses they make. In this way, White et al. (1986) identified all the 302 neurons of the hermaphrodite *C. elegans*, thus obtaining its complete wiring diagram.

White and colleagues succeeded to obtain the neuronal network because they were studying a very simple organism. The neurons of the *C. elegans* typically have few branches, and make few synapses, being mostly local connections. Nevertheless, the work to obtain the complete neuronal network from reconstructions of electron micrographs of serial sections represents already a huge effort.

1.2.2 Evolutionary perspective

From the metabolic viewpoint, it is really expensive to keep a nervous system. Nevertheless, following an evolutionary perspective, it seems intelligible that the nervous system favors the species by improving the behavioral repertoire of an animal. This, in turn, increases the probability of the individuals to survive and to generate offspring.

1.2. AN OVERVIEW OF THE FUNCTIONAL ANATOMY OF THE CENTRAL NERVOUS SYSTEM

Even unicellular organisms utilize several types of taxes to improve their chances of survival. These strategies consist on the movement of the organism towards or away from the external stimulus, typically attempting to reach an optimum concentration. The response could be associated to stimulus of several different qualities: chemical (chemotaxis), light (phototaxis), temperature (thermotaxis), sound (phonotaxis), gravity (gravitaxis), electric field (electrotaxis), concentration of oxygen (aerotaxis), and so on. In the case on chemotaxis, for example, the reliable discernment of shallow gradients of stimulus intensity might involve rather sophisticated mechanisms that combine cooperation and adaptation to perfect the sensitivity (Bray et al., 1998; Sourjik and Berg, 2002; Hansen et al., 2008; Skoge et al., 2011).

In the case of multicellular animals, the onset of the nervous system has long been thought to largely improve their fundamental capacities to respond to environmental changes (Parker, 1919). The sensitivity to stimuli increases in the presence of nervous system, and the response to a stimulus can be faster and stronger. These factors have been critical for many animals to survive under evolutionary pressure.

On the history of the nervous system. The Cnidaria was the first phylum to present nervous system (Squire et al., 2003). This phylum contains over 10,000 species of aquatic animals; it comprises jellyfish, corals, anemones and the hydra. The nervous system of an animal from Cnidaria phylum is a decentralized nerve net; they have no brain or central nervous system, see Fig. 1.1. The nerve net of the hydra is distributed rather uniformly throughout the cell body, with the exception of some zones of larger concentration, like the mouth and the base of the tentacles, which could be considered already as a tendency for centralization.

The flatworms are the simplest animals to display cephalization and centralization (Squire et al., 2003), which are fundamental organizational trends in the evolution of the nervous system. Besides from sensory and motor neurons, the flatworms have interneurons interpolated between sensory and motor neurons. The interneurons increase the capacity to transmit and process information. Differently of animals from cnidaria, the flatworms have a bilateral symmetry. As shown in the right panel of Fig. 1.1, their neurons form bundles of axons (nerve cords) extend along longitudinal and transverse directions. These nerve cords connect the clusters of neurons (ganglia), which are mostly concentrate in the rostral end (the head).

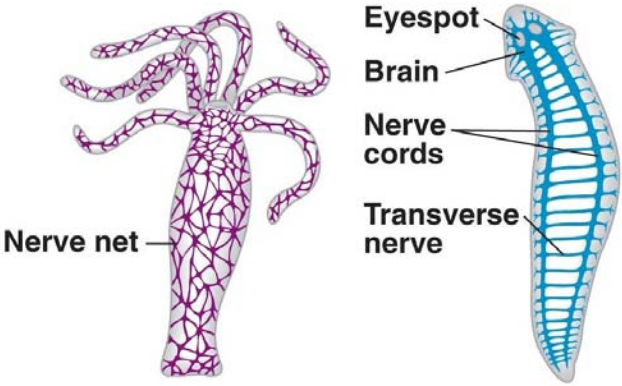

Figure 1.1: Left: the nerve net of a Hydra. Right: The nervous system with bilateral symmetry of a flat worm. Figure adapted from Bio1152 (2012).

Among the bilateral animals, there are two important configurations for the nerve cords. Arthropods, like insects, crustaceans, arachnids, and many other invertebrates, display a ventral nerve cord. Chordates, including all vertebrates, present a dorsal nerve cord surrounded by a notochord. The nerve cord generally defines a prime axis during the development of the chordates.

1.2.3 Developmental perspective

In an extremely faster time scale, the animals may develop the most complex nervous systems starting from a single cell. Remarkably, the early stages of embryogenesis follow basically the same steps for all vertebrates (Squire et al., 2003). This development leads straightforwardly to the main brain regions. The understanding of the development of the nervous system turns out to be an important guide for the modular anatomy of the brain (Kandel et al., 2000).

In the ectoderm, the outermost layer of the trilaminar gastrula (early embryo), there is the neural plate. The neural plate, shown in Fig. 1.2, is a spoon-shaped region that gives rise to the central nervous system. As illus-

trated in Fig. 1.2, the flat neural plate gets indented along the rostral-caudal axis forming the neural groove. Such invagination process is followed by the merging of the opposing lateral edges of the neural groove. This thin (one cell thick) closed tube is called neural tube.

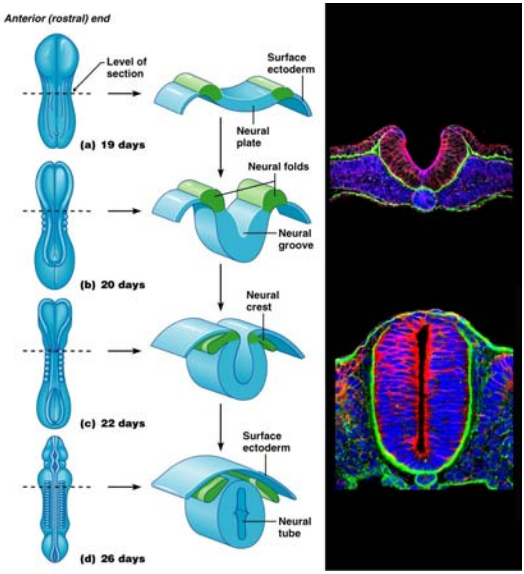

Figure 1.2: Development of a neural tube from a neural plate. Left and middle columns represent a diagram of human development. Right column shows a chick embryo of two days (top), and a mouse embryo of 9.5 days (bottom). Figure adapted from Trimble (2012); Cell (2012).

Along the rostral-caudal axis, the neural tube presents inhomogeneities that are already the first sign of regionalization. As in the spinal cord, the early neural tube also develops three swellings at its rostral end (Swanson, 1998). Figure 1.3 illustrates the primary vesicles, which correspond to prosencephalon (forebrain), mesencephalon (midbrain), and rhombencephalon (hinbrain) vesicles. Next, the right and left differentiation occurs and the vesicles divide further (Fig. 1.3). The prosencephalon differentiates into two secondary vesicles, telencephalon and diencephalon, whereas the rhombencephalon differentiates into two secondary vesicles, metencephalon and myelencephalon. Following neurulation, the telencephalon gives rise to the cerebral cortex, and cerebral nuclei; the diencephalon gives

rise to the thalamus and the hypothalamus; the mesencephalon gives rise to tectum and tegmentum; the rhombencephalon gives rise to rhombic lip, alar plate, and basal plate (Squire et al., 2003; Swanson, 1998).

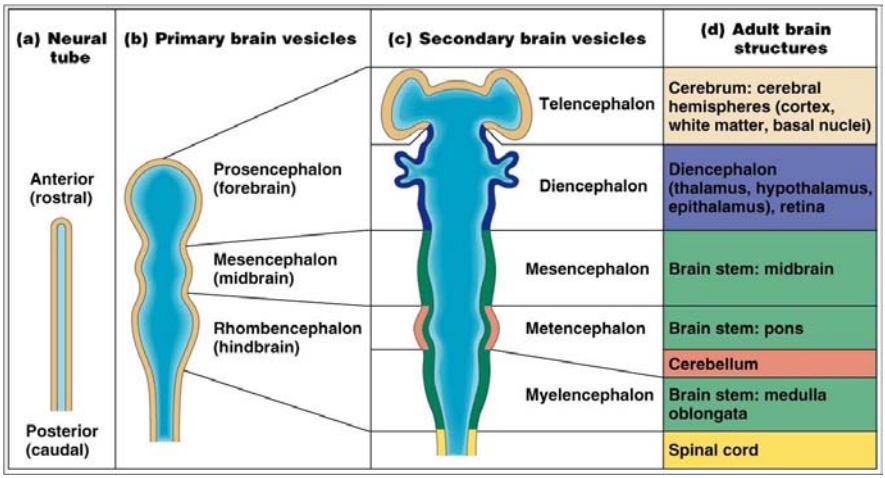

Figure 1.3: Schematic and nomenclatural representation of a human embryo early development from the neural tube to the secondary vesicles. Figure adapted from Trimble (2012).

1.2.4 Principles of functional anatomy of the central nervous system

The central nervous system comprises the brain and the spinal cord. The organization of the central nervous system of vertebrates follows the axis defined by the neural tube, i.e., the rostral-caudal axis. Along this axis, located between the spinal cord (most caudal) and the cerebral cortex (most rostral), there are six main regions (Kandel et al., 2000):

Spinal cord. The spinal cord connects the brain to the rest of the body: receiving somatosensory information through afferent pathways, sending motor information through efferent pathways, and coordinating certain reflexes and many autonomic functions.

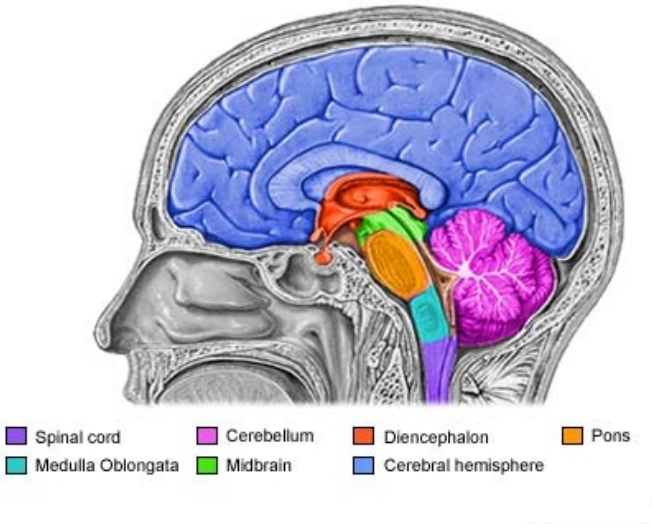

Figure 1.4: Main regions of the central nervous system. Figure adapted from Umm (2012).

Medulla oblongata. The medulla is the direct rostral extension of the spinal cord. Resembling the anatomy of the spinal cord, the medulla transmits information between the higher regions of the brain and the spinal cord. As well as the spinal cord, the medulla is also responsible for coordinating certain reflexes and many autonomic functions.

Pons and cerebellum. The pons is the rostral extension of the medulla, and the cerebellum is located dorsal to the pons. The pons is a relay center that transmits top-down signals from the telencephalon to the cerebellum, and to the medulla; and transmits bottom-up sensory signals to the thalamus. The human cerebellum has more neurons than the remainder of the brain combined (Williams and Herrup, 1988). Most of those neurons are tiny granule cells. Besides from these diminutive and numerous neurons, the Purkinje cells are also found in the cerebellum. These Purkinje neurons are widely known because of its fascinating and extensive dendrites (depicted in section 1.4.2). Among other functions, the cerebellum contributes to behavioral functions, and modulates cognitive information processing. For example, the

cerebellum plays the role of coordinating and correcting movements, during tasks involving fine motor skills.

Midbrain. The midbrain is the rostral extension of the pons, and is associated with different sensory systems: visual, auditory, and somatosensory. The midbrain also plays a role in temperature regulation, sleep/wake cycles, and alertness.

Diencephalon. The diencephalon, which lies rostral to the midbrain, is comprised of two main structures: the hypothalamus and the thalamus. Forming the ventral part of the diencephalon, the hypothalamus coordinates activities of the autonomic nervous system, and regulates metabolic process. The thalamus plays the role of the gateway to the cortex, because it relays most of the information coming from the lower regions. The thalamus is one of the key regions of this thesis. We shall discuss the function and organization of the thalamus in more detail below.

Cerebral hemispheres. The cerebral hemispheres are composed of cerebral cortex, and the basal ganglia (Kandel et al., 2000).

Next we discuss some general features of the cortex, and the hippocampus (which is located in the medial temporal lobe). Along with the thalamus, those regions are central for the results of the thesis.

cortex

Comprising more than three fourths of the volume of the human central nervous system (see table 1.1), the cerebral cortex is a major processing center. This region is concerned with perceptual awareness, memory, attention, thought, language, and consciousness.

Roughly speaking, the cortex can be viewed as a series of two-dimensional overlapping layers (up o six), which have been packed to cover a core brain region (basal ganglia and diencephalon) and to fit inside the approximately spherical surface constrained by the skull. This compression process gives rise to several folds: gyri and sulci. Despite a considerable fold variation among people (Toro et al., 2008), some notable divisions of the human cortex are invariant. These prime fissures, used as landmarks, separate each cortical hemisphere into four lobes: frontal, parietal, temporal, and occipital.

	proportions by volume (%)	
	rat	human
cerebral cortex	31	77
basal ganlgia	7	4
diencephalon	6	4
midbrain	4	1
hindbrain	7	2
cerebellum	10	10
spinal cord	35	2

Table 1.1: Table extracted from Swanson (1995).

The cortex surface has a gray color. This color arises from large collections of cell bodies, dendrites and unmyelinated fibers. Thus, this part is called gray matter, and it surrounds the deeper white matter. The white matter is manly composed by glial cells, and myelinated axons responsible for transmitting signals between separated regions. The name of this part of the nervous system comes from the lipid tissue of the myelinated axons, which has a white color.

Abounding in the white matter, the long-range connections are a general feature across several species. Comparing different mammalian species, there is a robust power-law scaling relating the volume of the gray matter to the volume of the white matter. This allometric relationship is shown in Fig. 1.5.

The division of brain tissue into gray and white matter is a ubiquitous feature of the vertebrate anatomy. Different sorts of explanations have been given for this intriguing fact. Some authors claim that the origin of this separation could be a consequence of minimizing the wiring volume (Ruppin et al., 1993; Murre and Sturdy, 1995). Based on scaling arguments, an alternative proposal to solve this conundrum suggests that the fundamental element to minimize is not the wiring volume, but the conduction delay (Wen and Chkolvskii, 2005). On top of that, this optimization of the latencies would also explain why the cortical thickness remains almost unchanged whereas the brain volume varies by orders of magnitude between species (Fig. 1.5).

Many efforts have been done to characterize the cortical networks. At the macroscopic level of cortical regions, which are connected by long-range

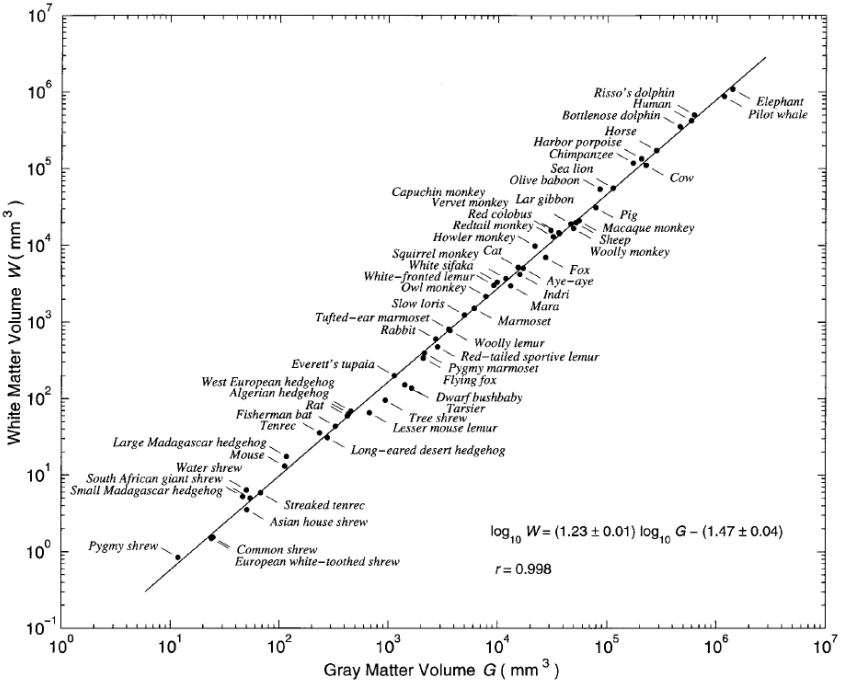

Figure 1.5: Scaling relation between the volume of neocortical gray and white matter. Figure extracted from Zhang and Sejnowski (2000).

fiber pathways, the mammalian cortex is characterized solely for a few of the most studied mammals like the cat (Scannell et al., 1999), and the monkey (Felleman and Van Essen, 1991; Kötter, 2004).

Sometimes considered as the basic functional units of the neocortex, a next modular level or organization is given by the cortical columns and microcolumns (Mountcastle, 1997; Mountcastle et al., 1957; Mountcastle, 1957). These columns are modules that extend vertically across the layers, perpendicular to the pial surface. What defines a column is the fact that the neurons within a given column encode similar features.

Despite the many efforts, like the neuronal reconstruction by electron microscopy (Briggman and Denk, 2006), the architectural network at the colum-

nar level, as well as the microscopic level, have remained elusive (Sporns et al., 2004). This structural information is a key feature to build more precise models. The absence of detailed structural information requires a workaround. For this reason, we stick to a less constrained relationship, which is generally satisfied by the cortex. Microscopically, the cortex is mainly composed of excitatory pyramidal cells, and local inhibitory interneurons, in a proportion of 80% and 20% respectively. Typically, we simply utilize random recurrent networks (following this recipe), or a mesoscale model (mimicking this recipe). This is a frequent issue, and, from now on, we shall implicitly or explicitly invoke this argument in almost every chapter.

The results of this work focus on the synchronization properties of cortical populations of neurons. Experimental observations of synchronization between distant neurons have long been observed (Engel et al., 1991; Frien et al., 1994; Roelfsema et al., 1997), however, the proposed mechanism explaining the observations (Traub et al., 1996) have not been entirely compelling. The hesitation appears especially because of the restricted robustness of the spike doublets model (Traub et al., 1996) with respect to key elements of the system, such as the broad range of cell types and delays in the connection. The *universality* of the synchronization found in the experiments suggests that a more general phenomenon must underpin this collective order. Based on recent advances in the synchronization aspects of delay-coupled systems [i.e., dynamical relaying (Fischer et al., 2006)], we attempt to identify and characterize the zero-lag long-range cortical synchronization. The first problem we tackle is how such isochronous cortical synchronization emerges in a generic cortical population of spiking neurons (Vicente et al., 2008b, 2009).

hippocampus

Historically, the brain was first analyzed by post-mortem inspections. Several regions were named based on the appearance that they had in the freshly dissected state (Squire et al., 2003). One example, as depicted in the Fig. 1.6, the hippocampus was thus named because of the similarities of its shape with the sea horse.

The hippocampus is among the most well studied brain areas. This region attracts much interest because it plays an important role in memory for-

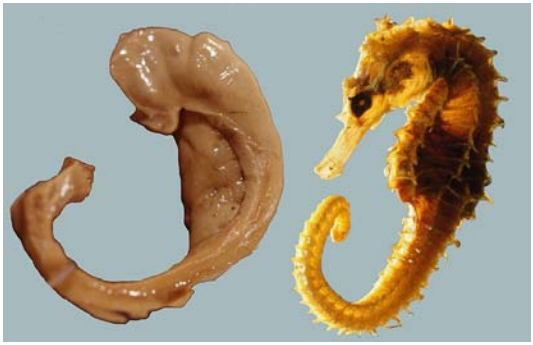

Figure 1.6: Comparison of a hippocampus with a sea horse. Extracted from Wikipedia (2012a).

mation, and spatial navigation (Buzsáki, 2010). The consolidation of both long-term and short-term memories depends on the hippocampus. Remarkable examples of hippocampal activity include the place cells (O'Keefe and Nadel, 1978) and the replay of waking assembly sequences during sleep (Lee and Wilson, 2002). For example, the hippocampal place cells have been proposed to constitute a cognitive map (O'Keefe and Nadel, 1978). Additionally, there are further practical reasons to understand the hippocampus and its relationship with the brain. Hippocampal damage is one of the first events of Alzheimer's disease. Moreover, schizophrenia and epilepsy have also been associated with abnormal activity of the hippocampus.

The hippocampal activity is characterized by some oscillatory rhythms, ranging from slow to hight gamma oscillations. Recently, the isolated hippocampus has been shown to generate theta oscillations (Goutagny et al., 2009). Such rhythms spans beyond the default activity of the hippocampus. In rodents, for instance, theta oscillations are even enhanced when the animal is moving.

The hippocampus exchanges a lot of information with cortical regions. For example, it has been recently proven that the prefrontal cortex and the hippocampus can develop phase locked oscillations (Siapas et al., 2005). As an attempt to establish a solid framework for such observations, we study the theta-band synchronization of distant cortical areas mediated by the hippocampus. As presented in chapter 6, our results suggest that such well-known phase-locking between prefrontal cortex and hippocampus is a facet

of a hippocampal dynamical relaying (Gollo et al., 2011). In addition to this phase-locking, a recurrent scenario, observed both in mice experiments and simulations, shows other cortical areas isochronously synchronized with the prefrontal cortex. This has been the prominent configuration generated by the hippocampal relaying. Moreover, in the experiments, such configuration appears with a higher probability when the mouse moves rather then quiet. This indicates that the dynamical relaying might play a key role in the integration of information from distant brain areas.

thalamus

The thalamus is a pivotal product of the embryonic diencephalon. Lying under the cerebral hemispheres, the thalamus is a collection of nuclei that occupies a core position in the brain. Such centrality confers the thalamus a remarkable capacity to exchange information with the cerebral cortex throughout extensive thalamocortical radiations. With the exception of the olfactory stimulus, which is primitive in evolutionary terms, all sensory stimuli intermediately pass through the thalamus. For this reason the thalamus is famous to be the gateway to the cortex. Figure 1.7 illustrates the central location of the thalamus in the brain, the anatomic configuration of its nuclei, and the areas bridged by the extensive thalamocortical radiations.

According to the functional role, each thalamic nucleus is classified as one of the three classes: specific relay nucleus, association nucleus, or nonspecific nucleus (Kandel et al., 2000). The specific relay nuclei receive sensory afferent input from a given sensory modality or motor function, project to and receive the feedback from the respective primary motor or sensory region of the cortex. The specific relay nuclei are: the medial geniculate (hearing), the lateral geniculate (vision), the ventral posteromedial (somatic sensation of the face), the ventral posterolateral (somatic sensation of the body), the ventral intermedial (motor), the ventral lateral (motor), the ventral anterior (motor), and the anterior nuclei (limbic function).

The association nuclei receive input from several regions of the brain and project to an association cortex. The association nuclei are: the lateral dorsal (emotional expression), lateral posterior (integration of sensory information), pulvinar (integration of sensory information), and the media dorsal (limbic function).

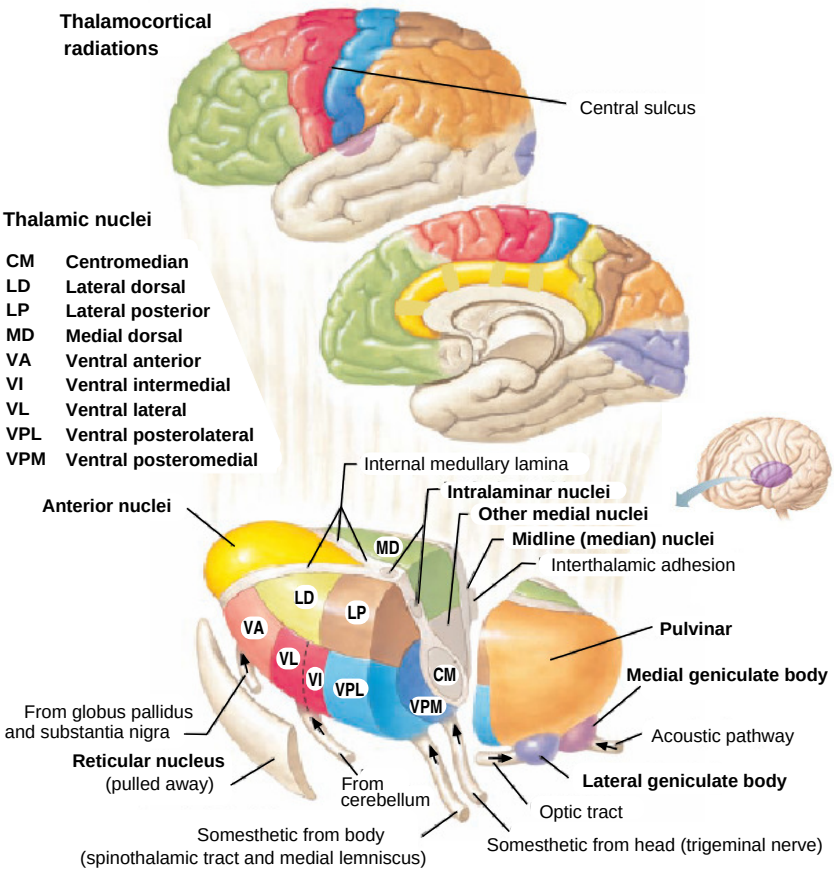

Figure 1.7: Thalamus in the human brain. The location of the thalamus (right panel), the position of the thalamic nuclei (bottom panel), and the thalamocortical areas connected by the thalamocortical radiations (top and bottom panels). See text for details. Figure adapted from Eneurosurgery (2012).

The other nuclei (midline, intralaminar, centromedian, centrolateral and reticular) have nonspecific functions. These nuclei have a widespread con-

nectivity pattern. They are thought to regulate the motivational and the arousal states, as well as the level of activity of the brain. Except for the reticular nucleus, their outputs consist of excitatory projections to other regions. The reticular nucleus, on the other hand, sends inhibitory projections to the other thalamic nuclei. It plays an important role in controlling and modulating the activity of the thalamus. Considering the thalamus as the gateway to the cortex, the reticular nucleus is the guardian of the gateway (McAlonan et al., 2008)

By analogy with the specific relay nuclei, it has been proposed that the olfactory bulb, which has also segregated and specialized moduli (glomeruli), plays the role of olfactory thalamus to pre-process the information, and to make the loops with the cortical areas involving the olfactory stimulus (Kay and Sherman, 2007).

The thalamus plays the important role of being a relay station. It is believed that the cortical areas would not be able to interpret the sensory stimuli without the pre-processing of the information at the thalamus. The first stride in the generation of sensory perception occurs through the reception and transmission of unimodal sensory stimulus to the primary cortical areas. In a series of back and forth thalamocortical exchanges of information, the perception of the different sensory stimulus is integrated. These thalamocortical loops represent a fundamental flux of information, ascending and descending along the hierarchical pathways (Llinás et al., 1999). Such loops have been proposed to be the neural mechanism underlying consciousness (Llinás and Ribary, 1993; Ward, 2011).

It has been argued that virtually any trivial task involves at least three distant brain regions (Kandel et al., 2000). This required integration is a central and recurrent topic of the thesis. A model of the thalamocortical circuit that attempts to elucidate a possible mechanism to give rise to such integration is presented in chapter 5. We consider the dynamical-relaying model in which the role of mediating element is played by the thalamus (Gollo et al., 2010). Remarkably, according to our results, the thalamus is not a passive element in the thalamocortical circuit, but instead its dynamics governs the long-distant zero-lag cortical synchronization. Due to the extensive thalamocortical radiations, the thalamus has always been the strongest candidate to mediate the cortico-cortical dynamics and synchronization. Not surprisingly, recent experimental evidences (Temereanca et al., 2008; Wang

et al., 2010a,b; Bruno, 2011; Poulet et al., 2012) support the fundamental importance of the thalamus in controlling the cortical activity.

1.3 A brief comparative overview on the experimental measurements of brain activity

Along the last century, during the course of the history of neuroscience, the anatomy of the nervous system has been studied thoroughly. Riding on top of such anatomical substrate, the neuronal dynamics is of exceptional relevance. Along a lifetime, there are certain changes in the anatomy, however, occurring at a much slower time scale than the changes in the dynamics. Thereby, the neuronal dynamics is asserted fundamental for cognition. The execution of essentially any task depends on some specific pattern of neuronal activity.

There is an important research field in neuroscience concerned to assess the neuronal activity. Brain activity can be assessed with recording methods or imaging techniques. The electrophysiological recordings capture the action potentials and the post-synaptic potentials. The electric signaling characterizes in a most reliable way the neuronal activity, however, this comes with a price: it requires an invasive method. There are also non-invasive neuroimaging methods based on electrophysiological principles. Two important examples are electroencephalography (Berger, 1929) (EEG) and magnetoencephalography (Cohen, 1968) (MEG). These popular neuroimaging techniques measure electrical potentials and magnetic fluxes respectively with high temporal resolution. However, as illustrated by Fig. 1.8, the spatial resolution is rather poor, even when taking into account the electromagnetic source imaging (Michel et al., 2004) (ESI), which improves the spatial resolution of EEG and MEG to the order of centimeter.

Other neuroimaging methods based on metabolic and hemodynamic principles can improve this limited spatial resolution. Some examples of such neuroimaging methods are functional magnetic resonance imaging (fMRI), near-infrared spectroscopy (NIRS), single-photon emission computed tomography (SPECT), and positron emission tomography (PET). The metabolic and hemodynamic activities reflect the neuronal dynamics in an indirect

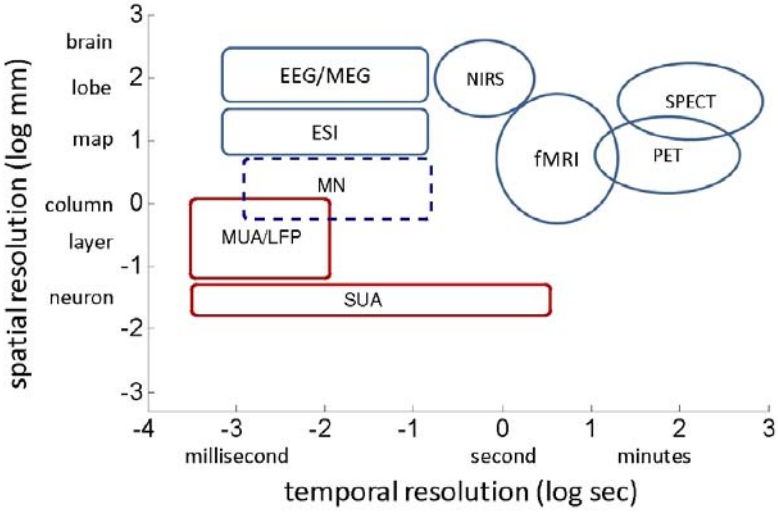

Figure 1.8: Limits of resolution of the different experimental techniques. Blue areas represent the ranges of resolution of the noninvasive techniques. Red areas represent the ranges of resolution of the invasive electrophysiological recordings from single-unit activity (SUA), multi-unit activity (MUA) and local field potential (LFP). Figure adapted from Liu (2008).

way. The neuronal activity consumes energy and triggers a cascade of metabolic and hemodynamic events. These events can be traced with fine spatial resolution but poor temporal resolution (see Fig. 1.8) because these indirect effects of neuronal activity take place at a much slower time scale.

For the time being, one cannot measure the brain activity with fine spatial and temporal resolutions by non-invasive methods. A promising advance in this direction is called the multimodal neuroimaging (Liu, 2008) (MN), which integrates different types of neuroimaging methods EEG/MEG and fMRI.

To detect synchronization between distant neurons (or specific neuronal regions) is among the most technical challenges. Such detection requires simultaneously recorded data with high temporal precision (~1 millisecond).

In addition, an accurate spatial precision, which to a great extent depends on the spot of interest, is often desired.

1.4 Biophysical overview of the neurons and neuronal interactions

The brain activity is a product of the neuronal dynamics combined with the neuron-to-neuron communication. This section addresses the fundamental problem of how the brain dynamics is generated. We start by identifying the building blocks of the brain; some authors (Izhikevich, 2007) claim that the neuron is the most important concept in neuroscience. Next, we describe the typical anatomy of a neuron, and the main functions of its constituents. We follow characterizing the neuronal dynamic states originated from the activity of the ionic channels. Finally, we discuss the types of neuronal communication.

1.4.1 Neurons

Cells are the basic structural unit in all living beings. This idea is credit to Schwann and Schleiden who in 1839 suggested that cells were the fundamental unit of life and all organisms were composed by one or more cells. In 1858, Rudolf Virchow, concluded that all cells derive from pre-existing cells, thereby completing the classical cell theory.

At that time, however, the nervous system was still considered to be an exception. The nervous tissue was thought to be a continuous reticulum system owing to its similarity to wire elements. This idea persisted until the Camillo Golgi's development of a new histological stained technique with a silver chromate solution, which allowed Ramón y Cajal to perform his experiments. The technique dyes only a few neurons [$\sim$ 2% of the cells (Kandel et al., 2000)], and enables the observation of single neuronal cells. Based on a deep investigation, Cajal concluded that the neurons were the fundamental building blocks of the nervous system (Squire et al., 2003).

The human brain has about 10^{10} neurons organized in a multilevel hierarchical system (Shepherd, 1998). The nervous system presents an enormous diversity of neuron types, connectivity, functionality, etc. Our description is solely restricted to the most common behavior, despite the large variability that exists. In this section we describe the neuron, first by its anatomical structure, and second by its central dynamical states: rest, spike and refractory period. At last, we comment on how the transitions between the dynamical states take place.

1.4.2 Neuronal morphology

Based on the neuronal morphology and on the cytological displaying features, Cajal proposed the principle of dynamic polarization (Kandel et al., 2000). This principle [which is part of the neuron doctrine (Golgi, 1906; Shepherd, 1991)] states that the activity coming from the dendrites are processed and passed from the axon to neighbor neurons. Despite of some exceptions (e.g., dendrodentric synapses), this directionality in the flow of activity typically occurs. In most cases the neuronal morphology can be understood as several parts adapted to fulfill its functional role. Some of the general morphological characteristics satisfied by most neurons (Kandel et al., 2000) are displayed in Fig. 1.9.

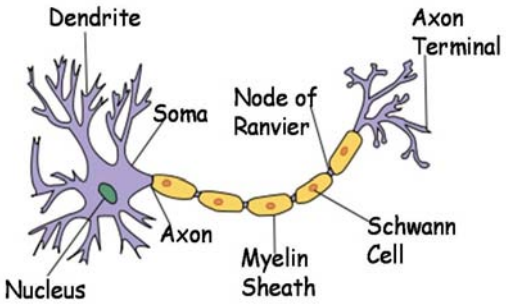

Figure 1.9: Sketch of a typical neuron with myelinated axon. Figure adapted from Wikipedia (2012b)

The three main parts of a neuron are the dendrites, the soma (cell body), and the axon. Most of the incoming inputs to a neuron come from the dendrites.

Presumably, the great distinctive feature of neurons is the presence of large dendritic trees. They are responsible for most of the variety in neuron size, shape and types [there are about 10^4 different morphological classes of neurons (Johnston et al., 1996)]. Figure 1.10, for example, compares two distinct types of neurons: The cerebellar Purkinje cell, and the cortical pyramidal cell.

The dendritic tree contains most of the postsynaptic terminals of the chemical synapses. Several functions (Stuart et al., 1999) of the dendritic arbors have also been claimed:

- to perform biological gates (Stuart et al., 1999; Koch, 1999);
- to detect the coincidences of incoming spikes (Agmon-Snir et al., 1998; Koch, 1999);
- to contribute with plasticity via dendritic spikes (Golding et al., 2002);
- to increase the learning capacity of the neuron (Poirazi and Mel, 2001);
- to improve the ability to distinguish the intensity of an incoming stimulus [i.e., to enhance the dynamic range] (Gollo et al., 2009, 2012a).

Despite such dendritic-computation properties, the role of dendrites seems yet distant from been clearly understood.

The cell body (soma) contains the nucleus and most of the cytoplasmic organelles. It is responsible for large part of the metabolic processes. Moreover, this region is where most recordings of the neuronal electrical activity take place.

In general, the axon can extent to regions far away from the soma. It might have different size (from 0.1 to 2,000 mm) depending on its functionality (Kandel et al., 2000). It starts at the axon hillock, where the action potential is generated (see section 1.4.4), and present ramifications at the extremities. Most of the pre synaptic terminals come out from those terminal buttons. The axon might be covered by myelin, which protects and controls some properties of neuronal activity, such as the velocity of the pulse propagation.

The axon is the crucial unit specialized to conduct the action potentials. Such propagation essentially occurs without distortion. This reliability property

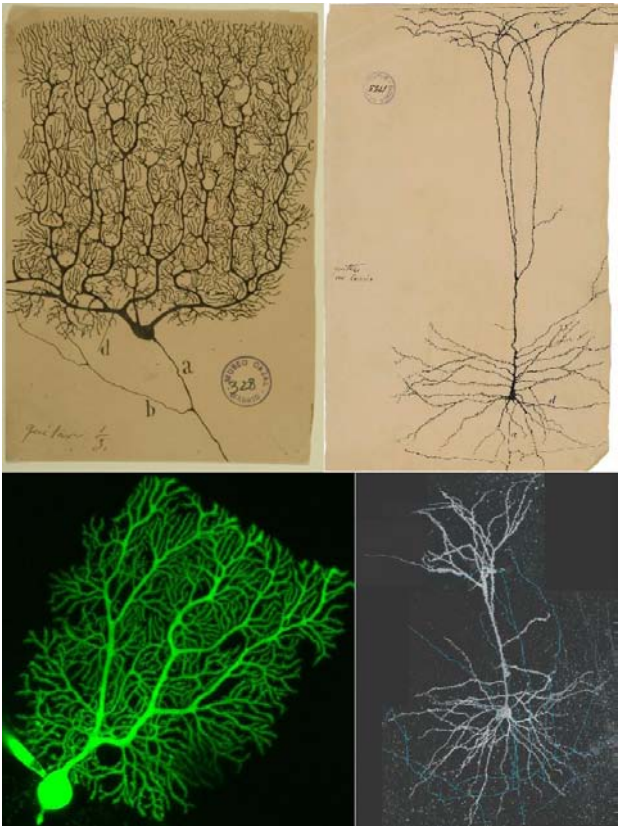

Figure 1.10: Examples of two different types of neurons. Top: Drawings by Ramón y Cajal of a human Purkinje cell (left), and a human pyramidal cell (right). Bottom: A rat Purkinje neuron injected with a fluorescent dye (left) [panel extracted from Rikenresearch (2012)], and a confocal laser scanning microscope image of a typical mouse frontal cortical layer 3 pyramidal cell (right) [panel extracted from Bumc (2012)].

is important because the action potentials (or spikes) are considered to carry most of the information of the neuronal activity (Gerstner and Kistler, 2002; Fries et al., 2007), either by the precise timing of the events, or by the firing rate over a certain period.

1.4.3 Nerst potential

The neurons are, as well as all other living cells, enclosed by a cell membrane. It separates the extracellular medium from the interior of the neuron. The neuronal membrane is a lipid bi-layer of 3 to 4 nm thick, which acts as a capacitor, separating the ions lying along its interior and exterior surface (Gerstner and Kistler, 2002; Dayan and Abbott, 2001).

Variations of the ionic concentrations give rise to the potential difference maintained by the cell membrane. This is called the membrane potential. Under normal conditions, the membrane potential remains around -90 to 50 millivolts. The membrane potential also defines the rest potential, a dynamical equilibrium state of ions coming back and forth.

Since the lipid bi-layer is impermeable in natural conditions, the ions might only cross the cell membrane via specialized structures (pore-forming proteins) called ionic channels, or by the active selective pumps. The operation process of channels does not involve metabolic energy, whereas the active movement of ions by the pumps requires the energy produced by the hydrolysis of adenosine triphosphate [ATP] (Kandel et al., 2000). Most channels possess gates that open in response to ligands (especially neurotransmitters), or voltage changes; they normally close by an intrinsic inactivation process (Lehmann-Horn and Jurkat-Rott, 2003). The ionic channels correspond to the molecular basis for the intracellular signal transduction, the maintenance of the resting potential, and the generation of action potentials.

There are a variety of different types of ionic channels; each neuron has more than ten types. Each channel type has its own properties; in particular, some of them are highly selective to a specific ion. Figure 1.11 illustrates the typical behavior of a voltage-gated ionic channel.

1.4.4 Neuronal activity

Neurons are nonlinear excitable elements, i.e., they generate a spike when its membrane potential exceeds a defined threshold [about 20-30 mV above the rest potential (Gerstner and Kistler, 2002)]. This excitation is also called action potential. When the membrane potential of a given neuron is perturbed without reaching the threshold, it relaxes back to its rest potential in a time scale governed by the membrane properties.

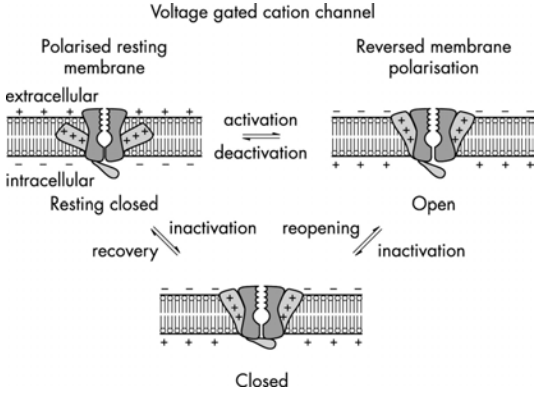

Figure 1.11: Diagram of the possible states of a voltage gated cation channels. This type of channels is important for the sodium, potassium, and calcium ions. A depolarization of the rest membrane (left) promptly opens the channel allowing a flux of cations according to their electrochemical gradients (right). The channel with a reverse polarization closes (bottom) and reopens very rarely. From refractory state, the membrane recovers back to the resting state. Owing to a slow depolarization process, a transition from the polarized to the inactivated state may also occur without channel opening (accommodation). Figure extracted from Lehmann-Horn and Jurkat-Rott (2003).

The spike is generated in a particular region called axon hillock located in between the soma and the axon. The pulse propagates (Fatt, 1957) mainly throughout the axon (forward propagation), but may also propagate to the dendrites [backpropagating spike (Stuart and Sakmann, 1994; Johnston et al., 1996; Falkenburger et al., 2001; Häusser and Mel, 2003)].

The spike occurs in a very narrow time window followed by a sudden decay of the membrane potential bellow the rest state. At this moment, the neuron is said to be hyperpolarized, and its potential difference with respect to the exterior region is greater than at rest. This stage is called refractory period. During the refractory period the neuron rarely gather enough contributions to spike. Typically, the membrane potential relaxes to the rest potential before another cycle happens. Figure 1.12 B shows an example of a whole cycle of microelectrode recording. This particular case corresponds to the seminal experiments of Hodgkin and Huxley in the squid giant axon (Fig. 1.12 A).

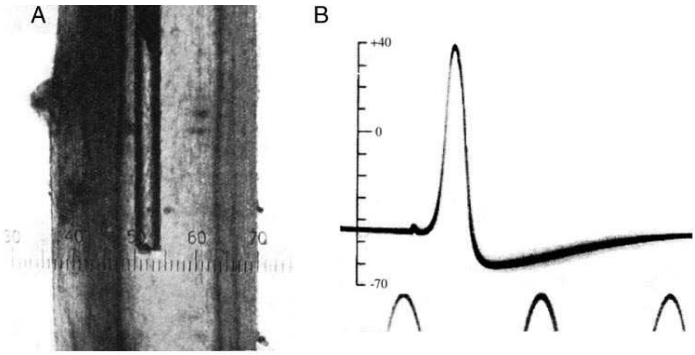

Figure 1.12: Intracellular recording of an action potential in the squid giant axon. (A) A microelectrode of 100 μm of diameter is inserted into the interior of a squid giant axon of about 1 mm. (B) The dynamics of an action potential dynamics. The y axis refers to the membrane potential (millivolts) while the x axis represents the time. The time interval between two peaks below equals to 2 ms. Figure adapted from original work of Hodgkin and Huxley (1939).

1.4.5 Neuronal communication

Charles Sherrington, in 1897, suggested that neurons perform functional contacts with other neurons and other types of cells through synapses. The existence of such structures was solely demonstrated 50 years later by electron microscopy (Squire et al., 2003).

Currently, we define the synapse as the specialized junctions through which cells of the nervous system signal to one another and to non-neuronal cells, such as muscles or glands. It is also the region in which two neurons are closest to each other. The cell transmitting a signal is known as pre-synaptic cell whereas the cell receiving the signal is the post-synaptic cell.

The brain is a highly connected tissue. Each neuron exchanges synaptic information with about 10^4 other neurons (Kandel et al., 2000). There are at least three different ways of communication among neurons: chemical synapses, electrical synapses and ephaptic interaction.

Chemical synapse

The predominant form of communication between neurons of vertebrates is the chemical synapse (Gerstner and Kistler, 2002). In this type of synapse there is a separation of the order of a few tens of nanometers called synaptic cleft, see Fig. 1.13. In the pre-synaptic terminals, there are collections of synaptic vesicles, each containing thousands of molecules of neurotransmitters. The vesicles release neurotransmitters in the synaptic cleft when the pre-synaptic neuron fires. After the spike, the neurotransmitters suffer a diffusion process in the extra cellular space of the synaptic cleft space. The molecules of neurotransmitters may bind to the post-synaptic cell receptors. The effective coupling of neurotransmitters triggers the opening of the ionic channels. This dynamics of the channels generates the postsynaptic potentials, which are local changes (excitatory or inhibitory) of the membrane potential. If the potential difference exceeds a certain threshold, the post-synaptic neuron fires, concluding the communication. Note that, in this case, there is an anatomical difference between two well-defined cells, which makes this type of communication unidirectional.

The resultant variation of membrane potential of the postsynaptic neuron depends on the type of neurotransmitter and the number of channels opened due to the binding of neurotransmitters. There are several types of neurotransmitters. Some of them excite (Brock et al., 1952) the postsynaptic neuron (increase its membrane potential, or depolarize); others inhibit (Wilson and Cowan, 1972; Duchamp-Viret and Duchamp, 1993; Rinzel et al., 1998) the postsynaptic neuron (decrease the membrane potential, or hyperpolarize). Our results focus on the chemical synapse because it is the most common type of interaction present in the brain.

Electrical synapse

Another route of neuronal communication is via electrical synapses. The electrical synapses occur through the electrical interaction between cells. In this case, the cellular membranes of neighbor neurons are located very close to each other. They are directly connected through specialized channels called gap junctions, see Fig. 1.14. These gap junctions are proteins that have the channels larger than the pores of the ionic channels. Various substances are simply free to spread by these channels. More importantly,

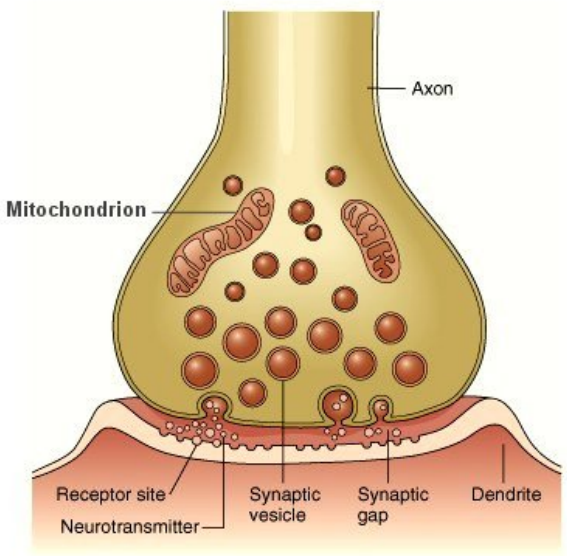

Figure 1.13: Diagram of the action of a typical chemical synapse, where the axon represents the presynaptic terminal and the dendrite represents the postsynaptic terminal. Figure extracted from Hrsbstaff (2012).

the gap junction enables a bidirectional and virtually instantaneous flow of current between the neurons.

Differently from the chemical synapses that are pulse-coupled, the electrical synapses have virtually instantaneous diffusive coupling. The effects of the chemical synapses are intermittent and sporadic, typically maintaining the communication active solely for brief time intervals. Such differences in the interactions can be reflected in the dynamics of neuronal networks (Balenzuela and García-Ojalvo, 2005; Rossoni et al., 2005; Feng et al., 2006; Pérez et al., 2011).

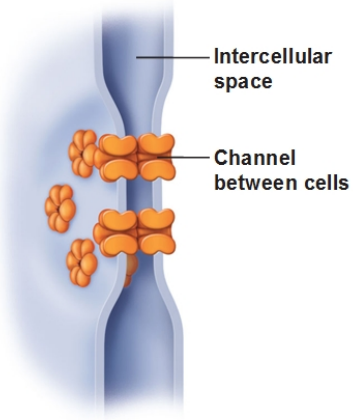

Figure 1.14: Schematic representation of a gap Junction. Two neurons get very closed together separated by an uniform gap, roughly 2-3 nm in width. Figure extracted from Antranik (2012).

Ephaptic interactions

A third, and less common type of neuronal communication is called ephaptic interaction. Formally, ephaptic coupling is the process by which neighboring neurons affect each other by current spread through the extracellular space (Lowe, 2003; Bokil et al., 2001; Furtado and Copelli, 2006). Eventually, in some cases of convergence of unmyelinated neurons, the axons gather into densely packed fascicles allowing the neuronal communication. An example of extreme convergence that occurs in mammals is the projections of the olfactory receptor neurons from the olfactory epithelium to the Mitral cells of the olfactory bulb.

Chapter 2

On the Different Modeling Levels

From subatomic elementary particles to universe(s), models span all spatial scales. The determination of the most appropriated modeling level highly depends on the features of interest. The best model for a given feature can be useless for another. The quest for better models is a fundamental and interminable task.

The brain, as a highly complex system, offers a multitude of functions, mechanisms, and behaviors. All of them become better understood after modeled (formally), or a set of experiments performed. Even the most pure empirical data demand a qualitative model to explain the results. Therefore, in science, one can never avoid modeling, which can indeed be of countless diverse natures. In particular, quantitative models, amenable to mathematical analysis, provide the advantage of enabling a formal consistency check. Furthermore, the understanding of suitable models of any kind frequently leads to successful predictions. Analogously to experiments, in which each experimental technique contains its own limitation, the validity of each model is also restricted by some boundaries. Thereby, it is important to take into account such restrictions to select the best model.

In neuroscience, where the quantum aspects have not been proved yet to play a role[1], probably, the smallest modeling scales correspond to the dynamics of the ionic channels. Several complex mechanisms of molecular interactions of the channels dynamics remain poorly understood. However, since the pioneer work of Hodgkin and Huxley, in a major conceptual leap, the opening and closing kinetics of the ion channels was deduced (Hodgkin and Huxley, 1952; Dayan and Abbott, 2001). They considered the conductance per unit of area of ion i (G_i) equals the maximal conductance per unit of area (g_i) times the probability of finding a channel in the open state P_i, i.e., $G_i = g_i P_i$. In turn, P_i might depend on one or more gates. In the case of persistent conductances (single gate), taking n $(1 - n)$ as the probability of a subunit gate being permissive (non-permissive), then $P_i = n^k$, where k represents the number of gating events (assumed independent). The probability of finding a channel in the open state is governed by the dynamics of n:

$$\frac{dn}{dt} = \alpha_n(V)(1 - n) - \beta_n(V)n \ , \tag{2.1}$$

where $\alpha_n(V)$ is the non-permissive to permissive transition rate, and $\beta_n(V)$ is the permissive to non-permissive transition rate. Finally, following the steps of the seminal work by Hodgkin and Huxley (1952), fitting these rates to the experimental data renders a biophysical model for the conductance.

Another important subcellular elements to model is the synaptic dynamics. The optimal synaptic model customarily depends on the precision craved. For example, the postsynaptic potentials can assume a variety of shapes: delta functions, exponential functions, alpha functions, and so on. The strength of the synapses also varies as a function of time (Bi and Poo, 1998; Abbott and Nelson, 2000). It has been claimed that the synapses play indeed a computational role (Abbott and Regehr, 2004). However, for many purposes, say whenever the focus is restricted to the events occurring in a fast time scale, it is a good approximation to assume a steady synaptic strength. To summarize, the phenomenology highlights that there are plenty of interesting behaviors at the subcellular level.

This chapter, however, aims at addressing the modeling strategies beyond the subcellular level, and to illustrate some of the major approaches that have been currently used. We start by the single neuron model. The approach of section 2.1 takes into account the neuronal tree topology and

[1]There is not only researches, but also a journal (Neuroquantology), handling with the interface of neuroscience and quantum mechanics.

considers the neuron as a spatially extended system. Although the most biophysically realistic model considers the neuronal structure, this strategy presents several limitations regarding its tractability. The most straightforward approximation to circumvent this limitations is to consider the neuron as a punctual element (section 2.2). To ignore the intricated morphology allows insights that, in several cases, justify the approximation. In particular, this compromise can be very convenient to study the behavior of a large number of interconnected neurons (section 2.3). In fact, it is already a considerable computational task to model populations of neurons using simple spiking neuron models. Frequently, a further simplification is advisable: to reduce the parameter space by the use of coarse-grained mesoscale models (section 2.4).

2.1 Detailed neuron models

The origin of the detailed neuronal modeling dates back to the development of the cable theory. Analogously to the heat equation, the cable theory comprises a partial differential equation that considers the membrane potential (V) as a function of space (x) (long axis of the neurite) and time (t) (Niebur, 2008):

$$\tau \frac{\partial V}{\partial t} - \lambda^2 \frac{\partial^2 V}{\partial x^2} = V_L - V\,; \tag{2.2}$$

where the parameters are: τ, a characteristic time scale; λ, a characteristic length; and V_L, the equilibrium membrane potential. The cable theory was further improved to study the cylindrical geometry of the cable (Rall, 1959, 1964), and its ramifications (Mel, 1993), as well as to understand the activity of pulses propagating through small buttons placed into the membrane called spines (Segev and Rall, 1988). These studies motivated the extensions to the two-compartmental model (Pinsky and Rinzel, 1994), and the multicompartmental model (Traub et al., 1991; Migliore et al., 2005; Rumsey and Abbott, 2006; Root et al., 2007).

The search for the most biologically realistic model has been a trend in neuronal modeling. The approach requires details concerning the neuronal morphology, the distribution of channels along the neuron, the precise behavior of each channel type, and so on. Those elements are largely unknown,

and usually vary in time. Therefore, they are either not included in the equations, or their setting relies on a prevalently speculative fashion. In addition, in the hypothetical case that all variables have been captured; the simulation of such a complex system represents a significant computational and interpretational challenge. This hampers the study, or allows only the simulations of idealistic situations in which, for example, the neuron receives rather artificial input signals.

It is essential to keep a balancement of detail and abstraction to model a single neuron (Herz et al., 2006). The greater the simplicity the better the topological description is allowed to be. This line of research aims at finding out the possibility that extensive neuronal regions could be the stage for some kind of *dendritic computation* (Gollo et al., 2009, 2012a).

Abstract models also provide further benefits. They are frequently the most appropriated to analytical investigations. Often a minimal model is the best to conspicuously show general features, which are also expected in more elaborate models. Moreover, the collective behavior of a multitude of connected units is typically better studied in simple models.

The most traditional approximation is to consider the neuron as a punctual element. Spiking neurons are typically modeled by differential equations (that we shall describe next). Other approaches to study punctual simplified models consist in assuming a network of neuron as a map (Chialvo, 1995; Kinouchi and Tragtenberg, 1996; Izhikevich and Hoppensteadt, 2004a), or neurons as cellular automata (Greenberg and Hastings, 1978; Ermentrout and Edelstein-Keshet, 1993; Furtado and Copelli, 2006; Kinouchi and Copelli, 2006; Gollo et al., 2012b). Those abstractions often allow analytical insights that would probably remain veiled otherwise.

To neglect the spatial structure of the neurons is the most widespread approximation in the art of neuronal modeling. The following section is devoted to discuss and to compare the different sorts of models that assume the neuron as a punctual element. Such modeling strategy either focuses on how its various ionic currents contribute to the subthreshold behavior and spike generation, or just mimics this entire process without monitoring each specific ionic contribution.

2.2 Spiking neurons

The dynamics of spiking neurons is mainly modeled by differential equations. One of the earliest models, which remains widely used, is the integrate and fire (I&F) neuron model (Lapicque, 1907; Knight, 1972; Abbott, 1999; Brunel and van Rossum, 2007). It is given by only one differential equation, which adds up the external input contributions and simultaneously relax exponentially to the rest state (see section 2.2.2). When the membrane potential reaches the threshold, it is reset to its rest state during a certain time interval called refractory period. Further features (mimicking the ionic channel time dependence) can be added to this model, to generate, for example:

Burst, this has been done by the so called integrate-and-fire-or-burst model (Smith et al., 2000);

Adaptation, as in the model of integrate-and-fire with adaptation (Izhikevich et al., 2004).

The neuronal models might also be more constrained to the detailed dynamics of several biophysical ionic channels, as, for example, the Hodgkin-Huxley (HH) model (Hodgkin and Huxley, 1952), which is based on a rather influential approach, motivating the study of numerous neuronal models (see section 2.2.1). The HH model inspired, for example, a simplified two-dimensional model called FitzHugh-Nagumo model (FitzHugh, 1961; Nagumo et al., 1962). Subsequently, both FitzHugh-Nagumo and HH were combined into a voltage-gated calcium channel model with a delayed-rectifier potassium channel called Morris-Lecar (Morris and Lecar, 1981). In order to describe different types of neurons with a better precision, some other models were also developed, like (for instance) the Hindmarsh-Rose (Hindmarsh and Rose, 1984), and the Izhikevich model. The last one reproduces several observed features, by two coupled differential equations (Izhikevich, 2000; Izhikevich and Hoppensteadt, 2004b). Mostly following Izhikevich (2004), next we discuss some of the major models of spiking neurons.

2.2.1 Biophysical models

The biophysically meaningful models of spiking neurons depend on measurable parameters. We first introduce the seminal work of Hodgkin and Huxley, which customarily influenced subsequent models.

Hodgkin-Huxley

Overcoming a series of experimental barriers, Hodgkin and Huxley studied in detail the dynamics of the squid giant axon. Such axon has a large length and diameter, which permitted electrophysiological intracellular recordings. Moreover, it has mainly two types of voltage gated ion channels (potassium and sodium). Compared to other conductance types that can influence the excitability of neurons (Llinás, 1988), this relatively simplicity endows the squid giant axon the ingredients required for the major conceptual advance provided by Hodgkin and Huxley.

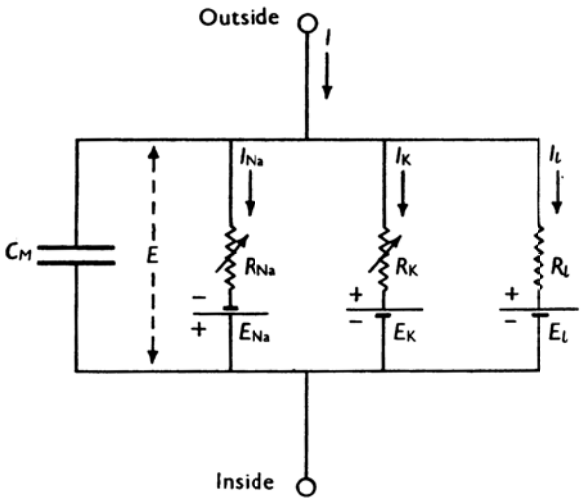

Figure 2.1: Equivalent electrical circuit representing membrane proposed by Hodgkin and Huxley for the squid giant axon. Figure extracted from Hodgkin and Huxley (1952).

The first assumption is to consider the membrane as the parallel electrical circuit shown in Fig. 2.1. The membrane current is thus divided into a capacity current and a ionic current:

$$C_m \frac{dV_m}{dt} + I_{ion} = I_{ext} \ , \tag{2.3}$$

where C_m is the capacitance of the membrane; V_m: the membrane potential; I_{ion}: the net ionic current; and I_{ext}: an applied current.

The ionic current is

$$I_{ion} = I_{Na} + I_K + I_L = G_{Na}(V - E_{Na}) + G_K(V - E_K) + G_L(V - E_L) \ , \tag{2.4}$$

where $G_i = 1/R_i$ is the conductivity per unit of area. Importantly, they found that G_{Na} and G_K are transient and persistent voltage dependent conductances that can be written as:

$$\begin{aligned} G_{Na} &= g_{Na} m^3 h \ , \\ G_K &= g_K n^4 \ , \end{aligned} \tag{2.5}$$

where g_{Na} and g_K are the maximal conductances. The transient conductances are controlled by two gates with opposite voltage dependences (in this case: m for activation and h for inactivation) (Dayan and Abbott, 2001). The persistent conductances are controlled by a single activation gate, as discussed previously (see Eq. 2.1).

Finally, The Hodgkin Huxley equations are found by combining Eqs. 2.3 to 2.5:

$$C \frac{dV}{dt} = -g_{Na} m^3 h (V - E_{Na}) - g_K n^4 (V - E_K) - g_L (V - E_L) + I \ . \tag{2.6}$$

The dynamics of the voltage-gated ion channels are described by the set of differential equations:

$$\frac{dm}{dt} = \alpha_m(V)(1 - m) - \beta_m(V) m \ , \tag{2.7}$$

$$\frac{dh}{dt} = \alpha_h(V)(1 - h) - \beta_h(V) h \ , \tag{2.8}$$

$$\frac{dn}{dt} = \alpha_n(V)(1 - n) - \beta_n(V) n \ , \tag{2.9}$$

where α_j and β_j are specific rate functions for each gate probability $j = m, n, h$. They were fitted experimentally in Hodgkin and Huxley (1952).

Morris-Lecar

To describe the oscillatory activity of the barnacle giant muscle fiber, Morris and Lecar (1981) proposed a leading biophysical model. The clarity of this nonlinear two-dimensional model enables insights with biophysical meaning, analogously to the Hodgkin-Huxley model. Although the model was proposed for a specific neuron type, its use has crossed remote boundaries (e.g., to represent a mammalian cortical neuron). The biophysical relevance of results under such distant conditions is debatable. Nevertheless, the model remains rather popular in the computational neuroscience community. The membrane potential depends on the K and Ca ionic currents, where the potassium (calcium) has a slow (instantaneous) activation:

$$C\frac{dV}{dt} = I - g_L(V - E_L) - g_{Ca}m_\infty(V)(V - E_{Ca}) - g_K n(V - E_K)\ ; \quad (2.10)$$

$$\frac{dn}{dt} = \lambda(V)[n_\infty(V) - n]\ ; \quad (2.11)$$

where

$$m_\infty = \frac{1}{2}\left[1 + \tanh\left(\frac{V - V_1}{V_2}\right)\right]\ ; \quad (2.12)$$

$$n_\infty = \frac{1}{2}\left[1 + \tanh\left(\frac{V - V_3}{V_4}\right)\right]\ ; \quad (2.13)$$

$$\lambda(V) = \bar{\lambda}\cosh\left(\frac{V - V_3}{2V_4}\right)\ ; \quad (2.14)$$

with parameters: $C = 20\ \mu F/cm^2$, $g_L = 2\ mmho/cm^2$, $g_{Ca} = 4\ mmho/cm^2$, $g_K = 8\ mmho/cm^2$, $E_L = -50\ mV$, $E_{Ca} = 100\ mV$, $E_K = -70\ mV$, $V_1 = 0\ mV$, $V_2 = 15\ mV$, $V_3 = 10\ mV$, $V_4 = 10\ mV$, $\lambda = 0.1\ s^{-1}$, and the external current $I[\mu A/cm^2]$.

2.2.2 Reduced models

Biophysical models have the advantage of allowing direct comparison with the experiments. On the other hand, most theoretical work are favored by simple models. A reduced number of parameters aids mathematical analysis to be amenable. Many simple models have been proposed since

the Hodgkin Huxley contribution. Typically, the simple models either focus on the integration properties of the neuron, or on reducing the amount of features involved in the conductances dynamics. Frequently, the most suitable model is not clearly identified. The purpose of the model restricts the most opportune choices. A brief description of some of the most featured reduced spiking neuron models is presented next.

FitzHugh-Nagumo

The FitzHugh-Nagumo model (FitzHugh, 1961; Nagumo et al., 1962) is a two-dimensional simplification of the Hodgkin-Huxley model. The idea was to qualitatively explain the excitability properties with an adapted van der Pol model. This set up was called Bonhoeffer-van der Pol model by FitzHugh, because its dynamics qualitatively resembles Bonhoeffer's theoretical model for the iron wire model of nerve (Bonhoeffer, 1948).

The model contains one equation that has a cubic nonlinearity, and another equation that is linear and describes a slower recovery variable:

$$\frac{dv}{dt} = a + bv + cv^2 + dv^3 - u \; ; \tag{2.15}$$

$$\frac{du}{dt} = \varepsilon(ev - u) \; . \tag{2.16}$$

Hindmarsh-Rose

The Hindmarsh-Rose model (Hindmarsh and Rose, 1984; Rose and Hindmarsh, 1989) is a three dimensional model:

$$\frac{dv}{dt} = u - F(v) + I - w \; ; \tag{2.17}$$

$$\frac{du}{dt} = G(v) - u \; ; \tag{2.18}$$

$$\frac{dw}{dt} = \frac{H(v) - w}{\tau} \; . \tag{2.19}$$

It can reproduce most neuronal behaviors depending on the choice of the functions $F(v)$, $G(v)$ and $H(v)$. In several cases, though, it is not straightforward to find the suitable set of functions (Izhikevich, 2004).

Izhikevich

A simple model that reproduces many computational features of spiking neurons was proposed by Izhikevich (2003):

$$\begin{aligned} \frac{dv}{dt} &= 0.04v^2 + 5v + 140 - u + I \; ; \\ \frac{du}{dt} &= a(bv - u) \; . \end{aligned} \tag{2.20}$$

v and u respectively represent the membrane potential and a membrane recovery variable. Additionally, there is a reset after each spike if $v \geq 30\, mV$: v is thereby reset to c; and u, to $u + d$.

This model is appropriated for simulations when diversity of neuronal activity plays a role, or different types of spiking modes coexists.

Integrate-and-fire (I&F)

This was perhaps the first neuronal model developed. It has been widely used ever since. The model, which is also known as leak integrate and fire, is very simple and intuitive. It allows fast simulations and analytical treatment. The dynamics is determined by a single equation describing the membrane potential:

$$\frac{dv}{dt} = a - bv + I \; ; \tag{2.21}$$

with an additional reset after each spike: if $v \geq v_{threshold}$, then v is reset to a constant value c. a and b are constants and I the applied current.

Integrate-and-fire with adaptation

By adding an extra equation to the integrate and fire model, more sophisticated features can be reproduced. The integrate-and-fire model with adaptation can be written as (Izhikevich, 2004):

$$\begin{aligned} \frac{dv}{dt} &= a - bv + g(d - v)I \; ; \\ \frac{dg}{dt} &= \frac{e - \delta(t) - g}{\tau} \; . \end{aligned} \tag{2.22}$$

v and g represent the membrane potential and slow recovery variable, respectively. a, b, d and e are constants; tau is a time constant; I, an applied current; and δ stands for Dirac delta function. This constitutes an option for a simple and intuitive model that present spike-frequency adaptation.

Integrate-and-fire-or-burst

Alternatively, one might be more interested in the coexistence of bursting and tonic spiking modes. For this purpose, the integrate-and-fire-or-burst can be an appropriated choice. The model also requires two equations (Smith et al., 2000; Izhikevich, 2004):

$$\frac{dv}{dt} = a - bv + gH(v - v_h)h(v_T - v) + I \; ; \tag{2.23}$$

with an additional reset after each spike: if $v \geq v_{threshold}$, then v is reset to c.

$$\frac{dh}{dt} = \begin{cases} -h/\tau^- \; , & \text{if} \quad v > v_h \; ; \\ (1-h)/\tau^+ \; , & \text{if} \quad v < v_h \; ; \end{cases}$$

where v represents the membrane potential, and h describes the inactivation calcium T-current with parameters g, v_h, v_T, τ^-, τ^+. H stands for the Heaviside step function.

Quadratic integrate-and-fire

The quadratic integrate and fire is a simple and canonical model, whose dynamics is described by a single variable:

$$\frac{dv}{dt} = a(v - v_{rest})(v - v_{threshold}) + I \; ; \tag{2.24}$$

with an additional reset after each spike: if $v \geq v_{peak}$, then v is reset to v_{reset}. In the trigonometric form, the model is also known as theta-neuron (Ermentrout and Kopell, 1986; Ermentrout, 1996). v represents the membrane potential a, v_rest and $v_threshold$ are constants and I is an applied current.

2.2.3 A comparative view of the most influential models of spiking neuron.

The number of models is increasingly large, and the competition between them can be quite fierce. Relevant inquiries in this regard include: What is the best model?; or which model to choose? A recent paper by Izhikevich (2004) tried to answer this question for spiking neurons.

The results, according to his evaluation, can be roughly summarized in a single plot, see Fig. 2.2. The criteria Izhikevich chose to quantify the plausibility of a model is controversial. The measure relies on the computational cost of the model, as well as the number of neuro-computational features reproducible by each model. In the top panel of Fig. 2.2, the x axis represents the number of computational steps to simulate the model for a period of 1 millisecond, which can be estimated with sufficient precision. However, the quantity measured by the y axis is subjective, and thereby the quantitative value is rather arbitrary. It is challenging to define a fair measure because presumably each feature should have a weight to separate the major from the minor functions. On top of that, the importance of a function is not steady, but it is highly dependent on the dynamical behavior of interest.

The biophysical models occupy the right edge positions because the computational effort is heaviest in these cases. This can be limiting, especially when the goal consists in simulating a large number of interacting units. The simplest models, on the left edge, are typically used to overcome such computational limitations. Furthermore, even the simplest model frequently suffices for the suggested purposes. It is not coincidently that, in our results, we have used only the extremal models for spiking neurons: HH (biophysically realistic), I&F (simple), and Izhikevich (flexible).

2.3 Neuronal populations of spiking neurons

It is important to understand and to acquire intuition on the behavior of single neurons. Neurons are considered building blocks of the nervous system, and the communication between two independent units occurs at the neuronal level. The neuronal activity is the basic dynamical element that ensures brain functioning.

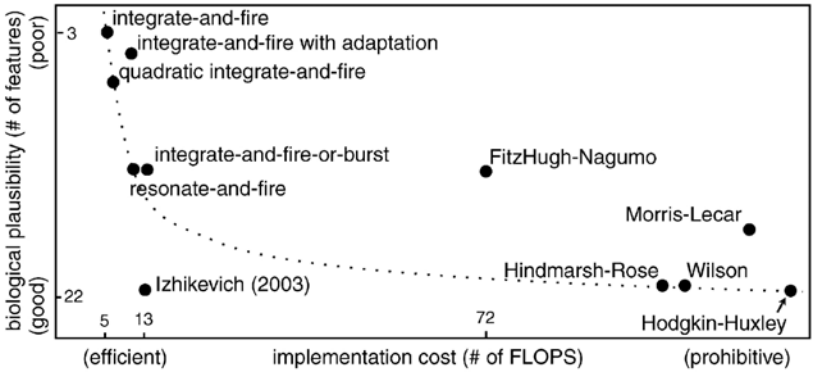

Models	biophysically meaningful	tonic spiking	phasic spiking	tonic bursting	phasic bursting	mixed mode	spike frequency adaptation	class 1 excitable	class 2 excitable	spike latency	subthreshold oscillations	resonator	integrator	rebound spike	rebound burst	threshold variability	bistability	DAP	accommodation	inhibition-induced spiking	inhibition-induced bursting	chaos	# of FLOPS
integrate-and-fire	-	+	-	-	-	-	-	+	-	-	-	-	+	-	-	-	-	-	-	-	-	-	5
integrate-and-fire with adapt.	-	+	-	-	-	-	+	+	-	-	-	-	+	-	-	-	-	+	-	-	-	-	10
integrate-and-fire-or-burst	-	+	+		+	-	+	+	-	-	-	-	+	+	+	-	+	+	-	-	-		13
resonate-and-fire	-	+	+	-	-	-	-	+	+	-	+	+	+	+	-	-	+	+	+	-	-	+	10
quadratic integrate-and-fire	-	+	-	-	-	-	-	+	-	+	-	-	+	-	-	+	+	-	-	-	-	-	7
Izhikevich (2003)	-	+	+	+	+	+	+	+	+	+	+	+	+	+	+	+	+	+	+	+	+	+	13
FitzHugh-Nagumo	-	+	+	-		-	-	+	-	+	+	+	-	+	-	+	+	-	+	+	-	-	72
Hindmarsh-Rose	-	+	+	+			+	+	+	+	+	+	+	+	+	+	+	+	+		+		120
Morris-Lecar	+	+	+	-		-	-	+	+	+	+	+	+		+	+	-	+	+	-	-		600
Wilson	-	+	+	+			+	+	+	+	+	+	+	+	+		+	+					180
Hodgkin-Huxley	+	+	+	+			+	+	+	+	+	+	+	+	+	+	+	+	+		+		1200

Figure 2.2: Comparing models of spiking neurons. Figure adapted from Izhikevich (2004).

Most of the information processing underlying brain functions, however, is thought to be carried out by a relatively large ensemble of neurons (Deco et al., 2008). Interesting behavior emerge from the collective behavior of numerous non-linear units (neurons): the whole system becomes more than

the sum of its parts (Anderson, 1972). Moreover, the collective behavior of a network of neurons can substantially overcome the behavior of a single neuronal unit [recent examples include Gollo et al. (2012b); Vasilkov and Tikidji-Hamburyan (2012)]. Thus, it seems unquestionable the need to elucidate the neuronal dynamics at the level of neuronal populations.

The straightforward route to assess the behavior of neuronal populations is to study the dynamics of large groups of spiking neurons. This approach is described in the following sections.

2.3.1 Building a network of excitatory and inhibitory spiking neurons

Once the cortical network gets mapped, and the columns get well characterized, it will be essential to understand the differences and the similarities of the dynamics in such networks compared with the recurrent networks. Meanwhile, invoking our ignorance (or our lack of knowledge) about the structure, we study recurrent networks because they are simple, and at the same time they are specially designed to fulfill a given function. In fact, the networks do not represent a specific structure; they are just random.

Most of the networks of spiking neurons involve both excitatory and inhibitory neurons. Typically, there are a series of standard methods that are observed in order to construct a neuronal network.

Dale's principle. A latter element of the neuron doctrine is the Dale's principle (Dale, 1934). This law, based on pharmacological evidences, states that the presynaptic contacts the neuron has release the same set of neurotransmitters. As a consequence, neurons can be classified in either excitatory or inhibitory: Excitatory (inhibitory) neurons cause excitatory (inhibitory) post-synaptic potentials. Although the functional implications of the Dale's principle to the network dynamics probably remain obscure, the principle is customarily taken into account in simulations of neuronal networks.

Balancement. Another indispensable element to take into account is the balancement of the amount of excitatory and inhibitory stimulus each neuron receive from the network. Excitatory neurons usually outnumber inhibitory ones, and neurons might receive much more excitation than inhi-

bition. Some aspects can be taken into account to equilibrate a network, such that, in average, neurons receive the same amount of excitation and inhibition, maintaining the same connectivity. The magnitude of the efficacy of the inhibitory synapse is often considered greater than the efficacy of the excitatory synapse. Alternatively, a larger firing rate of the inhibitory neurons can also compensate their minority. Unlike the dale's principle, the functional implications of the balancement are clearer understood (Brunel, 2000). The balancement of the network might strongly affects the dynamics. In a network of integrate and fire neurons, for example, the balancement is a control parameter that governs the synchronous state of the network.

2.3.2 Building modular structures

The segregation principle of organization of the brain is also represented by the cortex. Various modules are defined by the anatomical connectivity and observed by the dynamical activity of the brain (Hagmann et al., 2008). In fact, it is not clear weather there are intrinsic biophysical aspects that characterize each cortical module, or if they end up having different functions because of their connectivity and their position in the network (Wyss et al., 2006).

It is thus frequently desired to include modular features in the neuronal network. In such models, not only the behavior of the whole network is relevant, but also special attention is usually given to each module. The comparison of the dynamics of those modules can illuminate certain features of the dynamics, like the synchronization.

To model this specific modular aspect of the brain, recurrent networks can be joined together to give rise to a network comprised of modules. We indicate a set of remarks that might be useful to obtain modular networks mimicking reduced pieces of the brain.

Connectivity and delay. In general, most of the connections of a cortical neuron come from nearby neurons. The remainder connections come from separated neurons, and a few of those might come from quite distant neurons. High clustering and short path length have been observed from the cellular to the large-scale level (Sporns, 2010). This is the well-known

small-world property of the cortex, which promote economy and efficiency in brain networks.

On top of that, despite of the large connectivity, the number of neurons is so large that the network is astonishingly sparse. To reproduce such sparseness is a limitation because it requires an immense number of neurons. The typical workaround for this issue is to simulate a reduced network that only resembles the sparse connectivity.

Considering the small-world modular structure, and the sparse properties, it is possible to mimic reduced pieces of the brain. The local connectivity inside a module is assumed sparse. Furthermore, the connectivity among modules is assumed even sparser.

Another key element associated with the connectivity (via chemical synapse) is the delay. There are several dynamical processes that contribute to the synaptic delay. The prime contribution in most cases, especially for long-range connections, is designated to the axonal conduction latency time. Therefore, long-range connections (between different modules) are considered to have expressive delay. Intra-modular connections are considered to have significantly less delay, which are sometimes even assumed to be negligible.

2.3.3 Modeling meso- and large-scale brain dynamics with populations of spiking neurons

A large-scale network of spiking neurons necessarily requires numerous parameters. All of them must be adjusted in order to simulate the desired dynamics. The tuning of at least some parameters usually relies on an iterative process to set their values. The values of these parameters, in turn, depend on some aspects of the simulation results. Finding a fine set of parameters might take several attempts until all constrains get satisfied, especially when the parameters are strongly correlated (i.e., far from being independent). In order to simulate populations of spiking neurons, this is definitely the most routine obstacle to defeat. In this journey, short simulation time and few parameters to adjust are inevitably beneficial. It is thus crucial to reduce the number of free parameters and to choose simple models, which give rise to fast simulation times.

We have modeled meso-scale dynamics (motifs of neuronal populations) utilizing the integrate-and-fire model (chapters 4 and 5), and the Izhikevich model (chapters 6 and 7) for the spiking neurons. The integrate and fire model is very simple and fast, and the Izhikevich model is relatively fast and can reproduce different aspects of the neuronal dynamics.

Many works are restricted to study the dynamics of meso-scale models, say a unique neuronal population (Brunel, 2000; Izhikevich et al., 2004; Izhikevich, 2006), or motifs of neuronal populations (Chawla et al., 2001; Vicente et al., 2008b; Gollo et al., 2010, 2011). Others, however, go beyond the motifs of populations and attempt to simulate the entire cortex (Zhou et al., 2006; Zemanová et al., 2006; Zhou et al., 2007; Izhikevich and Edelman, 2008).

In Comparison with experiments, simulations have the benefit of being able to keep track of every single variable at any instant of time. However, the dimensionality of such system can be barely innumerable. Therefore, the investigation of only a small set of parameters (out of several) turns out to be feasible. The large complexity hampers a deep understanding of the system. To circumvent this limitation, there are several methods of reducing the dimensionality of the system.

2.4 Reduced meso- and large-scale models

There are several ways to reduce the degrees of freedom of a neuronal population. Firing-rate models are a prominent example (Wilson and Cowan, 1972, 1973). Instead of simulating the neuronal dynamics, or the dynamics of the time-dependent conductances, it concentrates on processes that occur at a slower time scale. Instead of actions potentials, which require short time scale, the output of each neuron-like unit simply consists of firing rates. Firing-rate models have comparatively few parameters, and are easier and faster to simulate than spiking neurons. Moreover, firing-rate models also provide insights via analytical calculations. However, crucially for our purpose, a firing-rate model fails when the presynaptic neurons are synchronous or highly correlated (Dayan and Abbott, 2001).

As recently showed by Deco et al. (2008), some alternative methods to reduce the degrees of freedom from a myriad to only few can be obtained by the

description of the probabilistic evolution of the distribution function. In particular, the probability distribution function can be represented by a set of scalars that parameterize it. This reduction gives rise to the neural mass models. An example of such model is discussed in chapter 7.

Reduced models have been successfully used to model and to elucidate meso- and large-scale brain activity (Breakspear and Stam, 2005; Zhou et al., 2007; Honey et al., 2007; Sotero et al., 2007; Deco et al., 2008; Pons et al., 2010; Bojak et al., 2010; Ursino et al., 2010; Ponten et al., 2010; Deco et al., 2011).

Chapter 3

Spatio-Temporal Neurodynamics: Rhythms, Synchronization and Coding

The brain dynamics that comprises perception, cognition, and consciousness ultimately emerge from the outcome of a multitude of neurons connected to around tens of thousands of neighboring neurons. Conspicuously, the incalculable dimensionality of the system generates the impressively rich and flexible patterns of neuronal activity of all brain functions. Neuronal oscillations at cortical networks, which occur across spatial and temporal scales, represent a general feature in this process. They have proven to subserve to functionally relevant patterns that are associated with cognitive behavior (Buzsáki and Draguhn, 2004). This chapter discusses some of these patterns of neuronal activity that are considered to play an important role in the brain functioning.

We restrict our focus to the dynamics of an isolated neuron solely in the next section. The other sections elaborate on the collective behavior of numerous coupled units. Section 3.2 discusses the neural oscillations observed in considerably large groups of neurons. The dynamical relaying, an inspiring mechanism to promote zero-lag synchronization between distant elements, is concisely presented in the section 3.3. Finally, section 3.4 introduces the binding by synchrony. This proposal constitutes an influential hypothesis

that bridges the neural code to the synchronized activity of neurons, which is ubiquitously found in the nervous system.

3.1 Single neuron activity: Excitability and oscillations

Analogously to lasers, chemical reactions, ion channels, climate dynamics, and other dynamical systems, most neurons display excitable properties (Lindner et al., 2004). In the absence of stimulus they are typically at rest. In response to a sufficiently strong input (injected current, or post synaptic potentials) they fire, i.e., generate an action potential. After such a spike, the neurons require a recovery time to fire again. Figure 3.1 exemplifies the response of a canonical excitable element to different kinds of input.

Neurons are non-linear elements that may exhibit a rather rich behavior even when isolated. Besides excitability, neurons can exhibit oscillations, and can also be posed in a bi-stable regime, in which both excitable and oscillatory states coexist. Interestingly, an oscillatory neuron in the bistable regime might stop firing if it receives a pulse of current driving the trajectory inside an unstable periodic orbit (Rinzel and Ermentrout, 1998).

3.1.1 Neuronal classification depending on the response to a driving current

Probably the simplest way to induce oscillations in most neurons is by injecting a current. There are different types of neuronal response to such stimulus. Figure 3.2 illustrates the two principal classes of neuronal excitability that have been characterized since the seminal work of Hodgkin (1948):

Class I neurons show all-or-none action potentials, arbitrarily low oscillatory frequency, and long delay to firing of an action potential after a transient stimulus;

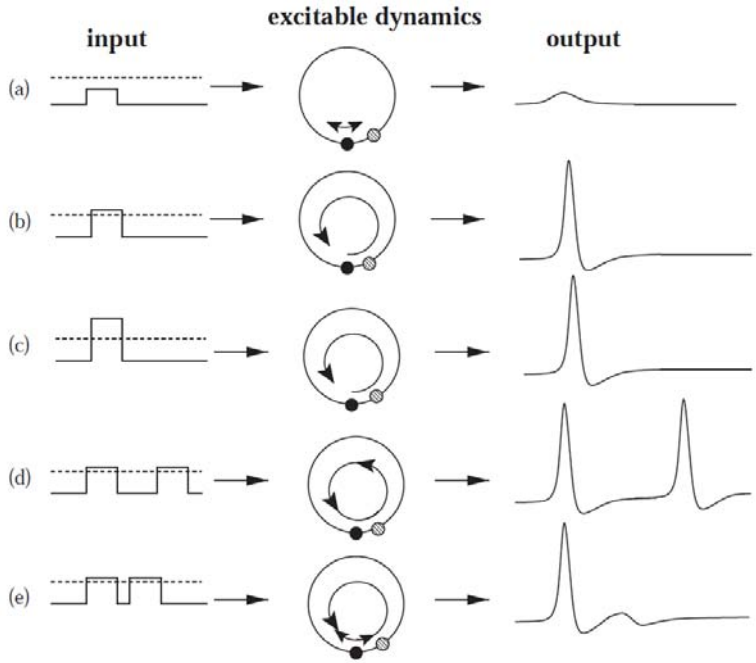

Figure 3.1: Responses of an excitable element to different kinds of input. Figure extracted from Lindner et al. (2004).

Class II neurons spike within a range of frequencies that precludes low rates, and evince short latencies to firing.

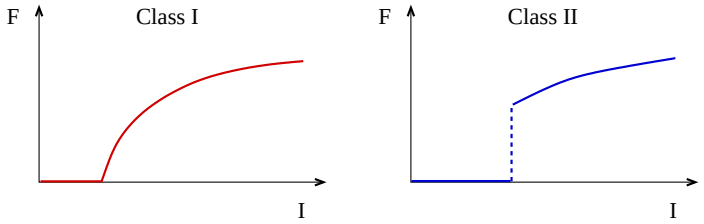

Figure 3.2: Neuronal firing rate as a function of the injected current.

The input-output function, which is given by the firing rate versus the injected current, of class I neurons is continuous. In contrast, the input-output function of class II neurons present an abrupt transition from rest to active firing. The minimal firing rate of class II neurons is relatively high, specially in comparison to class I neurons. Since the firing rate is a saturating function of the stimulus (it does not go to infinity), the firing rate dependence on the input of class II neurons is weaker than class I neurons.

Izhikevich (2007) suggests that class I neurons correspond to a snic (saddle-node on invariant circle) bifurcation, whereas class II neurons correspond to a saddle-node (off invariant circle) or a Hopf bifurcation. Such proposal considers the restriction to codimension-1 bifurcations of equilibrium, which depend on a single parameter (injected current). Naturally, the resting state can also lose stability or disappear by higher codimension bifurcations, eventually leading to counterintuitive behaviors.

3.2 Rhythmogenesis, neural synchrony and complexity

Synchronous rhythms sculpt the temporal coordination of brain activity. The rhythmic neuronal activity is associated with cognitive behaviors, and with a healthy brain functioning. In turn, dysfunctions in synchronization patterns are associated with some mental disorders.

It is fundamental to elucidate the mechanisms involved in such neuronal oscillations. The synchronous activity of oscillating networks is considered to be a fundamental link between events taking place at different spatial scales: the activity of single neurons at the micro scale, and the brain representations at the large scale (Buzsáki and Draguhn, 2004). Beyond the activity of single neurons previously described, an ensemble of coupled excitable neurons can also generate oscillatory activity in a spatially localized brain region. Within a larger scale, even rather distant oscillatory ensembles sparsely connected between one another can also coordinate their activity. The mutual relationship among the ensembles have been proposed to generate fast, complex and flexible patterns of neuronal activity that are required for the multiple brain states associated with cognition (Fries, 2005).

The long-range connections between distant ensembles typically involve a representative delay that crucially shapes the dynamics and should not be dismissed. The dynamics of delayed coupled neuronal regions shows complex behavior even for rather simple architectures due to frustration. A frustrated system could provide the substrate for flexible evolving patterns of oscillatory activity, and the coexistence of numerous metastable states.

3.2.1 Oscillatory brain activity associated with cognitive behaviors

The brain oscillations cover frequencies of about four orders of magnitude: ranging from approximately 0.05 to 500 Hz (Buzsáki and Draguhn, 2004). Within such a huge range, several bands have been characterized. Some of them are remarkably important for behavioral tasks (Buzsáki, 2006; Wang, 2010).

Nearby frequency bands compete with each other, and typically correspond to distinct functional modes (Buzsáki and Draguhn, 2004). Fast rhythms tend to exhibit a more localized neuronal representation than slow rhythms. Low frequencies present in each cycle a larger time period to recruit neurons, Thereby, such longer recruitment embraces more widespread neuronal portions. Different bands might work as parallel *independent* channels. However, the different frequency bands might also be correlated, as, for example, the remarkable interplay between the theta and the gamma bands (Lisman and Buzsáki, 2008).

Historically, the first rhythm to be described was the alpha (Bremer, 1958). This oscillatory band (from 8 to 12 Hz) is prominent in the wake-relaxed state. A variety of further brain rhythms have been classified across behavioral states (Wang, 2010):

Slow (<1 Hz) oscillations correspond to the transitions between up and down states (Steriade et al., 1993). Such oscillations occur during slow wave sleep and might play a role in memory consolidation.

Delta (1-4 Hz) rhythm has been suggested to accompany sensory signal detection and decision making (Başar et al., 2001).

Theta (4-8 Hz) rhythm is related to working memory, formation and retrieval of episodic and spatial memory.

Beta (12-30 Hz) rhythm is associated with sensorimotor integration and top-down signaling, and with preparation of movement (inhibitory control in the motor system).

Gamma (30-80 Hz) rhythm is associated with attention and integration of sensory information.

Ultrafast (>100 Hz) oscillations appear during anesthesia, behavioral immobility, and natural sleep. They might lead to the onset of seizures.

3.2.2 Oscillations as an emergent property of the network

Due to the universal collective behavior of interacting elements, even canonical networks of excitable units can generate oscillatory activity, e.g., Kinouchi and Copelli (2006). Generic cortical networks comprised of excitatory and inhibitory neurons, for example, can synchronize via diverse mechanisms involving chemical synapses (Wang, 2010): recurrent excitation, mutual interneuronal inhibition, and feed-back inhibition through the excitatory-inhibitory loop. Moreover, connections involving electrical synapses can also promote synchronization. Each of those mechanisms has its own characteristics, with commonalities and subtle differences among them. For a comprehensive and up-to-date review on the subject, please refer to Wang (2010).

3.2.3 Synchronization

Synchronization is an astonishing omnipresent collective phenomenon occurring at any known dimension, spanning from the subatomic to the astronomical scales. Synchronization requires the coordination of systems to operate at unison. Synchronized activities have been observed in the brain between neurons, between heart cells, in coupled lasers, in fireflies and in many other natural and man-made systems (Strogatz, 2003; Pikovsky et al., 2002).

Owing to such a great universality, one might consider that it is not surprising that synchronization also encompasses neuronal systems. Such that this temporal coordination could be just an epiphenomenon: merely an unavoidable side effect resulting from the coupling of multitudinous excitable units. However, growing evidence suggests that the brain developed (say

throughout evolution) to functionally benefit from neuronal synchronization. Synchronized groups of neurons, for example, are more effective than asynchronous groups to transmit a message via sparse long-distance connections. Exploring the time domain, this mechanism could operate as an alternative neural code that is simultaneously fast, and flexible (Singer, 1999).

Neuronal synchronization arises across spatial scales, from pairs of neurons to long-distance regions (Singer, 1999), which might even be in distinct cortical hemispheres (Mima et al., 2001). Synchronization by neural oscillations contributes to the formation of functional circuits at different spatial scales through a broad range of frequencies (Wang et al., 2010a; Kahana et al., 2001; Kahana, 2006; Buzsáki, 2002, 2006; Buzsáki and Draguhn, 2004). Specific patterns of neural synchronization have been largely associated with perceptual, motor skills, and higher cognitive functions, providing insights into how large-scale integration can be assisted by oscillatory codes in the mammalian brain (Varela et al., 2001; Cantero and Atienza, 2005; Womelsdorf and Fries, 2007; Uhlhaas et al., 2009; Crespo-Garcia et al., 2010; Gutierrez et al., 2010). The phase relationship of synchronized elements has been further suggested as a critical mechanism for the efficiency of such information exchange between neurons located in distant brain regions (Fries, 2005; Womelsdorf et al., 2007).

Delay

The presence of delayed interactions has been shown to play a critical role in dynamical systems (Niebur et al., 1991; Ernst et al., 1995; Ramana Reddy et al., 1998; Yeung and Strogatz, 1999; Atay, 2003; Atay et al., 2004; Sethia et al., 2008; D'Huys et al., 2008). Particularly for neuronal systems, non-negligible delays, which play an important role in long-distance connections, have been argued to shape spatiotemporal dynamics (Roxin et al., 2005) and to facilitate synchronization (Dhamala et al., 2004; Wang et al., 2008, 2009, 2011).

The presence of delay largely increases the dimensionality of the system, giving rise to a rich dynamical repertoire, as well as a possibly copious complexity. Accordingly, after extensive theoretical and experimental works, the effects of the delay in the system are not yet fully understood. There are examples of remarkable cutting edge exceptions in which the complexity of

delayed systems can be exploited for non-trivial computations (Appeltant et al., 2011). However, our first aim is to illustrate the order that emerges out of an infinite dimensional system described by complicated non-linear equations. A case, which is particularly suitable to illustrate this spontaneous organization, is the well known tendency of delayed-coupled oscillators to synchronize in anti-phase.

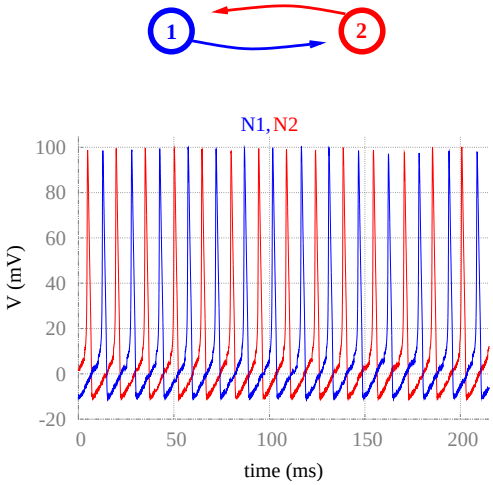

Figure 3.3: Anti-phase synchronization between two Hodgkin-Huxley neurons mutually connected with delay (6 ms). Details and parameters of the model are presented in chapter 7.

Figure 3.3 illustrates this tendency of anti-phase synchronization for a pair of delayed-connected Hodgkin-Huxley neurons in the oscillatory regime. The system is not deterministic because the neurons are driven by a Poisson process (to mimic the synaptic behavior). Nevertheless, the anti-phase synchronization is not disturbed, which highlights the robustness of this natural preference of the system.

3.2.4 Complexity and frustration

Cooperative behaviors have been proposed as a common thread between complex systems: Cooperation allows multiple and complex patterns to emerge from rather simple and local rules. However, a more universal

view of complexity, which comprises all sorts of complex systems (genetic algorithms, immune system, nervous system, protein folding, stock market, and others adaptive evolving systems), might require a unifying concept. Frustration has been proposed as a plausible unifying thread for complex systems that accomplish such generalization (Binder, 2008).

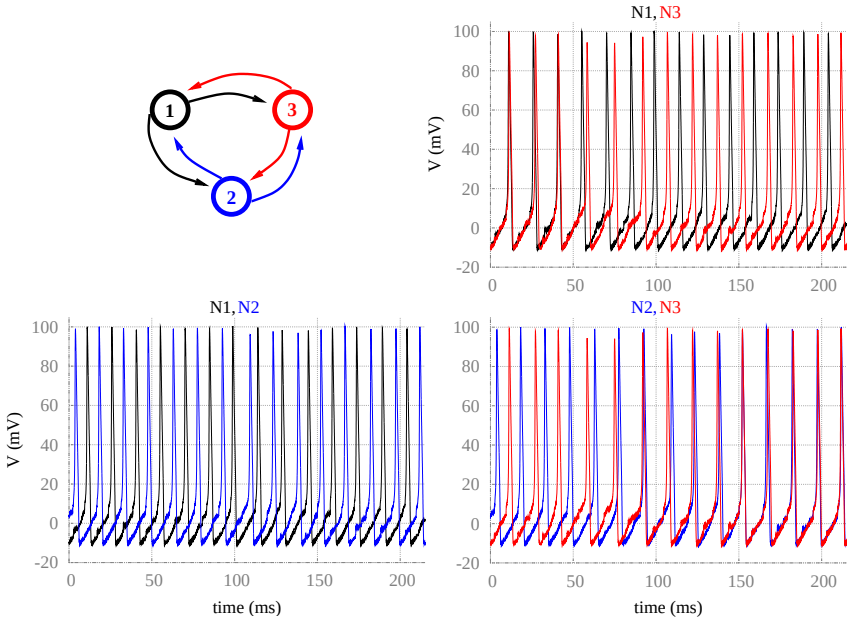

Figure 3.4: Example of frustration in a ring of three Hodgkin-Huxley neurons mutually coupled with delay (6 ms). The anti-phase synchronization between neighbor neurons cannot be satisfied simultaneously for all neighbor pairs. Details and parameters of the model are presented in chapter 7.

Frustrated systems show competing interactions that prevent all elements to satisfy their demands simultaneously: a piece of the system always remains against its natural tendency. The complexity of frustrated systems typically generates numerous metastable states without unbound grow. The concept of frustration was firstly developed by geometrical configurations that lack a unique minimal-energy state (Anderson, 1956; Toulouse, 1977; Villain, 1977; Vannimenus and Toulouse, 1977; Greedan, 2001). Nevertheless, this con-

cept can be largely extended to acquire a comprehensive formulation. For example, some kind of frustration is conspicuous in the presence of opposing tendencies among elements of microscopic and macroscopic scales, and could represent virtually all sorts of complex systems (Binder, 2008).

For us, an important and straightforward example is given by three all-to-all delayed-coupled elements. Figure 3.4 depicts a trial in which neurons 1 and 2 reasonably succeed to maintain their preferred dynamical relation (i.e., synchronized in anti-phase). However, neurons 1 and 3 start isochronously synchronized, and then switch to the anti-phase relation. In turn, neurons 2 and 3 start anti-phase synchronized, and then switch to the isochronous relation. The system lacks a fully stable relation between the three neurons. This is a rather simple geometry that can give rise to a rich dynamics due to frustration. This geometry has instigated several works, including for example D'Huys et al. (2011), who studied the role of the delay to shape the dynamics, or Aihara et al. (2011) who studied other biological systems composed of three *Hyla japonica* frogs in which delay can presumably be dismissed.

3.3 Dynamical relaying

The dynamical relaying is a mechanism to achieve isochronous synchronization between two delay-coupled oscillators. It has a general nature that allows zero-lag synchronization in a large variety of systems: oscillators, excitable systems, and maps. A prototypical motif of the dynamical relaying, for example, can be obtained from the scheme shown in Fig. 3.4 by removing the connections between neurons 1 and 3. In this case, the frustration of the system vanishes. Indeed, as shown in Fig. 3.5, the zero-lag solution appears even in the presence of stochastic inputs. The nearest neighbor neurons (1 and 2, or 2 and 3) show anti-phase synchrony, whereas the outer neurons (1 and 3) show zero-lag synchrony.

Furthermore, the dynamical relaying is not restricted to periodic systems. In fact, the dynamical relaying was originally formulated for a system of chaotic laser diodes bidirectionally coupled (see Fig. 3.6), and also additionally extended to other nonlinear systems such as neuronal elements satisfying the same coupling architecture (Fig. 3.7). A further generalization

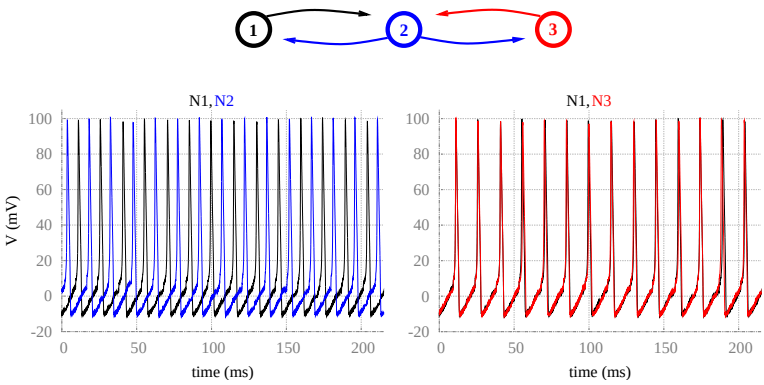

Figure 3.5: Example of dynamical relaying in a chain of three Hodgkin-Huxley neurons mutually coupled with delay (6 ms). The outer neurons synchronize isochronously, whereas neighbor neurons synchronize in anti phase. Details and parameters of the model are presented in chapter 7.

of this simple motif of neurons to motifs of neuronal populations was the first motivation for the original research of this manuscript.

In laser systems [solid-state and semiconductor lasers (Winful and Rahman, 1990; Terry et al., 1999)], investigations over three instantaneously coupled elements showed an intriguing behavior in which the first and the third lasers in the chain synchronized their activity. This motivated a deeper study in similar systems coupled with delay. Surprisingly, this configuration appeared to support the same isochronous activity (Fischer et al., 2006; Vicente, 2006). This first result was obtained experimentally and numerically in delay-coupled systems of semiconductor lasers. Figure 3.6 shows the experimental setup, time traces, and cross-correlations between pair of lasers. Delay, in coupled semiconductor lasers, occurs for short separation distance due to the fast internal time scale involved in such lasers. Moreover, Fischer et al. (2006) also showed analogous synchronization patterns in systems of bursting Hodgkin-Huxley thermoreceptor neurons, depicting an appreciable generality (Fig. 3.7).

The phenomenon engendered much interest both theoretically and experimentally. Thus, the dynamical relaying was subsequently deeper studied in a plethora of systems:

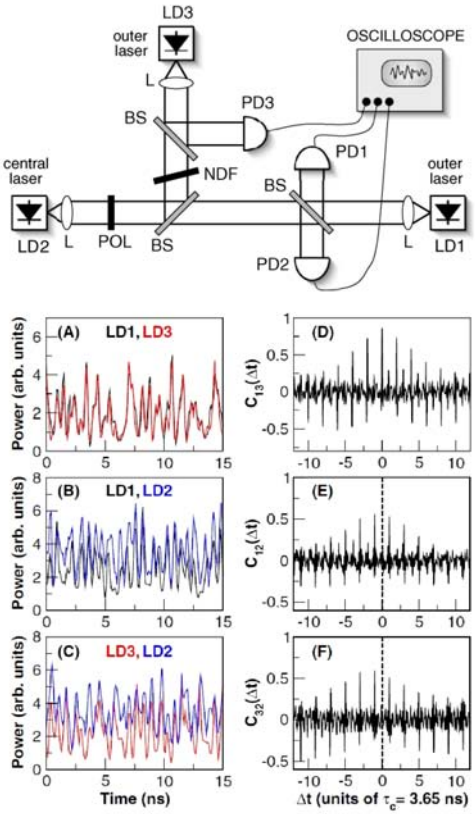

Figure 3.6: Dynamical relaying. (top panel): Experimental setup; (bottom panels): dynamics of a system of laser diodes (LD). Other abbreviations are polarizer (POL), aspheric lens (L), beam splitter (BS), photodetector (PD), neutral density filter (NDF), and C_{ij} corresponds to the correlation function between nodes i and j. The time series of the central laser is shifted τ_c. Figure panels extracted from Fischer et al. (2006).

- Semiconductor lasers (Vicente et al., 2006; Vicente, 2006; Landsman and Schwartz, 2007; Peil et al., 2007; Vicente et al., 2008a; Tiana-Alsina et al., 2012);

- Electronic circuits (Gomes et al., 2006; Wagemakers et al., 2007);
- Ikeda oscillators (Zhou and Roy, 2007);
- Josephson junctions (Chitra and Kuriakose, 2007);
- Mackey-Glass systems (Banerjee et al., 2012);
- Spatiotemporal chaotic systems (Jian-Ping et al., 2012);
- Coupled quadratic maps, Kuramoto, and Rösler oscillators (de Sousa Vieira, 2010);
- Diverse neuronal systems (Vicente et al., 2007, 2008b; Gollo et al., 2010, 2011).

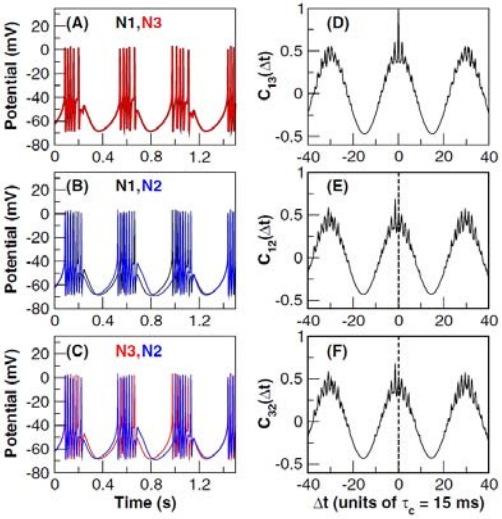

Figure 3.7: Dynamical relaying in a chain of three Hodgkin-Huxley neurons in the bursting mode. Figure extracted from Fischer et al. (2006).

3.3.1 Appraising the results in the dynamical-relaying framework.

Based on the dynamical-relaying mechanism, the results of this entire thesis can be elucidated. In fact, a shorter alternative title for this thesis could be: Dynamical relaying in neuronal systems. To begin with, the order of the result chapters reflects the chronological order in which the research projects were developed.

First (in chapter 4) we show that the dynamical relaying is not only consistent and robust in motifs of neurons but can be generalized to motifs of neuronal populations. This generalization represents the first step aiming to check whether the dynamical relaying could indeed play a functional role in the synchronization of large neuronal systems.

Our next endeavor (chapter 5) considers the thalamus as the relay center. Thalamocortical loops have been largely studied, and the thalamus has been identified as the strongest candidate to mediate cortical synchronization. The thalamus is the gateway for most sensory stimuli to reach the cortex. Such attribute, as suggested by our model, naturally endows the thalamus with the conditions to control and to coordinate cortical synchronization.

Ascribed to the previously satisfactory results, we acquired confidence to seek experimental evidence for the dynamical relaying. The data involved a dissimilar relay element: the hippocampus, which shows dominant oscillatory activity in the theta band. We thus show that the dynamical relaying is robust to these fine details of the dynamics, and that the phase relation between the areas obeys the pattern expected by the dynamical relaying. Even neglecting numerous interactions with other brain regions, the model accomplished to reproduce the data. This suggests a remarkable influence of the dynamical relaying in sculpting the large-scale brain dynamics.

Finally, we attempt to understand the fundamental lurking interactions that underpin the dynamical relaying. We find that a chain of bidirectionally-coupled nodes is not the minimal structure to promote zero-lag synchronization, but the common driving of a node which must be under the influence of a pair of anti-phase synchronized nodes. The effects of this pair induce the isochronous synchronization of the driven nodes. Thereby, we name this effect: Resonance-induced synchronization.

3.4 Binding by synchrony

The brain performs a myriad of parallel operations without the influence of a coordinating center. The binding by synchrony proposes that the synchronization of neuronal activity functions as a coordinating mechanism: to select and route signals, and, more importantly, to bind together simultaneous computations from spatially segregated regions, and to generate coherent percepts and actions (Singer, 2007). This proposal exploits the time domain for coding, which has advantages over the rate code, in particular, it allows a much faster processing speed. The binding-by-synchrony hypothesis was theoretically formulated by Milner (1974); Grossberg (1976); von der Malsburg (1981), and a few years latter the first experiments were accomplished to support the potential role of zero time-lag synchronization to code (Roelfsema et al., 1997; Varela et al., 2001; Singer, 2007).

Numerous experimental evidences have been gathered along the years, see for example the review by Uhlhaas et al. (2009). Moreover, owing to such potentially strong relation with the neural code, the binding by synchrony spurred numerous groups attempting to elucidate the phenomenon. It is particular important to generate, to sustain, and to control the synchronous oscillatory activity of the cerebral cortex. The next chapter sheds light in this topic by proposing the dynamical relaying as an overwhelming candidate mechanism to promote zero-lag synchronization among distant cortical populations of neurons.

Part II

Results

Chapter 4

Dynamical Relaying: A Robust Mechanism to Promote Zero-Lag Long-Range Cortical Synchronization

The development of multi-electrode recordings was a major breakthrough in the history of systems neuroscience (Nicolelis and Ribeiro, 2002). The simultaneous monitoring of the extracellular electrical activity of several neurons provided a solid experimental basis for electrophysiologists to test the emergence of neuronal assemblies (Singer et al., 1997). Specifically, the parallel registration of spike events resulting from different cells permitted the evaluation of temporal relationships among their trains of action potentials, an eventual signature of assembly organization. Modern multi-electrode techniques have now the capacity to simultaneously listen to a few hundreds of cells and, in contrast to serial single cell recordings, to reveal temporally coordinated firing among different neurons that is not linked

This Chapter is based on the paper: Vicente R, Gollo LL, Mirasso CR, Fischer I, Pipa G (2008) Dynamical relaying can yield zero time lag neuronal synchrony despite long conduction delays. Proc. Natl. Acad. Sci. 105: 17157–17162; and the book chapter: Vicente R, Gollo LL, Mirasso CR, Fischer I, Pipa G (2009) Far in space and yet in synchrony: neuronal mechanisms for zero-lag long-range synchronization. Coherent Behavior in Neuronal Networks. Springer Series in Computational Neuroscience 3: 143–167

to any external stimulus but rather to internal neuronal interactions. Only equipped with such class of technology it was possible to unveil one of the most interesting scenarios of structured timing among neurons, namely the consistent and precise simultaneous firing of several nerve cells, a process referred to as neuronal synchrony (Singer, 1999).

Neuronal synchronization has been hypothesized to underly the emergence of cell assemblies and to provide an important mechanism for the large-scale integration of distributed brain activity (Singer, 1999; Varela et al., 2001). One of the basic ideas in the field is called the binding by synchrony theory which exploits the dimension that temporal domain offers for coding (Singer, 1999; Milner, 1974; von der Malsburg, 1981; Gray et al., 1989; Gray, 1999). Essentially, it states that synchrony can be instrumental for temporally bringing together the processing output of different areas, which are functionally specialized, in order to give rise to coherent percepts and behavior. The differential effect that synchronous versus temporally dispersed inputs can exert onto a downstream neuron indicates how the temporal coherence of a set of neurons can become a flexible and potentially information-carrying variable that can modulate subsequent stages of processing (Singer, 1999; Salinas and Sejnowski, 2000, 2001). Despite the ongoing debate about its functional role in neuronal processing, the last two decades have seen the accumulation of large amount of data. Such results show evidence, at least in a correlative manner, for a role of synchrony (and the customary oscillations accompanying it) in a variety of cognitive processes ranging from perceptual grouping or stimulus saliency to selective attention or working memory (Gray et al., 1989; Castelo-Branco et al., 2000; Fries et al., 1997, 2001; Sarnthein J, 1998).

Interestingly, neuronal synchrony is not restricted to the local environment, e.g., of a single cortical column or area. Rather, long-range synchrony across multiple brain regions, even across inter-hemispheric domains, has been reported in several species including the cat and primate cortex (Roelfsema et al., 1997; Rodriguez et al., 1999; Mima et al., 2001; Uhlhaas et al., 2006; Soteropoulus and Baker, 2006; Witham et al., 2007). However, the zero-lag correlated activity of remote neuronal populations seems to challenge a basic intuition. Namely, one tends to tacitly assume that since the interaction among distant systems is retarded by the conduction delays (and therefore, that it is the past dynamics of one system what is influencing the other one at present) it is not possible that such interaction alone can induce the isochronous covariation of the dynamics of two remote systems. Actually,

the latencies associated with conducting nerve impulses down axonal processes can amount to several tens of milliseconds for a typical long-range fiber in species with medium or large sized brains (Swadlow et al., 1978; Swadlow, 1985, 1994). These ranges of conduction delays are comparable with the time-scale in which neuronal processing unfolds and therefore they cannot be simply discarded without further justification. Furthermore, profound effects in the structure and dynamics of the nervous system might have arisen just as a consequence of the communication conditions imposed by the time delays (Miller, 2000; Wen and Chkolvskii, 2005). As an example, several proposals of the origin of the lateralization of brain functions are based on the temporal penalty to maintaining information transferring across both hemispheres (Ringo et al., 1994; Miller, 1996).

The aim of this chapter is to illustrate that certain neuronal circuitries can circumvent the phase-shifts associated with conduction delays and give rise to isochronous oscillations even for remote-located areas. The chapter begins with a brief review of some theories that have been proposed to sustain long-range synchrony in the nervous system. Then we explore a novel and simple mechanism that accounts for zero-lag neuronal synchronization for a wide range of conduction delays (Vicente et al., 2008b; Fischer et al., 2006; Vicente et al., 2007; D'Huys et al., 2008). For that purpose, we investigate the synchronizing properties of a specific network motif which is highly expressed in the thalamo-cortical loop and in the cortex itself (Jones, 2002; Shipp, 2003; Honey et al., 2007). Such circuitry consists of the relaying of two pools of neurons onto a third mediating population which indirectly connects them. We then present numerical results on the dynamics of this circuit with two classes of models: first using Hodgkin and Huxley (HH) type of cells and second building large-scale networks of Integrate and Fire (IF) neurons. Finally, and after a detailed characterization of the influence of long-conduction delays in the synchrony of this neural module, we discuss our results in the light of the current theories about coherent cortical interactions.

4.1

How can zero-lag long-range synchrony emerge despite of conduction delays?

Before discussing different mechanisms proposed to cope with the long-range synchrony problem, it is first necessary to understand the origin of the delay that arises in neuronal interactions. As a rule, it is possible to dissect the latency in the communication between two neurons via a prototypical axo-dendritic chemical synapse in distinct contributions. For illustration purposes here we follow the time excursion of an action potential generated in a presynaptic cell up to becoming a triggering source for a new spike in a postsynaptic cell.

- The first component is due to the propagation of an action potential from the axon hillock to the synaptic terminal. The limited axonal conduction velocity imposes a delay ranging from a few to tens of milliseconds depending on the caliber, myelination, internodal distance, length of the axonal process, and even the past history of impulse conduction along the axon (Swadlow, 1994; Soleng et al., 1998; Swadlow and Waxman, 1975).

- A second element of latency occurs due to the synaptic transmission. After the action potential has reached the presynaptic terminal several processes contribute, to different degrees, to the so-called synaptic delay. These include the exocytosis of neurotransmitters triggered by calcium influx, the diffusion of the transmitters across the synaptic cleft, and their binding to the postsynaptic specializations. Altogether the complete process from the release to the binding to specialized channels can typically span from 0.3 ms to even 4 ms (Katz and Miledi, 1965).

- Another source of delay is the rise time of the postsynaptic potential. Different ionic channels have different time-scales in producing a change in the membrane conductance which eventually induces the building-up of a significant potential. For fast ionotropic AMPA or $GABA_A$ receptors it can take a time of the order of half a millisecond for such a process to rise a postsynaptic potential (Shepherd, 1998).

- Dendritic propagation toward the soma by either passive or active conduction is also a source of a small lag whose value prevalently depends on the dendritic morphology.

- Finally, the postsynaptic neuron can exploit several mechanisms, such as membrane potential fluctuations, to control to some degree an intrinsic latency in triggering a new action potential (Volgushev et al., 1998).

For long-distance fibers the most important contribution of delay typically comes from the axonal conduction. In human, an averaged-sized callosal axon connecting the temporal lobes of both hemispheres is reported to accumulate a delay of 25 milliseconds (Ringo et al., 1994). This is certainly not a negligible quantity, specially when a precise temporal relations among neuron discharges plays a role.

Nevertheless, a fiber connecting two brain regions is inevitably composed of non-identical axons, which give rise to a broad spectrum of axonal delays rather than a single latency value (Ringo et al., 1994; Aboitiz et al., 1992). Reciprocally connected fibers constitute one of the possible substrates for the establishment long-range synchrony. Within this framework the combination of a hypothetical extensive network of very fast conducting axons with the phase resetting properties of some class of neurons could in principle sustain an almost zero-lag long-range synchrony process. GABAergic neurons have been suggested to meet the second requirement. Via a powerful perisomatic control this type of cells can exert a strong shunting and hyperpolarizing inhibition which can result in the resetting of oscillations at their target cells (Dickson et al., 2003; Rizzuto et al., 2003; Mann and Paulsen, 2007). Their critical role in generating several local rhythms has been well described (Whittington et al., 2001; Buzsáki, 2006). However, their implication in the establishment of long distance synchrony is heavily compromised because the expression of fast long-range projections by interneurons is more the exception than the rule (Mann and Paulsen, 2007; Buzsáki, 2006). Another important consideration is that long-range connections in a brain do not come for free. Even a small fraction of long-distance wiring can occupy a considerably portion of brain volume, an important factor that severely restricts the use of fast large-diameter fibers (Ringo et al., 1994; Buzsáki, 2006).

Electrical synapses, and in special gap junctions, have also been involved in explaining spread neuronal synchrony (Bennet, 2004). Gap junctions consist of clusters of specialized membrane channels that interconnect the intracellular media of two cells and mediate a direct electrical coupling and the transferring of small molecules between them (Caspar et al., 1977). Evidence for the role of gap junctions to give rise to fast rhythmic activity has been put forward by observations that fast oscillations can be generated in conditions where chemical synaptic transmission was blocked (Draghun et al., 1998). Gap junctions also present two clear advantages over chemical synapses for inducing zero-lag synchrony. First, they are not affected by synaptic delays since no neurotransmitters are involved. Second, the electrotonic coupling between cells mainly acts via diffusion mechanisms and therefore it tends to homogenize the membrane potential of the both cells. Thus, gap junctions can be considered of synchronizing nature rather than excitatory or inhibitory class (Bennet, 2004). However, as we have pointed out before, for long-distance fibers the axonal delay is the largest component of latency and the saving corresponding the elimination of the synaptic delay can just correspond to a small fraction of the total time. In any case, electrical synapses are believed to underly homogenization of firing among neurons and to foster synchrony in moderately distributed networks (Bennet, 2004; Traub et al., 2001; Kopell and Ermentrout, 2004).

Proposals for explaining the observed long-range synchronous fast dynamics in the cortex have also been inspired by the study of coupling distant oscillations. In this context Traub et al. (1996) investigated the effect of applying dual tetanic stimulation in hippocampal slices. This influential work showed that, in a slice preparation, a strong simultaneous tetanic stimulation at two distant sites induced synchronous oscillations in the gamma-band. The concomitant firing of spike doublets by some interneurons with such double stimulation condition plus modeling support, led the authors to infer that a causal relationship between the interneuron doublet and the establishment of long-range synchrony should hold (Traub et al., 1996; Bibbig et al., 2002).

From another perspective, it is important to recall that neuronal plasticity is a key element in determining the structural skeleton upon which dynamical states, such as synchrony, can be built. Therefore, the experience-driven process of shaping neuronal connectivity can considerably impact the ability and characteristics of synchronization of a given neuronal structure. Interestingly, this interaction can go in both directions and correlated input

activity can also influence the connectivity stabilization via certain plasticity processes (Lowel and Singer, 1992). Modeling studies have shown that spike-timing-dependent plasticity rules can stabilize synchronous gamma oscillations between distant cortical areas. This is achieved by reinforcing the connections whose delay matches the period of the oscillatory activity (Knoblauch and Sommer, 2003; Izhikevich, 2006).

In summary, there are a number of factors and mechanisms that have been put forward to explain certain aspects of the long-range synchronization of nerve cells. Synchronization is a process or tendency toward the establishment of a dynamical order with many possible participating sources, and as a result it is not strange that several mechanisms can simultaneously contribute or influence it. Thus, neural systems might use distinct strategies for the emergence of coherent activity at different levels depending on the spatial scale (local or long-range), dynamical origin (intra-cortical or subcortical oscillations), and physiological state (sleep or awake), among others. Nevertheless, one should notice that a significant long-range synchronization is observed across different species with different brain sizes and at different stages of the developmental growth of brain structures. This point strongly suggests that any robust mechanism for generating zero time-lag long-distance cortical synchrony maintains its functionality for a wide range of axonal lengths. While it is possible that developmental mechanisms compensate for the resulting delay variations (Swindale, 2003) it is still difficult to explain all the phenomenology of long-distance synchronization without a mechanism that inherently allows for zero-lag synchronization for a broad range of conduction delays and cell types. In the following parts of this chapter we focus our attention on a recently proposed scheme, named dynamical relaying, which might contribute to such mechanism (Vicente et al., 2008b; Fischer et al., 2006; Vicente et al., 2007; D'Huys et al., 2008).

4.2 Zero-lag long-range neuronal synchrony via dynamical relaying

In this section we explore a simple network module that naturally accounts for the zero-lag synchrony among two arbitrarily separated neuronal pop-

ulations. The basic idea, which we shall further develop later, is that when two neuronal populations relay their dynamics via a mediating population, a robust and self-organized zero-lag synchrony among the outer populations can be reached (Vicente et al., 2008b; Fischer et al., 2006; Vicente et al., 2007; D'Huys et al., 2008).

At this point it is important to recall the difference between processes generating local rhythms or oscillations in a brain structure from the mechanisms responsible for their mutual synchronization. The model and simulations that are presented below provide a proof of principle for a synchronizing mechanism among remote neuronal resources despite long axonal delays. In contrast to the results present in the two following chapters, no particular brain structure or physiological condition is intended to be faithfully reproduced in this chapter. The main objective is the demonstration that under quite general conditions an appropriate connectivity can circumvent the phase lags associated to conduction delays and induce a zero-lag long-range synchrony among remote neuronal populations. In any case, it is worth mentioning that the diffuse reciprocal connectivity, the dynamical consequences of which we study below, is characteristic of the interaction of the neocortex with several thalamic nuclei (Jones, 2002; Shipp, 2003). Connectivity studies in primate cortex have also identified the pattern of connections investigated here as the most frequently repeated network motif at the level of cortico-cortical connections (Honey et al., 2007; Sporns and Kotter, 2004; Sporns et al., 2004).

4.2.1 Illustration of dynamical relaying in a module of three Hodgkin and Huxley cells

The simplest configuration to illustrate the effects of dynamical relaying corresponds to the study of the activities of two neurons that interact by mutually relaying their dynamics via a third one. We start investigating a circuit composed of three HH cells with reciprocal delayed synaptic connections (see top panel in Fig. 4.1 for an schematic representation of the network architecture). We first consider a condition in which the isolated neurons already operate in an intrinsic spiking state and observe how the synaptic activity modifies the timing of their action potentials. To this end we add an intracellular constant current stimulation (10 μA/cm^2) such that each isolated neuron develops a tonic-firing mode with a natural period of

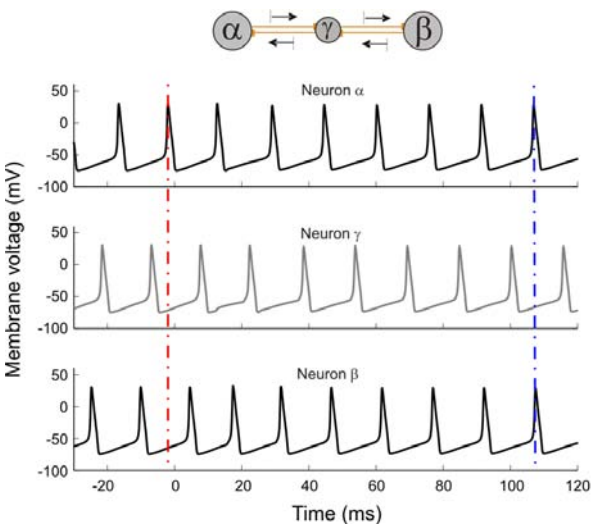

Figure 4.1: Time series of the membrane voltage of three coupled HH cells $N_\alpha - N_\gamma - N_\beta$. At time $t = 0$ the excitatory synapses were activated. Conduction delay $\tau = 8$ ms. Vertical lines help the eye to compare the spike coherence before and after the interaction takes place.

14.7 ms. The initial phase of the oscillations of each cell is randomly chosen to exclude any trivial coherent effect. Finally, we set all axonal conduction delays in the communication between neurons to a considerably long value of 8 ms to mimic the long-range nature of the synaptic interactions. Further details about the methodology used in the following simulations can be found at the *Methods* section at the end of the chapter. In Fig. 4.1 we show the time evolution of the membrane potentials under such conditions before and after an excitatory synaptic coupling among the cells is activated.

Previously to the switch-on of the synaptic coupling, the cells fire out of phase as indicated by the left vertical line to guide the eye in Fig. 4.1. However, once the interaction becomes effective at $t = 0$ and synaptic activity is allowed to propagate, a self-organized process is observed: the outer neurons synchronize their periodic spikes at zero-phase (even in the presence of long conducting delays). It is important to notice that no external agent

or influence is responsible for the setting of the synchronous state but this is entirely negotiated by the motif itself. Furthermore, we checked that the present synchrony is not just a phase condition between purely periodic oscillators but also a true temporal relationship. To that end, we added independent noisy membrane fluctuations to each neuron that resulted in a non-perfectly deterministic firing of them. In this case, the circuit maintained an approximated zero-lag synchrony between the outer neurons, reflecting both the robustness of the synchrony mechanism to moderate noise perturbations and showing that the synchrony process can be generalized beyond a phase relation. A condition akin has already been discussed in the previous chapter: Figure 3.5 illustrates the dynamical relaying taking place between three neurons, stochastically driven (Poisson input).

The mechanism responsible for the synchronization depends on the ability of an EPSP to modify the firing latencies of a postsynaptic neuron in a consistent manner. It further relies on the symmetric relay that the central neuron provides for the indirect communication between the outer neurons. The key idea is that the network motif under study allows for the outer neurons to exert an influence on each other via the intermediate relay cell. Thus, the reciprocal connections from the relay cell assure that the same influence that propagates from one end of the network to the other is also fed-back into the neuron which originated the perturbation and therefore, promoting the synchronous state.

It must be noticed, however, that the effect of a postsynaptic potential on a neuron strongly depends on the internal state of the receiving cell, and more specifically on the phase of its spiking cycle at which a postsynaptic potential (PSP) arrives (Ermentrout, 1996; Reyes and Fetz, 1993). Since the neurons of the module are, in general, at different phases of their oscillatory cycles (at least initially) the effects of the PSPs are different for the three cells. The magnitude and direction of the phase-shifts induced by PSPs can be characterized by phase response curves. The important point here is that the accumulation of such corrections to the interspike intervals of the outer neurons is such that after receiving a few PSPs they compensate the initial phase difference and both cells end up discharging isochronously, representing a stable state. Simulations predict that a millisecond-precise locking of spikes can be achieved already after the exchange of only a few spikes in the network (in a period as short as 100 ms). This value is found to be a function of the maximal synaptic conductivity and can be even shorter

for stronger synapses.

A key issue of the synchronization properties exhibited by such network architecture is whether the zero-lag correlation can be maintained for different axonal lengths or whether it is specific to a narrow range of axonal delays. To resolve this issue we test the robustness of the synchronous solution for other values of conduction delays. In Fig. 4.2 we show the quality of the zero-lag synchronization for two HH cells as a function of the conduction delay. The plot corresponds to two different scenarios: one in which the neurons are directly coupled via excitatory synapses (dashed line) and a second one in which the two neurons interact through a relay cell also in an excitatory manner (solid line). In both cases the connections are bidirectional. A quick comparison already reveals that the direct excitatory coupling exhibits large regions of axonal conduction delays where the zero-lag synchrony is not achieved. On the contrary, the relay-mediated interaction leads to zero time-lag synchrony in 28 out of the 30 delay values explored, $(1 - 30)$ ms. Only for the cases of $\tau = 3$ ms and $\tau = 10$ ms the network motif does not converge to the isochronous discharge for the outer neurons. For such latencies the three cells enter into a chaotic firing mode in which the neurons neither oscillate with a stable frequency nor exhibit a consistent relative lag between their respective spike trains.

Robust zero-lag synchrony among the outer neurons is also observed when the synaptic interaction between the cells is inhibitory instead of excitatory. Different synaptic rise and decay times within the typical range of fast AMPA and $GABA_A$ mediated transmission were tested with identical results as those reported above. These results indicate that the network motif of two neurons relaying their activities through a third neuron leads to a robust zero-lag synchrony almost independently of the delay times and type of synaptic interactions. We have also conducted simulations to test the robustness of this type of synchrony with respect to the nature of the relay cell. The results indicate that when a relay neuron is operating in a parameter regime different from the outer ones (such as different firing rate or conductances), the zero-lag synchrony is not disturbed. Remarkably, even in the case where the relay cell operates in a subthreshold regime, and thus only spiking due to the excitatory input from any of the outer neurons, the process of self-organization toward the zero-lag synchrony is still observed. It is also worth mentioning that in all cases such firing coherence is achieved

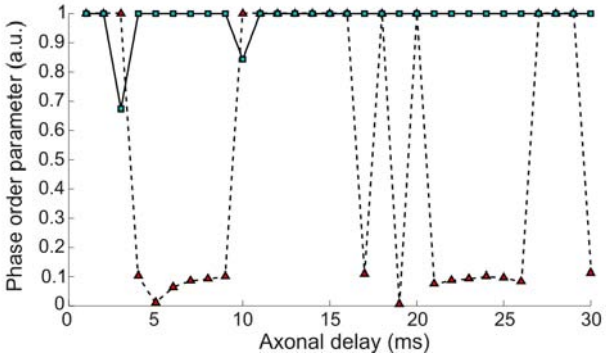

Figure 4.2: Dependence of zero time-lag synchronization as a function of the axonal delay for a scheme of two coupled cells (dashed line) and three coupled cells (solid line). In the case of the three interacting cells only the synchrony between the outer neurons is plotted here.

through small shifts in the spiking latencies which leave the mean frequency of discharges (or rate) almost unchanged.

4.2.2 Effect of a broad distribution of conduction delays

Axons show a significant dispersion in properties such as diameter, myelin thickness, internodal distance, and past history of nerve conduction. Within a fiber bundle the variability from one axon to another of these characteristics is directly related to the speed of propagation of action potentials along them and eventually translates into the existence of a whole range of latencies in the neuronal communication between two separated brain areas. Thus, conduction times along fibers are more suitably considered as a spectrum or distribution rather than a single latency value (Ringo et al., 1994; Aboitiz et al., 1992).

A crucial question is therefore whether the synchronization transition that we have described in the former section is restricted to single latency synaptic pathways or preserved also for broad distributions of axonal delays. To

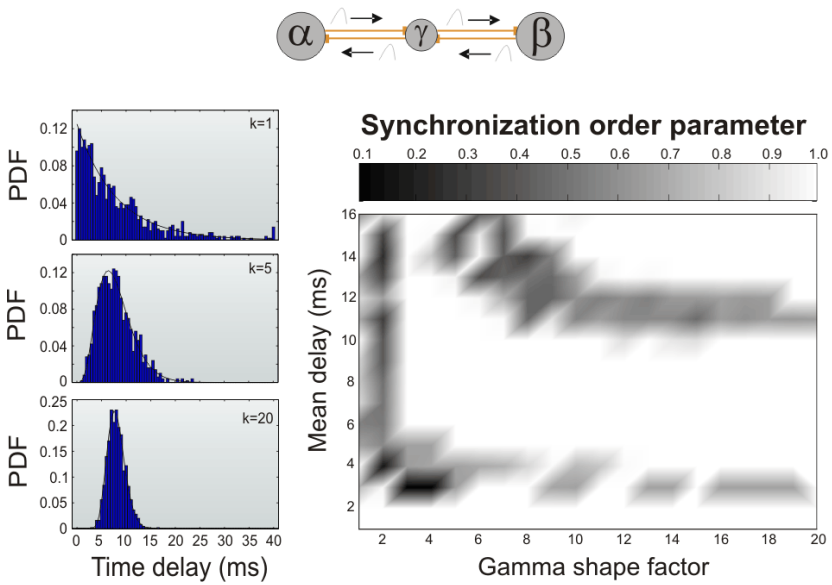

Figure 4.3: Left panels: gamma distribution of delays with different shape factors (k=1, 5, and 20) and the same mean (τ = 8 ms). Right panel: synchronization index at zero-lag of the outer neurons as a function of the shape factor and mean of the distribution of delays.

answer this issue we model the dispersion of axonal latencies by assuming that individual temporal delays of the arrivals of presynaptic potentials (i.e., latency times) are spread according to a given distribution. This intends to mimic the variability among the different axons within a fiber bundle connecting two neuronal populations. Since data about axonal distributions of conduction velocities in long-range fibers is limited, specially in the case of humans (Ringo et al., 1994; Aboitiz et al., 1992), and there is probably not a unique prototypical form of such distributions, we explore a whole family of gamma distributions with different shapes (see the *Methods* section). The left panels shown in Fig. 4.3 illustrate different gamma distributions of axonal delays for three different shape factors.

Our numerical simulations indicate that for a large region of mean delays (between 3 and 10 ms) the outer neurons synchronize independently of the shape of the distribution. These results can be observed in the right panel of Fig. 4.3 where we plot the zero-lag synchronization index of the outer neurons of the network motif as a function of the shape of the gamma distribution of axonal delays and its mean value. Only distributions with unrealistic small shape factor (i.e., exponentially decaying distributions) prevent synchrony irrespective of the average delay of the synaptic connections. For more realistic distributions, there is a large region of axonal delays that gives rise to the zero-lag synchrony among the outer neurons. As in the case of single latencies, we find a drop in the synchrony quality for distributions with a mean value around $\hat{\tau} \sim (10-12)$ ms, where chaotic firing is observed. The isochronous spiking coherence is in general recovered for larger mean delay values.

So far we have considered a rather symmetric situation in which similar distributions of axonal delays are present in each of the two branches that connect the relay neuron to the outer units. This assumption can only hold when the relay cell is approximately equidistant from the outer ones. In the final section of this chapter we refer to several results pointing to the thalamic nuclei and their circuitry as ideal relay centers of cortical communication which approximately satisfy this condition. It is nevertheless advisable to investigate the situation in which the axonal delays of each of the two pathways of the network motif are described by dissimilar distributions. In this case, we find that if the distributions of delays for each branch have different mean values then a nonzero phase-lag appears between the dynamics of the outer neurons. This effect is illustrated for gamma distributions of different shape factors in Fig. 4.4. For delta distributions of delays (which is equivalent to the single latency case) the lag amounts to the difference in mean values. Thus, if one of the pathways is described by a delta distribution of delays centered at $\tau_a = 5$ ms while the other is represented by a latency of $\tau_b = 7$ ms, then after some transient the neuron closer to the relay cell consistently fires 2 ms (i.e., $\tau_b - \tau_a$) in advance to the other outer neuron. It is worth to note that such value it is still much smaller than the total delay accumulated to communicate both neurons ($\tau_a + \tau_b = 12$ ms). When studying the effect of broader distributions of delays we observed that outer cells tend to fire with a lag even smaller than the difference in

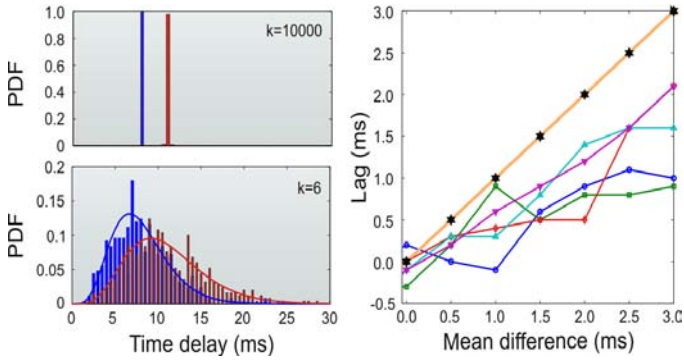

Figure 4.4: Left panels: different gamma distributions of delays used for the two dissimilar branches of the network module. Upper left panel shows distributions with shape factor k=10000 (quasi-delta) and means of 8 and 11 ms. Bottom left panel shows distributions with shape factor k=6 and means of 8 and 11 ms. Right panel: lag between the discharges of the outer neurons as a function of the difference in the mean of the distributions of delays for the two branches. Shape factors k=6 (squares), k=8 (circles), k=10 (diamonds), k=12 (up-triangles), k=14 (down-triangles), and k=10000 (stars) were tested.

the mean values of the distributions. Thus, our results suggest that broader distributions of delays can help distant neurons to fire almost isochronously.

4.2.3 Dynamical relaying in large-scale neuronal populations

A further key step in demonstrating the feasibility of synchronizing widely separated neurons via dynamical relaying is the extension of the previous results to the level of neuronal populations, the scale at which neuronal micro-circuits develop their function (Douglas and Martin, 2004). Far from being independent, the dynamical response of any neuron is massively affected by the activity of the local neighborhood and by the long-range afferents originating in distant populations. It is also important to consider the random-like influences usually referred to as background noise, a term that collects a variety of processes from spontaneous release of neurotrans-

mitters to fluctuations of unspecific inputs (Pare et al., 1998; Arieli et al., 1996). In such a scenario, we explore whether long-range fibers supporting dynamical relaying, and thus indirectly connecting pools of neurons, are suitable to promote remote interpopulation synchrony in the presence of local interactions and noise sources.

Balancement between excitation and inhibition

The scale extension, from motifs composed of a few neurons to motifs composed of a few populations of neurons introduces a myriad of degrees of freedom in the system. In a cortical region, there are about 4 excitatory neurons for each inhibitory one. Moreover, the dynamical behavior of a population of neurons strongly depends on the amount of excitatory and inhibitory currents received by each neuron from its presynaptic neighbors (Brunel, 2000). The balancement is an effective means to control the proportion of excitatory to inhibitory current received by each population in a random population (see section 2.3.1). As showed by Brunel (2000), the balancement is perhaps the most efficient control parameter to tune the populations into synchronous or asynchronous states.

We compare results for the same motifs and two different balancements. First, we utilize unbalanced populations in which the excitation overcomes the inhibition. Even isolated, each population synchronizes and generates an intrinsic oscillatory rhythm. Second, we utilize balanced populations in which neither excitation or inhibition overcomes the other. The dynamics in this configuration is such that the isolated populations do not synchronize. However, the system is tuned to a regime in which the addition of the long-range excitatory connections between the pairs of populations synchronizes each population. Both types of populations, regardless of the balancement lead to the phase synchrony of the populations when connected following the dynamical-relaying structure.

We built three large networks of sparsely connected excitatory and inhibitory IF neurons. We interconnect the three populations following the topology of the network motif under study, i.e. the mutual relaying of activities of two external populations onto an intermediate pool of relay neurons. For details on the building of each network and their connectivity see the *Methods* section.

Unbalanced populations We first begin by initializing the three networks without the long-range inter-population connections. Thus only the recurrent local connections and the Poissonian external background are active and then responsible for any dynamics in the stand-alone networks. Consequently, each population initially exhibits incoherent spiking of their neurons with respect to neurons belonging to any of the other populations. Once the long-range synapses are activated at t = 100 ms, we observe how the firing of the neurons organize toward the collective synchrony of the outer populations. Thus, the firing cycles of the outer networks of neurons occur with decreasing phase lags until both populations discharge near simultaneously and exhibit almost zero-phase synchrony. Fig. 4.5 illustrates the typical raster plots, firing histograms, and cross-correlograms of neurons among the three inter-connected networks for a long conduction delay of 12 ms. Similar results are observed when other axonal delays in the range of 2 to 20 ms are explored.

The effective coupling of the networks modifies the relative timing among their spikes yielding populations 1 and 3 to rapidly synchronize. However, the qualitative dynamics of each single neuron seems to be not so much altered by the interaction. Periodic firing of comparable characteristics is found in both the coupled and the uncoupled case (compare the firing of the central population in Fig. 4.5 and Fig. 4.7 where in the latter the population 2 remains uncoupled from other populations). Indeed, the mean period of the coupled oscillatory activity (~32 ms) is found to be close to the local rhythm of an isolated network (~34 ms), and therefore the coupling has little effect on the frequency of the oscillation. This indicates that zero-lag synchrony can be developed by this mechanism via small latency shifts without affecting the nature of the neuronal dynamics.

Balanced populations We repeat the same procedure, but utilizing a balanced population (see the *Methods* section). As depicted in Fig. 4.6, this test indicates the robustness of the dynamical relaying with respect to the details of the model to generate zero-lag synchronization of populations 1 and 3. Despite this resilience of the dynamical relaying regarding the balancement of excitation and inhibition, there are some marked differences in the dynamics. The delay in the communication plays an important role in the system composed of balanced populations, in which there is no prominent oscillatory activity of the isolated populations before they are functionally coupled. In this case, the excitatory reciprocal coupling between the popu-

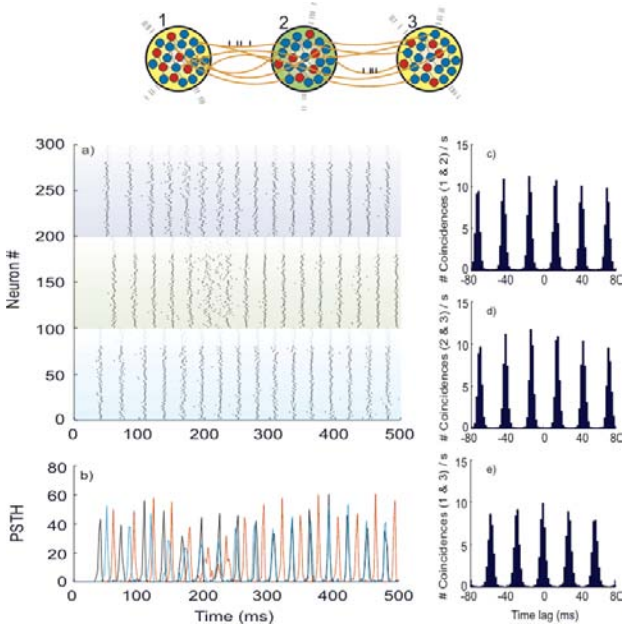

Figure 4.5: Dynamics of three unbalanced large-scale networks interacting through dynamical relaying. Panel a): raster plot of 300 neurons randomly selected among the three populations (Neurons 1-100 are from Pop. 1, 101-200 from Pop. 2, and 201-300 from Pop. 3). The top 20 neurons of each subpopulation (plotted in gray) are inhibitory, and the rest excitatory (black). Panel b): firing histogram of each subpopulation of 100 randomly selected neurons (black, red, and blue colors code for populations 1, 2, and 3, respectively). Panel c): averaged cross-correlogram between neurons of Pop. 1 and Pop. 2. Panel d): averaged cross-correlogram between neurons of Pop. 2 and Pop. 3. Panel e): averaged cross-correlogram between neurons of Pop. 1 and Pop. 3. At t=100 ms the external inter-population synapses become active. Bin sizes for the histogram and correlograms is set to 2 ms. Inter-population axonal delays are set to 12 ms. Parameter values are $C = 0.25\%$, $g = 3.5$ and $\nu = 5$Hz.

lations is essential to synchronize the populations internally. Subsequently, the populations adapt their period of oscillations by small amounts, ending up phase synchronized. As a result of the coupling, the period of the oscillations is strongly influenced by the conduction delays. The period is generally given by a multiple of the delay in the connection, mostly twice the long conduction delay.

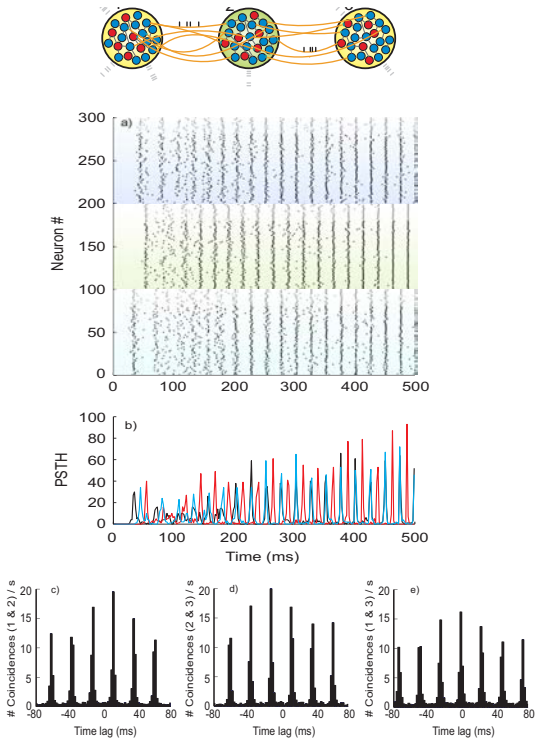

Figure 4.6: Same as figure 4.5, but for balanced populations: Parameter values are $C = 0.8\%$, $g = 4$ and $\nu = 5.4$Hz.

Control motif To better determine the role of the relay cells (Pop. 2) in shaping the synchronization among cells belonging to remote neuronal net-

works (Pop. 1 and Pop. 3), we designed the following control simulation. We investigated the neuronal dynamics obtained under exactly the same conditions as shown in Fig. 4.5 for the unbalanced populations with the only variation that this time the two outer networks interacted directly. The results are summarized in Fig. 4.7. Although only the topology of the connections has been changed, this is enough to prevent zero-lag synchronization of networks 1 and 3 to occur, highlighting the essential role of the relaying population.

Robustness

Direct connection So far we have focused on studying how a V-shaped network motif with reciprocal interactions determines the synchronization properties of the constituent neurons, and compared them to the case of a direct reciprocal coupling between two populations. The results above indicate that the V-shaped structure can promote the zero-lag synchrony between their indirectly coupled outer populations for long delays, while direct connections between two populations can sustain zero-lag synchrony only for limited values of axonal latencies. However, usually both situations are expected to occur simultaneously, this is neuronal populations that need to be coordinated might be linked by both direct (monosynaptic) and non-direct (polysynaptic) pathways. In fact, there exists much more cortico-cortical connections than connections with subcortical structures. It is fundamental to understand the dynamics when all the populations presumably belong to the cortex. Therefore, we also conducted numerical studies including bidirectional coupling between the populations 1 and 3 (closing the open end of the sketches shown in top of Fig. 4.5 or 4.6 to a ring form) to study how it modifies the synchronization properties formerly described, which were due only to their indirect communication via population 2. Thus, we introduce a reciprocal connection between populations (1 and 3) with variable strength (measured as the number of synaptic input received by both population).

For both balanced and unbalanced populations, we observed that when the connectivity (or number of synapses) between the pools of neurons 1 and 3 is moderate and smaller than the connectivity between these populations and the relay population 2, a zero-lag synchronous dynamics between the outer populations still emerges. This holds even for the case in which the synapses linking Pop. 1 and Pop. 3 have a different delay than the ones linking these

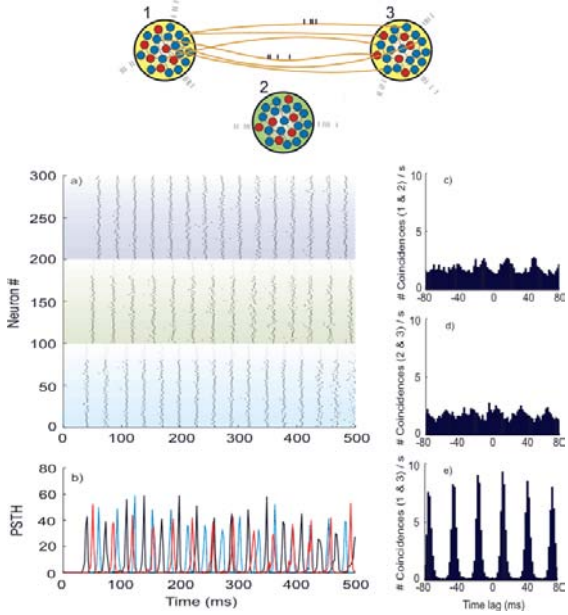

Figure 4.7: Dynamics of two unbalanced large-scale networks interacting directly. Population 2 is disconnected from other populations. Panel a): raster plot of 300 neurons randomly selected among the three populations (Neurons 1-100 are from Pop. 1, 101-200 from Pop. 2, and 201-300 from Pop. 3). The top 20 neurons of each subpopulation (plotted in gray) are inhibitory, and the rest excitatory (black). Panel b): firing histogram of each subpopulation of 100 randomly selected neurons (black, red, and blue colors code for populations 1, 2, and 3, respectively). Panel c): averaged cross-correlogram between neurons of Pop. 1 and Pop. 2. Panel d): averaged cross-correlogram between neurons of Pop. 2 and Pop. 3. Panel e): averaged cross-correlogram between neurons of Pop. 1 and Pop. 3. At t=100 ms the external inter-population synapses become active. Bin sizes for the histogram and correlograms is set to 2 ms. Inter-population axonal delays are set to 12 ms. Parameter values are $C = 0.25\%$, $g = 3.5$ and $\nu = 5$Hz.

to the relay center. As expected, when the reciprocal connectivity between pools 1 and 3 is stronger, direct coupling dominates, and, depending on the delay, it can impose a non-zero lag synchronous solution. Consequently, the connectivity weight plays a fundamental role in this case of a ring.

Asymmetrical external driving In natural conditions, we don not expect the external incoming activity over the involved populations to be equivalent. Actually, a rather asymmetric amount of stimulus driving the neurons located at the distant populations can be expected. Inspired by this possibility, we checked whether the results previously described are robust to asymmetric external driving. We characterize how much variation is allowed in order to guarantee the zero-lag synchronization via the dynamical-relaying mechanism.

Contrary to the ring test, previously discussed, asymmetric inputs developed noticeably different robustness for the balanced and the unbalanced populations. In particular, the former displays more robustness, i.e., the dynamical relaying do synchronize the outer populations for almost any asymmetry for balanced neuronal populations. The only condition is that the three population must to be active, in the sense that neurons should fire spontaneously. On the other hand, the unbalanced case is much sensible to the input asymmetry: Accordingly, we found the dynamical relaying to be effective only for asymmetries smaller than 10% of the external driving input to the outer populations. These results suggest that, given the dynamical-relaying substrate, the regulation of input asymmetry could function as a dynamic control of zero-lag synchronization. Furthermore, a larger star motif embedded in a much large structure could in principle select which regions should be engaged in the coordinated spiking mode by modulating the external driving.

Further structures Amongst other relevant networks that might sustain the emergence zero-lag synchrony between some of its nodes stands the star topology where a central hub is reciprocally connected to other nodes. For such arrangement, which in some sense can be understood as to be composed of several V-shaped motifs, numerical simulations show that the outer elements of the star that are bidirectionally connected to the central hub also tend to engage in a zero-lag synchronous spiking.

4.3 General discussion, conclusions and perspectives

In this chapter we have dealt with the intriguing problem of explaining how long-range synchrony can emerge in the presence of long conduction delays. This challenging question, that has attracted the attention of many researchers, is still far from being fully clarified. Nevertheless, our main goal in the previous pages was to disseminate the idea that, in addition to intrinsic cellular properties, an appropriate neuronal circuitry can be essential in circumventing the phase shifts associated with conduction delays. In particular, we have explored and showed how a simple network topology can naturally enhance zero-lag synchronization of distant populations of neurons. The neuronal micro-circuit that we have considered consists of the relaying of two pools of neurons onto a third mediating population which indirectly connects them. Simulations of Hodgkin & Huxley cells as well as large networks of integrate and fire neurons arranged in the mentioned configuration demonstrated a self-organized tendency toward the zero-lag synchronous state despite of large axonal delays. These results suggest that the presence of such connectivity pattern in neuronal circuits may contribute to the large-scale synchronization phenomena reported in a number of experiments in the last two decades (Singer, 1999; Varela et al., 2001).

The question immediately pops up: Is there brain any particular structure in the where such connectivity pattern is significantly common? Within the brain complex network, the thalamus and its bidirectional and radial connectivity with the neocortex form a key partnership. Several authors have indicated that the reciprocal coupling of cortical areas with the different thalamic nuclei may support mechanisms of distributed cortical processing and even form a substrate for the emergence of consciousness (Llinás and Pare, 1997; Llinás et al., 98; Ribary et al., 1991; Sherman and Guillery, 2002). It has also been explicitly proposed that diffuse cortical projections of matrix cells in the dorsal thalamus together layer V corticothalamic projections are an ideal circuitry to extend thalamocortical activity and sustain the synchronization of widespread cortical and thalamic cells (Jones, 2002; Shipp, 2003). The resemblance of such circuitry with the topology we studied here is evident if we identify the associative nuclei of the thalamus with our relay population. Altogether, the results described in this chapter point to the direction that long axonal latencies associated with cortico-thalamo-

cortical loops are still perfectly compatible with the isochronous cortical synchronization across large distances. Within this scheme the most important requirement for the occurrence of zero-lag synchronization is that the relay population of cells occupies a temporally equidistant location from the pools of neurons to be synchronized. It is then highly significant that recent studies have identified a constant temporal latency between thalamic nuclei and almost any area in the mammalian neocortex (Salami et al., 2003). Remarkably, this occurs irrespectively of the very different distances that separate the thalamus and the different cortex regions involved, and it relies on the adjustment of conduction velocity by myelination. Thus, thalamic nuclei occupy a central position for the mediation of zero-phase solutions.

Coherent dynamics between remote cortical populations could certainly be generated also by reciprocally coupling these areas to yet another cortical area or other subcortical structures. It is important to remark that connectivity studies in primate cortex identified the pattern of connections studied here as the most frequently repeated motif at the level of cortico-cortical connections in the visual and other cortical systems (Honey et al., 2007; Sporns and Kotter, 2004; Sporns et al., 2004). The functional relevance of this topology in cortical networks is unclear but according to our results is ideally suited to sustain coherent activity.

In general, it is quite possible that a variety of mechanisms are responsible for bringing synchrony at different levels (distinguishing for example, among local and long-distance synchrony) and different cerebral structures. The fact that each thalamic nucleus projects almost exclusively ipsilaterally (the massa intermedia is clearly inadequate for supporting the required interthalamic communication) is already an indication that the callosal commissure should play a prominent role in facilitating interhemispheric coherence. Studies including lesions in the corpus callosum sustain this view (Engel et al., 1991). However, within a single hemisphere the disruption of intracortical connectivity by a deep coronal cut through the suprasylvian gyrus in the cat cortex did not disturb the synchrony of spindle oscillations across regions of cortex located at both sides of the lesion (Contreras et al., 1996). This suggests that subcortical, and in particular cortico-thalamic interactions, could be responsible not only for the generation of oscillations but also for maintaining both the long-range cortical and thalamic coherence found in such regimes. It is likely then that subcortical loops with widespread connectivity such as the associative or non-specific cortico-thalamo-cortical circuits could run in parallel as an alternative pathway for the large-scale

integration of cortical activity within a single hemisphere (Shipp, 2003; Douglas and Martin, 2004; Sherman and Guillery, 2002). As we have shown here, with such connectivity pattern even large axonal conduction delays would not represent an impediment for the observation of zero time-lag coherence.

We would like to stress here that conduction delays are an important variable to consider not only for synchronization but in any temporal coding strategy. They contribute with an intrinsic temporal latency to neuronal communication that adds to the precise temporal dynamics of the neurons. Thus, they could have an important implication in gating mechanisms based in temporal relationships. For instance, when assisted by membrane oscillations, neurons undergo repetitive periods of interleaved high and low excitability and it has been reported that the impact of a volley of spikes bombarding one of such oscillatory neuron is strongly influenced by the phase of the cycle (variable influenced by conduction delays) at which the action potentials reach the targeting neuron (Volgushev et al., 1998). Conduction delays along with the frequency and phase difference of two respective oscillatory processes determine the timing of the arrival of inputs and therefore can control whether the incoming signal is relatively ignored (when coinciding the trough of excitability) or processed further away (when reaching the neuron at the peak of the fluctuating depolarization) (Salinas and Sejnowski, 2001; Fries, 2005). By this mechanism it has been hypothesized that a dynamically changing coherent activity pattern may ride on top of the anatomical structure to provide flexible neuronal communication pathways (Fries, 2005). Based on the properties formerly reviewed subcortical structures, such as some thalamic nuclei, might be in an excellent situation to play a role in regulating such coherence and contribute to the large-scale cortical communication.

In summary, the network motif highlighted here has the characteristic of naturally inducing zero-lag synchronization among the spikes of two separated neuronal populations. Interestingly, such property is found to hold for a wide range of conduction delays, a highly convenient trait not easily reproduced by other proposed mechanisms, which have a more restricted functionality in terms of axonal latencies. Regarding its physiological substrate, the associative thalamic nuclei have the cortex as their main input and output sources and seem to represent active relay centers of cortical activity with properties well suitable for enhancing cortical coherence (Shipp, 2003). The advantage of this approach in terms of axonal economy, spe-

cially compared to an extensive network of fast long-range cortical links, is overwhelming. Ongoing research is being directed to a detailed modeling of the interaction between cortex and such nuclei with an emphasis in investigating the role of limited axonal conduction velocity. From the experimental side the relatively well controlled conditions of thalamocortical slice experiments, allowing for the identification of synaptically coupled neurons and cell class, might be a first step for testing whether the topology investigated here provides a significant substrate for coherent spiking activity. An important issue related to the physical substrate of synchrony is how the dynamic selection of the areas that engage and disengage into synchrony can be achieved, but that is a subject beyond the scope of the present chapter.

4.4 Methods

4.4.1 Models

Two neuronal models were simulated to test the synchronization properties of the neuronal circuits investigated here.

In the most simplified version we focused on the dynamics of two single-compartment neurons that interact with each other via reciprocal synaptic connections with an intermediate third neuron of the same type (see top panel in Fig. 4.1). The dynamics of the membrane potential of each neuron was modeled by the classical Hodgkin-Huxley equations (Hodgkin and Huxley, 1952) plus the inclusion of appropriate synaptic currents that mimic the chemical interaction between nerve cells. The temporal evolution of the voltage across the membrane of each neuron is given by

$$\begin{aligned} C\frac{dV}{dt} &= -g_{Na}m^3h(V-E_{Na}) - g_K n^4(V-E_k) \\ &- g_L(V-E_L) + I_{ext} + I_{syn}\ , \end{aligned} \tag{4.1}$$

where $C = 1\ \mu\text{F/cm}^2$ is the membrane capacitance, the constants $g_{Na} = 120$ mS/cm^2, $g_K = 36$ mS/cm^2, and $g_L = 0.3$ mS/cm^2 are the maximal conduc-

tances of the sodium, potassium, and leakage channels, and $E_{Na} = 50$ mV, $E_K = -77$ mV, and $E_L = -54.5$ mV stand for the corresponding reversal potentials. According to Hodgkin and Huxley formulation the voltage-gated ion channels are described by the following set of differential equations

$$\frac{dm}{dt} = \alpha_m(V)(1-m) - \beta_m(V)m \ , \tag{4.2}$$

$$\frac{dh}{dt} = \alpha_h(V)(1-h) - \beta_h(V)h \ , \tag{4.3}$$

$$\frac{dn}{dt} = \alpha_n(V)(1-n) - \beta_n(V)n \ , \tag{4.4}$$

where the gating variables $m(t)$, $h(t)$, and $n(t)$ represent the activation and inactivation of the sodium channels and the activation of the potassium channels, respectively. The experimentally fitted voltage-dependent transition rates are

$$\alpha_m(V) = \frac{0.1(V+40)}{1-\exp\left(-(V+40)/10\right)} \ , \tag{4.5}$$

$$\beta_m(V) = 4\exp\left(-(V+65)/18\right) \ , \tag{4.6}$$

$$\alpha_h(V) = 0.07\exp\left(-(V+65)/20\right) \ , \tag{4.7}$$

$$\beta_h(V) = \left[1+\exp\left(-(V+35)/10\right)\right]^{-1} \ , \tag{4.8}$$

$$\alpha_n(V) = \frac{(V+55)/10}{1-\exp\left(-0.1(V+55)\right)} \ , \tag{4.9}$$

$$\beta_n(V) = 0.125\exp\left(-(V+65)/80\right) \ . \tag{4.10}$$

The synaptic transmission between neurons is modeled by a postsynaptic conductance change with the form of an alpha-function

$$\alpha(t) = \frac{1}{\tau_d - \tau_r}\left(\exp\left(-t/\tau_d\right) - \exp\left(-t/\tau_r\right)\right) \ , \tag{4.11}$$

where the parameters τ_d and τ_r stand for the decay and rise time of the function and determine the duration of the response. Synaptic rise and

decay times were set to $\tau_r = 0.1$ and $\tau_d = 3$ ms, respectively. Finally, the synaptic current takes the form

$$I_{syn}(t) = -\frac{g_{max}}{N} \sum_{\tau_l} \sum_{spikes} \alpha\left(t - t_{spike} - \tau_l\right)\left(V(t) - E_{syn}\right) , \qquad (4.12)$$

where g_{max} (here fixed to 0.05 mS/cm^2) describes the maximal synaptic conductance and the internal sum is extended over the train of presynaptic spikes occurring at t_{spike}. The delays arising from the finite conduction velocity of axons are taken into account through the latency time τ_l in the alpha-function. Thus, the external sum covers the N different latencies that arise from the conduction velocities that different axons may have in connecting two neuronal populations. N was typically set to 500 in the simulations. For the single-latency case, all τ_l were set to the same value, whereas when studying the effect of a distribution of delays we modeled such dispersion by a gamma distribution with a probability density of

$$f(\tau_l) = \tau_l^{k-1} \frac{\exp(-\tau_l/\theta)}{\theta^k \Gamma(k)} , \qquad (4.13)$$

where k and θ are shape and scale parameters of the gamma distribution. The mean time delay is given by $\hat{\tau}_l = k\theta$.

Excitatory and inhibitory transmissions were differentiated by setting the synaptic reversal potential to be $E_{syn} = 0$ mV or $E_{syn} = -80$ mV, respectively. An external current stimulation I_{ext} was adjusted to a constant value of 10 μA/cm^2. Under such conditions a single HH type neuron enters into a periodic regime firing action potentials at a natural period of $T_{nat} = 14.66$ ms.

The second class of models we have considered consists of three large balanced populations of integrate and fire neurons (Brunel, 2000). Top panel in Fig. 4.5 depicts a sketch of the connectivity. Each network consisted of 4175 neurons, 80% of which were excitatory. The internal synaptic connectivity was chosen to be random, i.e. each neuron synapses with 10% of randomly selected neurons within the same population, such that the total number of synapses in each network amounts to about 1,700,000. Additionally, to model background noise, each neuron was subjected to the influence of an external train of spikes with a Poissonian distribution as

described below. The inter-population synaptic links were arranged such that each neuron in any population received input from a small number of the excitatory neurons in the neighboring population, 0.8% for the systems of balanced populations and 0.25% for the systems of unbalanced populations. This small number of inter-population connections, compared to the much larger number of intra-population contacts, allowed us to consider the system as three weakly interacting networks of neurons rather than a single homogeneous network. Intra-population axonal delays were set to 1.5 ms, whereas the fibers connecting different populations were assumed to involve much longer latencies in order to mimic the long-range character of such links.

The voltage dynamics of each neuron was then given by the following equation

$$\tau_m \frac{dV_i}{dt} = -V_i(t) + RI_i(t) \ , \tag{4.14}$$

where τ_m stands for the membrane constant and $I(t)$ is a term collecting the currents arriving to the soma. The latter decomposes in postsynaptic currents and external Poissonian noise

$$RI_i(t) = \tau_m \sum_j J_j \sum_k \delta(t - t_j^k - \tau_l) + A\xi_i \ , \tag{4.15}$$

where J_j is the postsynaptic potential amplitude, t_j^k is the emission time of the k-th spike at neuron j, and τ_l is the transmission axonal delay. The external noise ξ_i was simulated by subjecting each neuron to the simultaneous input of 1000 independent homogeneous Poissonian action potential trains with an individual rate of 5.4 Hz for the systems of balanced populations and 5 Hz for the systems of unbalanced populations. Different cells were subjected to different realizations of the Poissonian processes to ensure the independence of noise sources for each neuron. J_{exc} and A amplitudes were set to 0.1 mV. The balance of the network was controlled by setting $J_{inh} = -gJ_{exc}$ to compensate the outnumber of excitatory units. We used $g = 4$ for the systems of balanced populations, and $g = 3.5$ for the systems of unbalanced populations.

The dynamics of each neuron evolved from the reset potential of $V_r = 10$ mV by means of the synaptic currents up to the time when the potential of

the i-th neurons reached a threshold of 20 mV, value at which the neuron fired and its potential relaxed to V_r. The potential was clamped then to this quantity for a refractory period of 2 ms during which no event could perturb the neuron.

4.4.2 Simulations

The set of equations (4.1-4.12) was numerically integrated using the Heun method with a time step of 0.02 ms. For the first class of models that we investigated, i.e. the three HH cells neuronal circuit, we proceeded as follows. Starting from random initial conditions each neuron was first simulated without any synaptic coupling for 200 ms after which frequency adaptation occurred and it settled into a periodic firing regime with a well-defined frequency. The relation between the phases of the oscillatory activities of the neurons at the end of this warm up time was entirely determined by the initial conditions. Following this period, and once the synaptic transmission was activated, a simulation time of 3 seconds was recorded. This allowed us to trace the change in the relative timing of the spikes induced by the synaptic coupling in this neural circuit.

The second class of model involving the interaction of heterogeneous large populations of neurons was built with the neuronal simulator package NEST (Brette et al., 2007). The simulation of such networks uses a precise time-driven algorithm with the characteristic that the spike events are not constrained to the discrete time lattice. In a first stage of the simulation the three populations were initialized isolated from each other and evolved just due to their internal local connectivity and external Poissonian noise. In a subsequent phase, the three populations were interconnected according to the motif investigated here and simulated during 1 second.

4.4.3 Data analysis

The strength of the synchronization and the phase-difference between each individual pair of neurons (m, n) were derived for the first model of three HH neurons computating the order parameter defined as

$$\rho(t) = \frac{1}{2}|\exp(i\phi_m(t)) + \exp(i\phi_n(t))| \,, \tag{4.16}$$

which takes the value of 1 when two systems oscillate in-phase and 0 when they oscillate in an anti-phase or in an uncorrelated fashion. In order to compute this quantifier it is only necessary to estimate the phases of the individual neural oscillators. An advantage of this method is that one can easily reconstruct the phase of a neuronal oscillation from the train of spikes without the need of recording the full membrane potential time series (Pikovsky et al., 2002). The idea behind this is that the time interval between two well-defined events (such as action potentials) define a complete cycle and the phase increase during this time amounts to 2π. Then, linear interpolation is used to assign a value to the phase between the spike events.

The synchrony among the large populations of neurons of the second model described above was assessed by the computation of averaged cross-correlograms. For that purpose, we randomly selected three neurons (one from each of the three populations) and computed for each pair of neurons belonging to different populations the histogram of coincidences (bin size of 2 ms) as a function of the time shift of one of the spike trains. We computed the cross-correlograms within the time window ranging from 500 to 1000 ms to avoid the transients towards the synchronous state. The procedure was repeated 300 times to give rise to the estimated averaged distributions of coincidences exhibited in Figs. 4.5, 4.6 and 4.7.

Chapter 5

Controlling Cortical Synchronization via Thalamic Dynamical Relaying

In the central nervous system (CNS) it is assumed that the information is mainly represented by the activity of neurons that is transmitted to other neurons through synaptic links. The extent of the neural network activated by a specific *piece of information* is a never-ending matter of investigation but it is accepted that both average levels of discharges, firing rate (Gollo et al., 2009), and precise spike timing contribute to neural coding. Spatiotemporal firing patterns (Villa et al., 1999b; Hayon et al., 2005) and coherent oscillatory neural activity (Fries et al., 2007) associated to sensory and behavioral events support the hypothesis that temporal information plays a key role in brain processing. Empirical phenomena and extensive experimental data, validated across different species (Gray et al., 1989; Engel et al., 1991; Castelo-Branco et al., 2000; Tiesinga et al., 2008), emphasize the importance of an emerging cortico-cortical synchrony as a major phenomenon for binding features associated to distributed neural activities (von der Marlsburg, 1973; Fries, 2005; Desbordes et al., 2008). Despite the success of physical models to reproduce oscillatory patterns of neural activity it is not clear whether

This Chapter is based on the paper: Gollo LL, Mirasso C, Villa AE (2010) Dynamic control for synchronization of separated cortical areas through thalamic relay. NeuroImage 52: 947–955.

the synchronization is the result of network processing exclusively limited to cortico-cortical interactions or subcortical structures might also intervene (Contreras et al., 1996; Traub et al., 1996; Vicente et al., 2008b; Chawla et al., 2001), for a recent review please refer to (Uhlhaas et al., 2009).

The thalamus is a structure of CNS that could play an important role in the emergence or control of cortico-cortical synchronization because the exchange of information between the thalamus and cerebral cortex is a general feature of all ascending sensory pathways but olfaction (Jones, 1985; Sherman, 2005). The connectivity pattern between thalamus and cortex is usually viewed as been characterized by thalamocortical integration and corticothalamic feedback (Steriade and Llinas, 1988; Villa et al., 1999a; Villa, 2002). Multiple thalamocortical modules characterized by the same basic connectivity may be assumed to work in parallel and include three main components (see Fig. 5.1): (i) dorsal thalamic neurons (e.g. from the medial geniculate body for the auditory pathway or from the lateral geniculate body for the visual pathway) recipient of the sensory input from the periphery; (ii) cells of the thalamic reticular nucleus (R), a major component of the ventral thalamus; (iii) the cortical area receiving the corresponding thalamic input. The thalamic reticular nucleus receives collateral inputs from both thalamocortical and corticothalamic fibers and sends its inhibitory projections to the dorsal thalamus, thus regulating the firing mode of the thalamocortical neurons. The thalamic reticular nucleus receives inputs also from several forebrain and midbrain areas known to exert modulatory functions (McCormick and Bal, 1994), in particular from basal forebrain cholinergic cells (Villa et al., 1996) that are involved in many cognitive functions and whose dysfunction is associated to Alzheimer's disease. In the auditory system evidence exists that corticofugal activity regulates the response properties of thalamic cell assemblies by changing their bandwidth responsiveness to pure tones (Villa et al., 1991) thus allowing to selectively extract information from the incoming sensory signals according to the cortical activity (Villa et al., 1999a). This model suggests that the thalamocortical circuit carries embedded features that enable the build-up of combined supervised and unsupervised information processing akin to produce an adaptive filter (Tetko and Villa, 1997) aimed to select behaviorally relevant information processing (von Kriegstein et al., 2008).

The current study is not intended at simulating any detailed thalamocortical circuit, but rather to assess the contribution of simple variables that could play a major role in controlling the emergence and maintenance of synchro-

nized activity in distributed cortical areas that project to the same thalamic nuclei. Our model predicts that small changes in the cortical neurons firing rate, due to non-correlated background synaptic activity in the thalamic region, is capable of generating single or multiple frequency oscillations along with zero-lag synchronization between distant cortical regions. We quantify this synchronized state by measuring the signal-to-noise ratio, which does not monotonically increase with the firing rate. According to our model, thalamic activity plays a key role in controlling the appearance of lag free synchronization between cortical areas. In addition, despite its simplification, the model provides hints about the conditions necessary to achieve that synchronization. We report an efficient control set as the ratio of dorsal over ventral thalamus external input activity to switch on thalamocortical synchronous dynamics. That switch occurs at a fast time scale, without any need of synaptic plasticity that would require longer time scales (Fries, 2005). The type of control that we suggest is not limited to an "*On - Off*" switch, but it allows to control the appearance of synchronous activity over an extended range of frequencies despite the delays involved in the long-range cortico-cortical interactions (Ringo et al., 1994; Vicente et al., 2009).

5.1 Methods

To study the synchronization of cortical activity facilitated by the thalamic relay we conducted extensive numerical simulations of a reduced thalamocortical model of spiking integrate–and–fire neurons subject to background noise and an external driving. The model included both local synapses and long-range interactions with different delays according to functional connectivity in a four populations motif (Milo et al., 2002), as illustrated in Fig. 5.2. The simulations were performed using NEST, the neuronal simulation tool (Brette et al., 2007) with the PyNEST interface (Eppler et al., 2009).

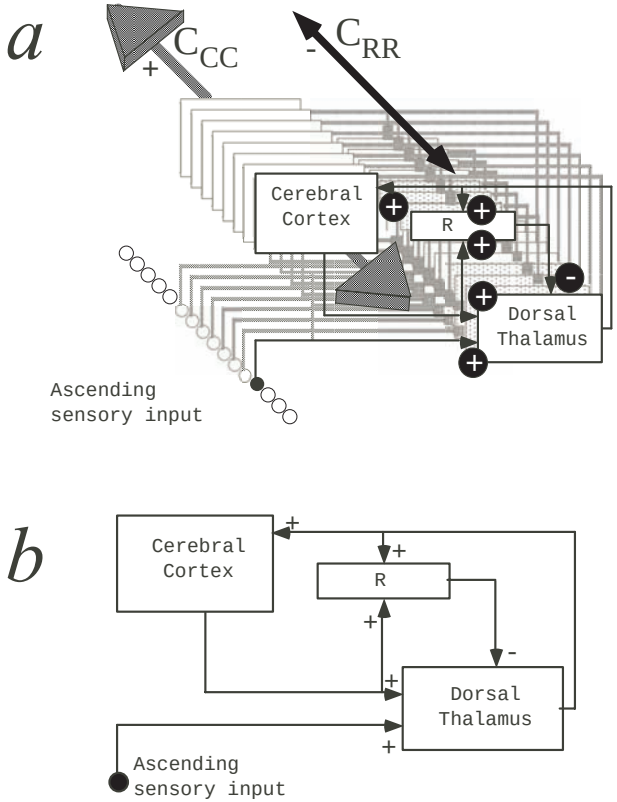

Figure 5.1: **(a)** A functional scheme of the modular organization of the typical thalamocortical sensory pathway (somatosensory, visual, sensory). The signs indicate the nature of the connections, (+) excitatory and (-) inhibitory. Notice the big arrows labeled C_{CC} corresponding to long-range excitatory cortico-cortical connections and C_{RR} corresponding to the inhibitory connections within the reticular and perigeniculate nucleus of the thalamus (R). Note the excitatory input from the ascending sensory pathway to the dorsal thalamus, the excitatory projection from the thalamus to the cortex with a collateral to R, and the excitatory projection of the cortex to the thalamus with a collateral to R. The only output of R is an inhibitory backprojection to the thalamus. **(b)** Explicit connections within one thalamocortical module.

5.1.1 Neuronal model

The integrate-and-fire neuron model (Brunel, 2000) for each neuron i satisfies the following dynamical equation for the membrane potential $V_i(t)$:

$$\tau_{mem}(m)\frac{dV_i(t)}{dt} = -V_i(t) + RI_i(t)\ , \tag{5.1}$$

where $\tau_{mem}(m)$ is the membrane time constant of neuron i belonging to the population m (as in Fig. 5.2); $I_i(t)$ is the total current arriving to the soma. The last term in the above equation is given by the sum of all postsynaptic potentials (PSP) of neurons belonging to the network plus the total PSP of all external neurons, the latter being modeled as a Poisson process. Thus,

$$RI_i(t) = \tau_{mem}(m)\sum_j J(j)\sum_k \delta(t - t_j^k - \tau(z,m)) + V_{ext}\ . \tag{5.2}$$

The first sum is taken over all presynaptic neurons j, each neuron receives $C_e(m,z)$ excitatory synapses and $C_i(m,z)$ inhibitory synapses and they depend on the inter-population (long-range) connections z if both neurons belong to different populations or otherwise on the population m to whom they belong. t_j^k is the time of the $k-th$ spike received by neuron i from its neighbor j. The axonal conduction delay is given by $\tau(z,m)$, which corresponds to a spike of a presynaptic neuron j that reaches neuron i. $J(j)$ stands for the PSP efficacy and depends on whether its presynaptic neighbor neuron j is excitatory ($J(j) = J_e$) or inhibitory ($J(j) = J_i$). V_{ext} is the PSP generated by neurons from outside the thalamocortical network. It is given by an independent and homogeneous Poisson process of N_{ext} external neurons, each one firing with a fixed average rate $\nu(m)$. The external spike contributes with a change of the membrane potential by J_{ext} whenever it impinges upon neuron i. The dynamics of the neurons can be described as following: the neurons start at a rest potential $V_r(m)$ which can be changed by the synaptic current. If the potential $V_i(t)$ of the i-th neuron reaches the threshold $\theta(m)$ a spike is generated and its membrane potential is reset to $V_r(m)$ after an absolute refractory period ($\tau_{rp} = 2$ ms).

5.1.2 Thalamocortical model

The topology of the model is characterized by two thalamic and two cortical neural populations (Shepherd, 1998; Huguenard and McCormick, 2007).

The overall layout of our model is depicted in Fig. 5.2. The thalamus is composed by two segregated populations, one of excitatory thalamocortical principal cells (T) and another of inhibitory neurons corresponding to the thalamic reticular and perigeniculate nuclei (R). The two thalamic populations are also characterized by recurrent intrathalamic connections. The cortical populations are formed by an excitatory cell type with local, long range cortical, and feedback corticothalamic projections and by an inhibitory type characterized by only local efferent projections. In addition, the two cortical populations are distributed in two *areas* (C_1 and C_2) which may or may not be interconnected (depending on the value of parameter C_{CC}). It is a hierarchical network, with an intra-population random structure and a simple inter-population pattern of connectivity with longer delays. The populations have both internal and external connectivity. Then, the topology satisfies the following constrains: both R (C_{CR}) and T (C_{CT}) populations receive cortical feedback, the cortical populations are innervated by T (C_{TC}) but do not receive inhibitory feedback from R. There are also direct connections from R to T (C_{RT}) and from T to R (C_{TR}). Long-range cortico-cortical connections are determined by C_{CC}. Assuming that the thalamus is composed by both R and T populations, the thalamocortical model may also be reduced to a three populations network formed by a central thalamic region (T and R) and two balanced cortical areas. Each neuron of a given population receives the same amount of postsynaptic connections. The presynaptic neurons are chosen randomly; therefore, the postsynaptic distribution is binomial for each type of neuron (excitatory or inhibitory) within a given population.

After a brief parameter search and according to the range of values described in the literature, we have set characteristic parameters for each population m as presented in Table 5.1. The rational of our choice was to preserve the main dynamical features, though retaining the simplicity of a reduced thalamocortical circuit. The values of the threshold, the resting membrane potential, and the membrane time constants were selected such that the neurons in R were the most excitable and those in T were the least excitable because T neurons are meant to receive the external input arising from the ascending sensory pathways. For the sake of simplicity, the refractory period and the excitatory/inhibitory postsynaptic efficacies were chosen to be the same for all neurons.

The connectivity parameter values described in Table 5.2 were set arbitrarily in order to maintain their relative proportion for cell types usually

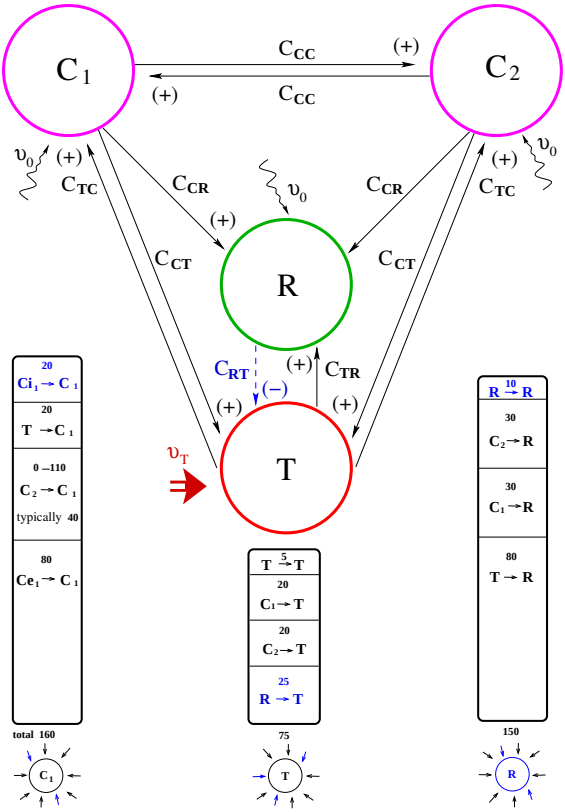

Figure 5.2: Thalamocortical connectivity. The populations are randomly connected. The two cortical populations (C_1 and C_2) are balanced with both excitatory (80%) and inhibitory (20%) neurons. The parameters which define the neuronal model are presented in Table 5.1. All populations are sparse with exception of the thalamic reticular and perigeniculate nuclei region (R). The thalamus can be considered as both R and the excitatory thalamocortical relay neurons (T) together. The inter-population connectivity is described by the parameters of Table 5.2. The dashed blue arrow (C_{RT}) stands for inhibition while black arrows stand for excitatory connections. The background noise and the external driving consists of independent Poisson train impinging in each neuron with parameters of Table 5.3. Neurons in T are externally driven at rate ν_T meanwhile the other ones receive background activity at rate ν_0. The external input is uncorrelated and defines the key parameter: $\frac{\nu_T}{\nu_0}$. A scheme of all the synaptic inputs innervated in the neurons of each population is presented at the bottom panels.

Table 5.1: Neuronal parameters for the neurons in population m. *Each neuron receives from random neighbors of the same population.

m	C_1, C_2	R	T	population
$N_e(m)$	800	0	200	# of excitatory neurons
$N_i(m)$	200	40	0	# of inhibitory neurons
$\tau_{mem}(m)$	20	25	15	membrane time constant (ms)
$\theta(m)$	20.5	24.65	15	threshold value (mV)
τ_{rp}	2	2	2	refractory period (ms)
$V_r(m)$	10	12.5	7.5	membrane rest potential (mV)
$C_e(m)$	80	0	5	# of excitatory synapses*
$C_i(m)$	20	10	0	# of inhibitory synapses*
$\tau(m)$	1.5	2	1	synaptic delay (ms)
J_e	0.05	0	0.05	excitatory synaptic efficacy (mV)
J_i	-0.2	-0.2	0	inhibitory synaptic efficacy (mV)

described in the literature (Jones, 1985; Sherman, 2005). The number of connections was set to keep 160 afferences to each neuron of C, 75 afferences to each neuron of T and 150 afferences to each neuron of R. This pattern of convergence-divergence is meant to preserve the known anatomical thalamocortical and corticothalamic pattern of connectivity (Jones, 1985; Sherman, 2005). The specific proportion of afferences generated by each population is indicated in the boxes at the bottom of Fig. 5.2. The delays were set to account for typical axonal delays described in the thalamus and cortex of mammals (Swadlow, 2000; Knoblauch and Sommer, 2004). Despite the fact that we have not systematically investigated all ranges of axonal delays, we observed that the results are robust for different delays. The most relevant parameter is the delay between the thalamus and the cortical areas (τ_{TC}) which must be kept identical for all ascending projections. If this latency time is not the same for the different cortical areas, say $\tau_{TC_1} \neq \tau_{TC_2}$, the maximum number of coincident spikes in the cross-correlograms would not occur at zero-lag, but at a lag that depends on the difference between the TC connections time delays. It is worth mentioning that a constant latency between thalamus and cortex, irrespective of the distances, has been reported

due to regional myelination differences that compensate for the conduction velocities (Salami et al., 2003).

Table 5.2: Synaptic parameters for inter-population (long-range) connections z between any two regions. **Each neuron of the target population receives input from randomly selected neurons belonging to the efferent population.

z	CR	CT	TC	RT	TR	CC	inter-population connection
$C_e(z)$	30	20	20	0	80	0-110	# of excitatory synapses**
$C_i(z)$	0	0	0	25	0	0	# of inhibitory synapses**
$\tau(z)$	8	8	5	2	2	5	synaptic delay (ms)

5.1.3 Background activity and external input

To model the background activity we assume that each neuron in the network is connected with N_{ext} excitatory external neurons subject to an independent random Poisson processes with average rate ν_0 for neurons of all regions. The thalamic region (T) receives the background activity combined with an external input also modeled by independent Poisson process, such that both the overall external input to T is a process characterized by a rate ν_T. The parameters used for the Poisson background and the external driving are presented in Table 5.3.

Table 5.3: Synaptic efficacy, Poisson external driving and background activity parameters.

J_{ext}	0.1	external synaptic efficacy (mV)
ν_0	10.0	external driving Poisson mean rate to C and R (Hz)
ν_T	8.0-45.0	overall external driving Poisson mean rate to T (Hz)
N_{ext}	450	number of external neighbors

5.1.4 Cross-correlation analysis

We run extensive simulations and analyze the spike trains over several trials. In order to quantify the results from the numerical simulations, we define two values from the cross-correlogram: a) the mean value evaluated over the time lag representing the *noise* level that quantifies the expected number of coincidences by chance; b) the peak of the cortico-cortical cross-correlogram (typically at zero-lag) that stands for the *signal*. Those quantities are used to compute the signal-to-noise ratio (SNR) for different values of v_T and different strengths of cortical interconnectivity (C_{CC}). The cross-correlograms are measured during $2,000$ ms in a stationary regime after 500 ms of transient dynamics. The result is condensed in a single cross-correlogram, which quantify the mean number of coincidences (in a 2 ms bin) of $3,000$ randomly selected neuron pairs belonging to different populations averaged over 100 trials. This procedure allows us to assess the mean behavior of the dynamics and eliminate single trial fluctuations.

The *noise* is determined by the mean over the time lag in the averaged cross-correlogram. In the stationary regime, the noise can also be calculated analytically considering the activity of the two populations just as been independent: Let $F(p)$ be the mean firing rate of a population p and b the bin size of the computed cross-correlogram. Therefore the mean cross-correlogram (noise) of two arbitrary populations i and j is given by $\langle XCOR_{i-j} \rangle = F(i)F(j)b$. For a typical thalamocortical circuit the two cortical areas have either maximum synchrony at zero-lag or no synchrony (unless C_{CC} is greater than the number of internal excitatory cortical connections C_{eC}). Thus the *signal* of the cortico-cortical dynamics is defined as the number of coincidences in the cross-correlogram at zero time lag.

5.2 Results

We have simulated the activity of large populations of interacting neurons with delayed connections. We used a simple integrate and fire (I&F) neuronal model in order to keep the problem more tractable. The model is such that if the membrane potential reaches the threshold a spike is fired. The membrane potential is reset after the firing to its resting potential with

an absolute refractory period (2 ms). The spike is transmitted to all target neurons which receive an excitatory or inhibitory PSP according to the type of synapse. The spike is transmitted with a delay depending on the connection type. Large delays are associated with inter-population connections and short delays with local connections within each population. Obtained from extensive numerical simulations, the results analyze the firing rate, cross-correlation indicators, oscillation and synchronization information calculated from the spike trains of individual neurons and neuron populations. It is worth mentioning that the neuronal spike times were reliably reproduced despite the simplicity of the I&F model.

5.2.1 Thalamocortical circuit dynamics

In the most symmetrical case, the T region is set in order to receive external driving with the same rate as the other populations ($\nu_T = \nu_0$). The firing rate in R is higher than in the cortex which is also higher than in T. For a typical number of cortico-cortical interaction, say $C_{CC} < 40$, due to the network connectivity and the difference in the neuronal parameters, there is no correlation among the different areas, and the activity is random and irregular. For $\nu_T > \nu_0$ other scenario takes place. The raster plots of 150 neurons randomly chosen among all neuronal populations illustrate the network dynamics. Such a typical raster plot is depicted in Fig. 5.3a. It shows the case in which the cortico-cortical connections are set to $C_{CC} = 40$ and the thalamus is receiving an external input of mean rate $\nu_T = 7/3\nu_0$. The neurons within the populations T and R are synchronized at a high frequency. The two cortical areas exhibit a large number of coincidences at zero-lag, meaning that they are synchronized and *in-phase*. The cross-correlograms (see Methods section for details) between the cortical areas and between the T region and one cortical area are shown in Fig. 5.3, b and c. The plots clearly indicate *in-phase* correlation among cortical areas while the thalamus and the cortical area are out of phase (with the cortical area delayed by 6 ms).

The synchronization of the cortical regions depends on the external input to T. Fig. 5.4 shows the raster plot of a single trial characterized at $t = 50$ ms by a sudden increase of the T activity from the mean rate ν_0 to $7/3\nu_0$. Synchronization does not occur in the system for low values of input ν_T, for instance $\nu_T = \nu_0$, from 0 – 50 ms or after the input is switched off, say for time $t > 250$ ms.

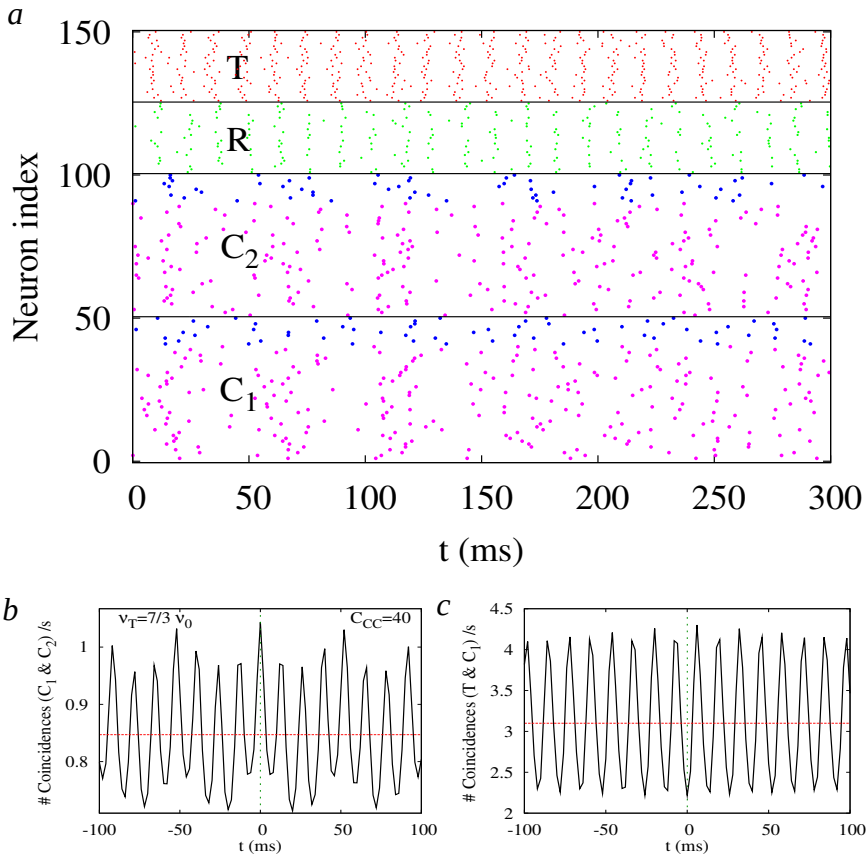

Figure 5.3: Thalamocortical dynamics. Panel **(a)** shows raster plots of 150 neurons randomly chosen, 50 neurons from each cortical population and 25 neurons from R and T. In the cortical areas, the spikes in magenta (blue) stand for excitatory (inhibitory) neurons. The spikes of neurons in R are in green and those of T in red. Neurons in the cortical populations and in R receive external stimulus of ν_0 Hz. The rate in T is $\nu_T = \frac{7}{3}\,\nu_0$. The average cross-correlogram over 100 trials of 3,000 random neuron pairs of different populations with bin size 2 ms are presented in panels **(b)** for C_1 and C_2 areas and **(c)** for T and C_1. The red horizontal line is the mean cross-correlogram value (noise) and the C_1-C_2 peak at zero-lag stands for the signal, see text for details. The vertical point line is set at zero-lag only to guide the eye. The maximum of C_1-C_2 crosscorrelation occur exactly at zero-lag while the maximum of T-C_1 happen at 6 ms.

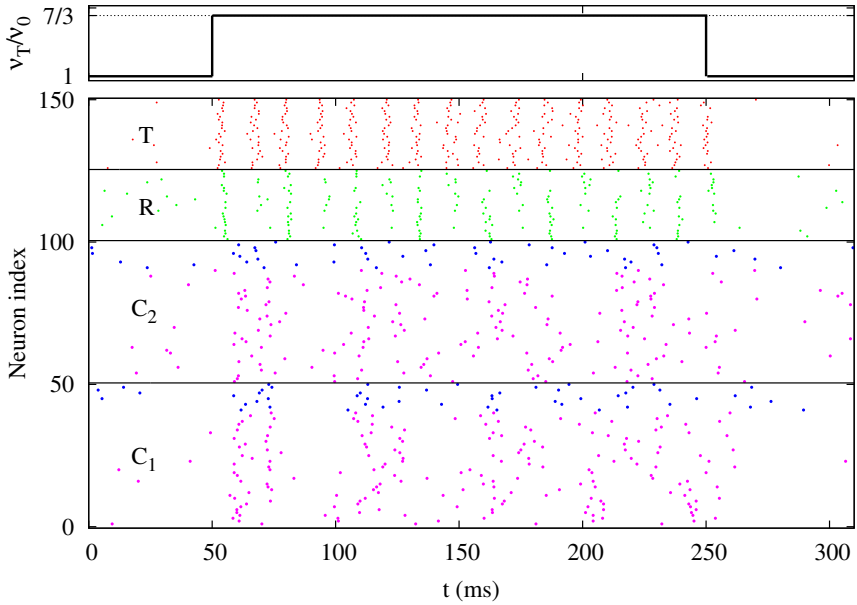

Figure 5.4: Example of *On - Off* synchronization. The ratio $\nu_T = \nu_0$ is increased to $\nu_T = \frac{7}{3}\ \nu_0$ at time $t = 50$ ms and switched back to the original value at $t = 250$ ms. The cortico-cortical connection is set as $C_{CC} = 40$.

The mean firing rate of T, C, and R neurons, computed over 2,000 ms, increases monotonically as a function of the input rate ν_T (Fig. 5.5a). The dependency of the cortical oscillation frequency as a function of ν_T/ν_0 is shown in Fig. 5.5b for directly interconnected ($C_{CC} = 40$) and disconnected ($C_{CC} = 0$) cortical areas. The frequencies are determined from the power spectrum analysis of the cross correlograms. Only those components whose power is larger than 20% of the maximum power are considered here. In the case where the cortical areas were disconnected, they oscillate at a single frequency close to the thalamic firing rate (see rate in Fig. 5.5a). When they are connected ($C_{CC} = 40$) a single frequency dominates the oscillatory dynamics only if $\nu_T < 2\nu_0$. Beyond this threshold at least two frequencies of oscillation appear. For $\nu_T = \frac{7}{3}\nu_0$ three different frequencies are observed (as in Fig. 3b). The lowest frequency is related to the firing rate of the neurons within the cortical areas. The intermediate frequency is related to the thalamic firing rate like in the disconnected case. The oscillatory frequency in the cortical areas enhances for increasing input fed into the T region due to the stronger interaction between the cortex and the thalamus. The highest frequency component in the interconnected case ($C_{CC} = 40$) is observed only for a very small range of input values.

The SNR, as defined in the Methods section from the cross-correlograms, as a function of ν_T/ν_0 is illustrated in Fig. 5.5c. The firing rate and the *signal* increase monotonically with the external rate of the input, but interestingly the SNR is characterized by a local maximum for uncoupled cortical areas as well as for coupled cortico-cortical areas with connectivity $C_{CC} = 40$. The SNR was quite flat for low values of ν_T, and then increases until reaching the local maximum. After decreasing from the local maximum the SNR increases again monotonically for very large values of the rate ν_T. To gain insight whether the synchronization among the cortical areas is induced by the T-R circuit into this aspect, we simulated the system without the cortico-thalamic connections ($C_{CR} = C_{CT} = 0$). The results are shown with solid dots in Fig. 5.5c. This curve shows that for $2 < \nu/\nu_0 < 3$ the SNR is much smaller than the one obtained with the whole connectivity, indicating that the synchronization is not driven by the thalamus circuit. Instead, a true collective behavior emerges from the whole interaction. For $\nu/\nu_0 \sim 3$ the curve increases suddenly, thus indicating that the synchronization starts to be driven by the activity of the thalamus. The SNR as a function of the strength of the cortico-cortical connection for different values of ν_T/ν_0 is illustrated in Fig. 5.5d. Interestingly, for low values of ν_T/ν_0 the SNR

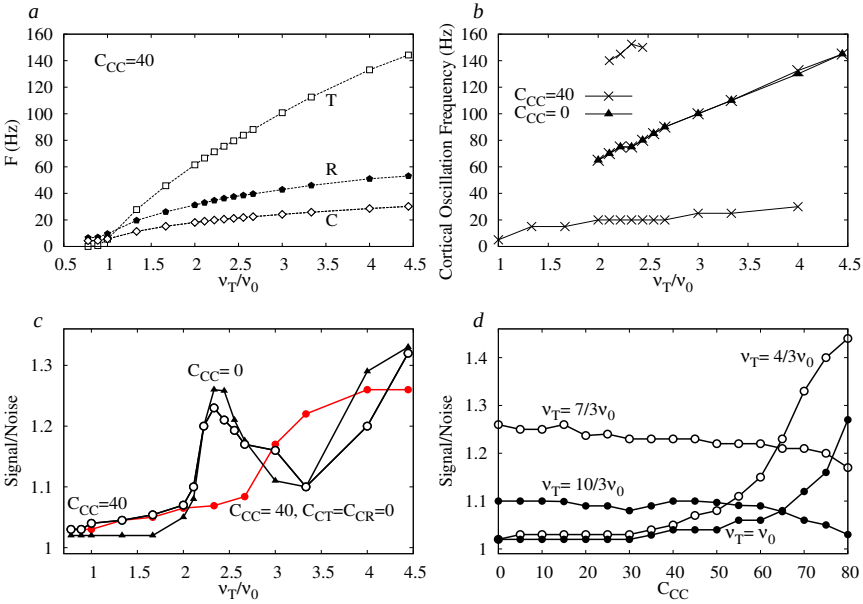

Figure 5.5: Unveiling the dynamics - 100 trials analysis. **(a)**: the mean firing rate as a function of the external input ν_T incoming into T population. **(b)**: the cortical oscillation frequency for increasing ν_T for the case of coupled and uncoupled cortical areas. The frequencies are measured from the Fourier transform of the cross-correlograms. **(c)**: SNR for two values of the cortico-cortical interaction: when the areas are coupled (open circles) and when they are uncoupled (triangles). Solid circles correspond to the SNR obtained when there is no cortical feedback ($C_{CR} = C_{CT} = 0$). **(d)**: SNR for an increasing value of the cortico-cortical interaction strength for different values of ν_T.

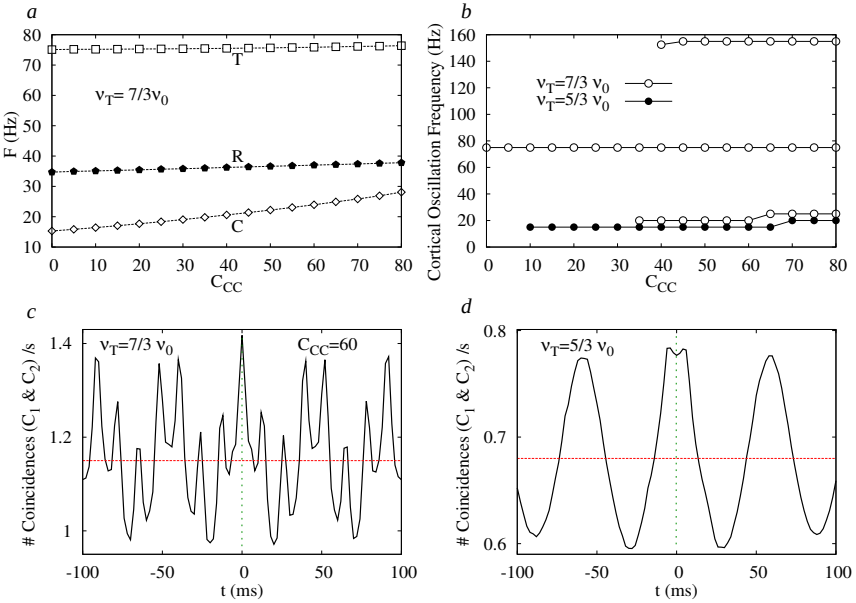

Figure 5.6: Effect of the cortico-cortical connection. Panel **(a)**: firing rate of the T, R and C areas as a function of the cortico-cortical interaction strength for $\nu_T = 7/3\nu_0$. Panel **(b)** cortical oscillation frequency vs. C_{CC} for two different values of ν_T ($5/3\nu_0$; $7/3\nu_0$). Panel **(c)**: Cross-correlogram between C_1 and C_2 areas for $C_{CC} = 60$ and $\nu_T = 7/3\nu_0$, the local maximum closest to zero are located at ±12 ms. Panel **(d)**: same as panel (c) but for $\nu_T = 5/3\nu_0$, and the maximum are not exactly at zero-lag but at ±6 ms.

response is flat but increases for large C_{CC} while it is flat but decreases for higher values of ν_T/ν_0.

5.2.2 Effect of the cortico-cortical connection

The mean firing rate F of the three neuronal populations as a function of the strength C_{CC} at an input level $\nu_T = 7/3\nu_0$ is illustrated in Fig. 5.6a. This figure shows that the cortical firing rate is indeed the most affected rate and increases monotonically with an increase in the cortico-cortical connectivity.

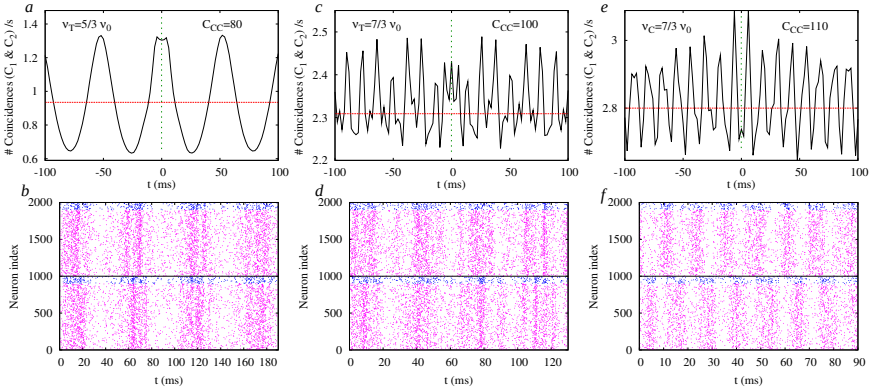

Figure 5.7: Dynamics of the cortical area as a function of the cortico-cortical interaction strength. Panel **(a)**: cross-correlogram for $\nu_T = 5/3\nu_0$ and $c_{cc} = 80$; Panel **(b)**: corresponding raster plot of all the cortical neurons in both cortical areas. Panel **(c)**: cross-correlogram for $\nu_T = 7/3\nu_0$ and $c_{cc} = 100$; Panel **(d)**: corresponding raster plot. Panel **(e)**: cross-correlogram for $\nu_T = 7/3\nu_0$ and $c_{cc} = 110$; Panel **(f)**: corresponding raster plot.

The dominant frequencies of cortical oscillations determined by the power spectrum analysis are displayed in Fig. 5.6b as a function of cortical connectivity and for two levels of external input to the thalamus. For a value $\nu_T = 5/3\nu_0$ a single frequency appears almost constant and independent of the C_{CC} strength. On the contrary, at $\nu_T = 7/3\nu_0$ three frequency components appear for $C_{CC} > 35$. Like in Fig 5.5b the lowest frequency is associated to the cortical firing rate and the intermediate frequency is associated to the firing rate of population T. The highest frequency became more important for higher values of C_{CC}. The presence of multiple oscillatory frequencies can be clearly observed in the cross-correlogram for $C_{CC} = 60$ and $\nu_T = 7/3\nu_0$ (Fig. 5.6c), whereas a single frequency component dominates the dynamics for $\nu_T = 5/3\nu_0$ (Fig. 5.6d).

The observation of the raster plots and of the cross-correlograms illustrates further the dynamics emerging from the interaction between the cortical areas. In Fig. 5.7, a and b it can be observed that for $C_{CC} = 60$ and $\nu_T = 5/3\nu_0$ the slow frequency component related to the cortical firing frequency is predominant. The peak is not sharp, at ±4 ms from the zero-lag, and a

master-slave dynamics can be observed in the region of high instantaneous firing rate (say from 50 – 80 ms after the external input onset). Multiple frequencies are observed in the raster plot and in the cross-correlogram (Fig. 5.7, c and d) for $C_{CC} = 100$ and $\nu_T = 7/3\nu_0$. In this case, both the zero-lag cortical synchronization and the leader-laggard dynamics present a strong competition. The cortico-cortical connection dominates and gives rise to an out-of-phase cortical synchronized dynamics between the two areas for very large connectivity values, e.g. $C_{CC} = 110$ as shown in Fig. 5.7, e and f. The signature of this dynamics appears both in a double peak at ±6ms (corresponding to the cortico-cortical coupling time in the cross correlation function) and in the raster plot where zero-phase synchronization does not occur between the cortical areas.

5.3 Discussion

We have presented the dynamics of a simplified thalamocortical circuit. Our results suggest that the thalamus could be a central subcortical structure that is able to trigger the emergence of zero-lag synchrony between distant cortical areas due to a dynamical relaying (Fischer et al., 2006; Vicente et al., 2008b). According to this phenomenon a central element can enable two populations to synchronize at zero-lag. Other subcortical areas, such as the brainstem (Scheller et al., 2009) and the hippocampus, are likely to play a similar role in dynamical relaying. However, the peculiar recurrent connections of the thalamic reticular nucleus (Jones, 1985; Sherman, 2005) might provide the thalamocortical circuit with specific features that do not account just for the synchronized pattern, but also for switching *On* or *Off* the asynchronous state. Furthermore, considering that large scale integration may occur as a consequence of neuronal coherence, the critical question about how the dynamical selection of integrated areas is achieved remains open (Salinas and Sejnowski, 2001; Fries, 2005; Vicente et al., 2008b; Uhlhaas et al., 2009). We suggest that an increase in the external activity fed into the T population with respect to that of R yields the cortical areas synchronize at zero-phase lag as depicted in Fig 5.3. That means the thalamus would be able to control the cortical synchronous state and regulate large scale integration. This control can occur at a fast time scale in agreement with experimental data (Fries, 2005) and without any need of plasticity or adap-

tation mechanisms which typically require longer time scales (Knoblauch and Sommer, 2004). The main input sources to T are the ascending sensory input and the descending cortico-fugal pathway, thus suggesting that both inputs may play an important role in controlling cortical synchrony. This hypothesis for the cortico-petal projections is complementary to the hypothesis of *adaptive filtering* suggested elsewhere for the cortico-fugal projections (Villa et al., 1991, 1999a; Tetko and Villa, 1997).

According to our model, see Figs. 5.5b, 5.6b, the thalamocortical circuit is able to generate fast oscillations in the frequency ranges of the beta or gamma bands triggered by an external input into the thalamus formed by independent Poisson trains. The question of how to generate such fast oscillations has been largely discussed in the literature (Traub et al., 1996; Doiron et al., 2003; Doiron et al., 2004; Börgers et al., 2005; Marinazzo et al., 2007; Börgers et al., 2008) but, as recently pointed out (Nikolić, 2009), empirical phenomena, like the cycle skipping, were not satisfactorily described. Cycle skipping is observed experimentally in our thalamocortical model when each cortical neuron spikes according to a gamma frequency modulation but with a smaller firing rate. In the raster plots of Fig. 5.3a it can be observed that few neurons spike at a given gamma cycle. Then, the oscillations are in fact shared by a whole population while single neurons skip cycles. As shown in Fig. 5.5, a and b the cortical oscillations, for instance at a signal-to-noise ratio local maximum $\nu_T \simeq \frac{7}{3}\ \nu_0$, occur at frequencies near 80 Hz for disconnected areas and in multiple frequencies for $C_{CC} = 40$, while the average firing rate is approximately $\frac{1}{4}$ of it, 20 $spikes/s$. In general, the firing rate of the cortical populations (see Figs. 5.5a, 5.6a) was found to be related to the lowest frequency component in the case of multiple frequency oscillations.

The current results emphasize the hypothesis that the thalamus could control the dynamics of the thalamocortical functional networks enabling two separated cortical areas to be either synchronized (at zero-lag) or unsynchronized. Remarkably, the cortical feedback contributes substantially to generate the collective phenomena that give rise to the robust synchrony control (Fig. 5.5c). Correlations in the output firing rate of two neurons have been shown to increase with the firing rate (de la Rocha et al., 2007). We observed that for increasing input rates (ν_T) the firing rate of all populations increases monotonically, accordingly to a sigmoidal function (Fig. 5.5a). Under the same conditions, the correlations among the cortical areas were also enhanced. However, the SNR developed a more complex pattern, namely a pronounced local maximum appeared as shown in Fig. 5.5c. König and

collaborators (König et al., 1995) reported physiological evidence of long-range synchrony with oscillations, whereas short-range synchrony may occur with or without oscillations. Our results, especially for low number of cortico-cortical inter-population synapses (say smaller than the internal connectivity), are in agreement with this finding. However, synchronization without oscillations in the local circuit may appear due to extensive sharing of common excitatory inputs which typically generates the zero-lag coincidence observed when neurons fire at high rates (de la Rocha et al., 2007). Conversely, neurons correlated by long-range connections are likely to share very few synaptic drivings, such that synchronization without oscillations should be very rare.

In order to suggest an insight of the model with the anatomical pattern of the circuit one should consider that the thalamocortical and corticothalamic projections are reciprocal to a great extent but corticothalamic projections are characterized by a dual pattern of synapses on the thalamic neurons. Small endings formed the major corticothalamic terminal field, whereas giant terminals were less numerous and formed additional terminal fields together with small terminals. (Rouiller and Welker, 2000; Takayanagi and Ojima, 2006). The modal switch of corticothalamic giant synapses controlled by background activity was recently reported (Groh et al., 2008). We speculate that this finding and our results may suggest that each pattern of corticothalamic synapse might correspond to a different function. One synaptic type might be involved in assessing the circuitry necessary for the build-up of cortico-cortical synchronization. The other synaptic type would be involved in transmitting stimulus-related information. Which is which is a question that the current study is unable to answer. We must also consider the fact that our model of individual dynamics of the integrate-and-fire neurons does not produce burst discharges (Sherman, 2001; Krahe and Gabbiani, 2004). This is a clear limitation and the inclusion of a more physiologically realistic model, as well as greater neuronal diversity (Buia and Tiesinga, 2008), are scheduled for our future work. Despite the simplification of our circuitry and the neuronal network modeling in general, the robustness of our model is a remarkable outcome of this study. The zero-lag synchronization between the cortical areas depends only on the identical axonal delays $\tau(TC)$. If these delays are not the same for all TC connections the maximum number of coincident spikes in the cross-correlograms does not occur at zero-lag but at a lag that depends on the difference between the TC time delays. However, it is worth mentioning that regional myelination, that

compensates for changes in the conduction velocity, has been reported as a mechanism that could keep constant latency between thalamus and cortex, irrespective of the distances. Moreover, our results are in agreement with the suggestion reported by (Chawla et al., 2001) about the key role of the thalamus favoring the zero-lag synchronization.

We have arbitrarily kept the external input ν_0 over R and the cortex populations fixed but we might have kept fixed T and the cortex populations with a variable external input into R (ν_R). In fact it is the dependency on the variable $\frac{\nu_T}{\nu_R}$ which represents the control key of the dynamic activity of the system as both rates of external inputs (ν_T, ν_R) are varying over time (McAlonan et al., 2008; Yu et al., 2009). The importance of uncorrelated inputs can be viewed as emphasizing the role of the so-called *background activity*, which was already reported to play an important role in controlling the thalamocortical circuit dynamic state (Wolfart et al., 2005). We are convinced that further investigations with more accurate details of the neuronal models and with embedded models of the dual cortico-fugal connectivity could provide critical clues for better understanding the mechanisms of the dynamical control subserving the synchronization of cortico-cortical distributed activity.

In conclusion, supported by extensive numerical simulations of the thalamocortical circuit, we found that the thalamus can play the role of a central subcortical area capable of facilitating zero-lag synchrony among distant cortical regions via dynamical relaying. It can also be responsible for the dynamic selection of separated cortical areas to synchronize (at zero-lag). Moreover, the system supports multiple frequency cortical oscillations when driven by uncorrelated inputs. We hope our results will guide future experiments aiming at the understanding of the thalamocortical circuit and the large-scale brain communication. Ultimately, the binding by synchrony theory might be finally tested once the zero-lag synchronization underling mechanisms are well known.

Chapter 6

Hippocampal Dynamical Relaying: Simulations and Experiment

In vivo and in vitro experiments suggest that zero-lag neuronal synchrony occurs in the brain even in the presence of large axonal conduction delays (Roelfsema et al., 1997; Rodriguez et al., 1999; Soteropoulus and Baker, 2006). From a theoretical viewpoint, modeling zero-lag synchronization in long delayed systems has typically been a challenging task. As mentioned in previous chapters, different mechanisms have been proposed to account for this phenomenon (Ermentrout and Kopell, 1998; Kopell et al., 2000; Knoblauch and Sommer, 2003). More recently, Fischer et al. (2006) introduced a novel and robust concept of synchronization via dynamical relaying. This concept suggests that two distant neuronal populations are able to synchronize at zero or near zero time lag if a third element acts as a relay between them. This relay symmetrically redistributes its incoming signals between the two other regions. Interestingly, this mechanism has proven to be remarkably robust for a broad range of conduction delays and cell types (Vicente et al., 2008b). A requirement for achieving synchrony without time lag is that the involved brain generators oscillate endogenously or

This Chapter is based on the paper: Gollo LL, Mirasso CR, Atienza M, Crespo-Garcia M, Cantero JL (2011) Theta Band Zero-Lag Long-Range Cortical Synchronization via Hippocampal Dynamical Relaying. PLoS ONE 6(3): e17756.

by coupling with other areas. In this context, the thalamus (chapter 5) has been recently proposed as a pivotal region generating isochronal gamma range synchronization between distant cortical areas by means of the dynamical relaying mechanism (Gollo et al., 2010).

Although the main generators of theta oscillations are located in the hippocampus, this oscillatory activity has been observed in many cortical and subcortical regions (Alonso and García-Austt, 1987; Leung and Borst, 1987; Mitchell and Ranck, 1980). However, none of them are capable of generating theta activity on their own (Buzsáki, 2002) despite some models of recurrent excitation predicted the generation of coherent theta oscillations in neocortical networks (Budd, 2005). Functional coupling between hippocampal and neocortical theta waves have recently been observed in rodents, likely revealing binding of cortico-hippocampal systems modulated by cognitive and behavioral demands (Tejada et al., 2010; Young and McNaughton, 2009). Long-range cortico-cortical synchrony without time lags has been previously reported between areas subserving related functions (Roelfsema et al., 1997; Murthy and Fetz, 1992), but the impact of the hippocampus on cortico-cortical theta oscillatory dynamics has been unexplored to date. We hypothesize that if the hippocampus acts as a dynamical relaying center connected to distant regions of the neocortical mantle, then the hippocampus might act as a relay station inducing zero-lag synchronization between long-distance cortical regions where theta oscillations do not appear prominently.

This chapter tests this hypothesis by modeling local field potentials (LFP) arising from the combined dendritic activity of a large number of neurons in the hippocampus and two distant cortical areas in mice either during spontaneous motor exploratory behavior (active) or motor quiescence (passive). We found that zero-lag synchronization between both cortical regions was mediated by prominent theta oscillations in the hippocampal formation in the two behavioral states, although it was enhanced during motor exploratory state, where the hippocampus has been suggested to play a critical role in sensorimotor integration (Bland and Oddie, 2001).

6.1 Results

Zero-lag long-range synchronization emerged between the anterior (frontal) and posterior (occipital) cortical regions when the amplitude of theta oscillations was prominent in the hippocampus. The cortico-cortical zero-lag correlation was approximately 45% higher in the active (when exploring) than in the passive state (when quiet), as revealed by our experimental and modeling results. The theta oscillations recorded in the hippocampus (relay element) were delayed by 30 ms, which is a strong signature of the dynamical relaying phenomenon (Fischer et al., 2006; Vicente et al., 2008b; Gollo et al., 2010).

In the following, we show results obtained from numerical simulations and LFP recorded data. We start by analyzing the neuronal population dynamics and show how theta frequency emerges in the system. Then, we simulate synchronization patterns within the neocortical-hippocampal circuit in passive and active states. Finally, we compare the simulations with the experimental data.

6.1.1 Modeling theta oscillations generated in the hippocampus

We modeled the hippocampus and the frontal and occipital cortices. Each area contains 500 sparse and randomly connected neurons described by the Izhikevich model (Izhikevich, 2003). This model uses two variables: the membrane potential v and a recovery variable u, associated with slow ion channels. We assume that, within each area, 80% of the neurons project excitatory synapses (AMPA) and 20% inhibitory synapses (GABA). Synapses are mathematically described in equation (4) (see Materials and Methods section). Each neuron in the hippocampus (cortical areas) is assumed to receive 35 (50) synaptic inputs from randomly chosen neurons of the same area with negligible conduction delay. The connectivity between areas is considered even sparser. Neurons of a given area are innervated by three excitatory synapses with long conduction delays (8-20 ms) from each of the other areas. The ultimate goal of the model is to compare the neuronal activity of the three areas during the active moving and passive quiescent

motor behavioral states. The active state is modeled by assuming a 6% larger external driving over the hippocampus with respect to the cortical areas. This is obtained by increasing the Poisson rate of the external driving.

The capacity of the rodent hippocampus to generate theta oscillatory activity is well documented (Buzsáki, 2002; Buzsáki et al., 2003; Leung, 1998; Goutagny et al., 2009). Our model assumes that the hippocampus is mainly composed of neurons operating in a burst regime whose activity is modulated by slow theta oscillations (frequency range from 6.5-7.5 Hz) and an interspike frequency of 35-45 Hz. We consider that most neurons in the cortical areas fire in the regular spiking regime. Diversity within each population is added to the internal neuronal parameters of the model (see Materials and Methods section). The spiking activities of the different regions are illustrated in Fig. 6.1. Time traces of ten randomly chosen neurons, eight excitatory (black) and two inhibitory (gray), are plotted in Figs. 6.1 A to F, corresponding to the hippocampus (A & D) and the visual (B & E) and frontal (C & F) cortical regions, respectively. In panels A to C, neurons are completely disconnected from each other, at both global and local levels. The lack of correlation between neuronal activities was due to the assumed random initial conditions. When neurons are coupled within each population, keeping the inter-population coupling strength equals to zero, hippocampal neurons start to synchronize, as displayed in panel G. This synchronization pattern gives rise to a theta oscillation reflected in the time evolution of the average membrane potential shown in panel G. On the contrary, cortical neurons do not fire synchronously, as illustrated in panels E and F, resulting in an almost flat time trace of the average membrane potential (panel G). This behavior is also evident in the raster plots shown in panel H. To determine the level of synchronization, we computed the auto-correlation function as the number of spike coincidences of neurons belonging to the same population (bins of 2 ms), subtracted from the number of coincidences expected by chance, as shown in Fig. 6.1 I. A coherent behavior was observed in the hippocampus, but not in the cortical areas.

6.1.2 Dynamical relaying in the theta range

Results from our model predict the emergence of zero-lag synchronization between frontal and occipital cortices, but not between the cortical regions and the hippocampus when the long-range connection is switched on (this will be discussed later). The proposed reduced model, as will be shown

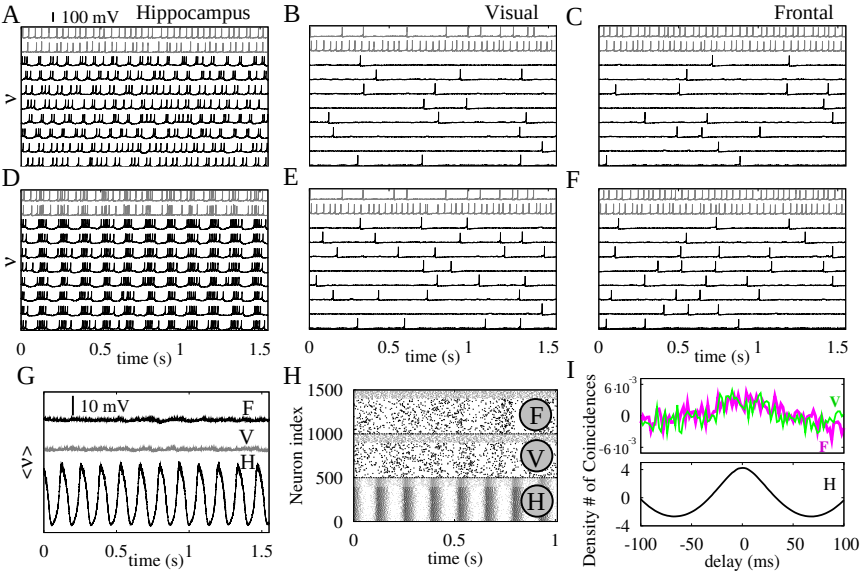

Figure 6.1: Dynamical characterization of the hippocampus and cortical regions during the generation of theta oscillations. Panels A, B and C show the voltage v time traces of 10 randomly chosen neurons (8 excitatory in black and 2 inhibitory in grey) of each population in the absence of local and long-range connections. Panels D, E and F show the same time traces of neurons locally connected within each population. Panel G shows the ensemble average voltage v of each area: Frontal cortex (F), Visual cortex (V) and the Hippocampus (H). Panel H shows raster plots. Panel I shows an average number of coincident spikes of neuron pairs of the same population, obtained from the auto-correlation function and subtracted from the mean number of coincidences over the delay window. The upper figure in panel I displays cortical groups while the bottom figure stands for the hippocampus. External driving to each neuron is given by 100 independent excitatory neurons spiking according to a Poisson distribution with average rate r = 16.3 Hz.

below, captures the main features observed experimentally. A large-scale integration is maintained by interconnecting the cortical populations and the hippocampus via long-range fibers, with large conducting delays. Our simple motif depicted in Fig. 6.2 A, is sufficient to reproduce the two behavioral states. In the model, the difference between the two states is on the Poisson rate of the external driving. Both states present zero-lag synchronization between cortical areas as revealed by the mean-voltage time traces represented in Figs. 6.2 B and C, as well as in the raster plots (Figs. 6.2 D and E). In the network, cortical activity becomes locally synchronized due to theta oscillations generated in the hippocampus, when both the internal and long-range connections between the different areas are active. Raster plots also reveal the presence of two different groups of neuronal activity in each area: one of excitatory neurons (black) and the other of inhibitory ones (gray). Unlike neural assemblies in the two cortical areas that synchronize at zero-lag, neural activity in the hippocampus was phase locked, but shifted with the activity in cortical neurons.

6.1.3 Large-scale motifs

Our choice of motif is not arbitrary. From a physiological point of view, recurrent connections among the three involved areas are expected. From the modeling point of view other options could be considered. One possibility is to couple bidirectionally only the two cortical areas, as suggested in ref. (Ermentrout and Kopell, 1998). However, in this scenario the out-of-phase solution is the one that appears more often (Vicente et al., 2008b). Moreover, for our parameter values, the two areas do not synchronize (Fig. 6.3 A-C). It is worth stressing that theta oscillations are not observed in either these cortical areas. We have also tested a motif with unidirectional coupling between the hippocampus and the cortices, keeping the two cortical regions bidirectionally connected. As shown in Fig. 6.3 D-F, this motif does not yield zero-lag synchronization among cortical areas when using the same parameter values. The motif that yields the most robust results is the one chosen in the present study, as depicted in Fig. 6.3 G-I.

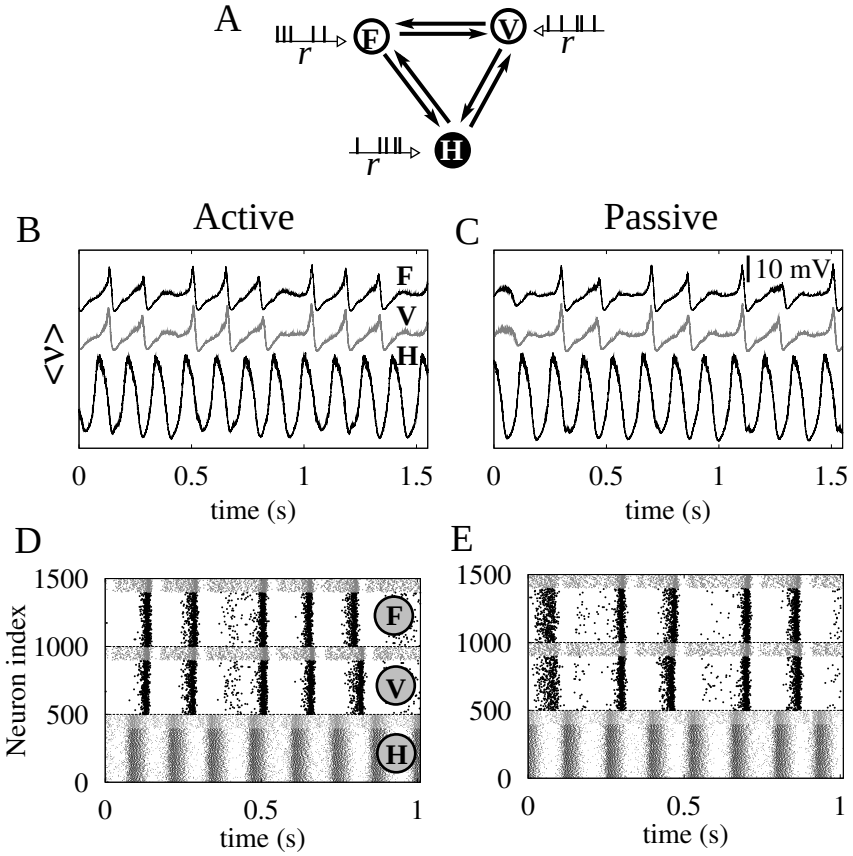

Figure 6.2: Modeling neuronal dynamics underlying passive and active behavioral states. Panel A represents the simple motif connecting the brain regions F, V and H. Each neuron is driven by an independent Poisson process of rate r = 16.3 Hz (r = 15.4 Hz) for the active (passive) state. In panels B and C, the ensemble average voltage for the passive and active states are plot respectively. Panels D and E include the corresponding raster plots.

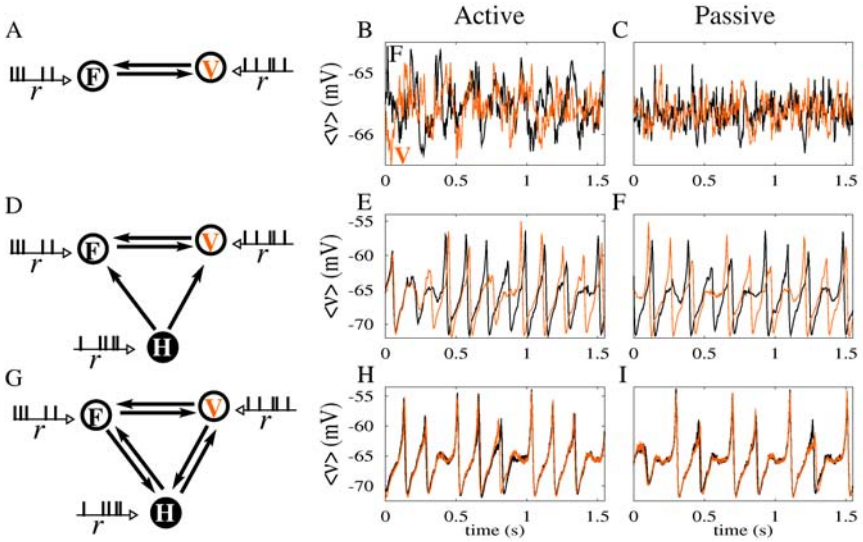

Figure 6.3: Zero-lag cortico-cortical synchronization for different motifs. Simulation results for the ensemble average voltage of the cortical regions are shown for two external drives corresponding to the active (r = 16.3 Hz) and passive (r = 15.4 Hz) states. Regardless of the behavioral state, we found that the two cortical areas (frontal and visual) do not synchronize at zero-lag when mutually connected without the hippocampal relay (panels A-C). Neither we observed zero-lag synchronization when only the hippocampus drives them (panels D-F). The cortical feedback to the hippocampus (as depicted in panel G) is critical to promote zero-lag cortico-cortical synchronization, as depicted in panels H and I.

6.1.4 Zero-lag synchrony is enhanced during motor exploratory behavior

The reduced model proposed here is justified due to the remarkable equivalence with the experimental data in neocortical-hippocampal neuronal systems during both behavioral states. Although our simulations might only reveal a keen difference for the two states, we demonstrate that noticeable differences are present. With both simulated and experimental data, we proceeded as follows. First, the LFP time traces (for the experimental data) and the ensemble average membrane potential (in the simulations) were filtered around the dominant frequency of theta oscillations recorded in the hippocampus (6.5-7.5 Hz). Next the cross-correlogram of the resulting signals of two different areas was performed within a 300-ms window with delays varying from -300 to 300 ms. The time series were shifted by 50 ms to account for the experimental data variability; the procedure was repeated to cover the 60 s time series. The delay corresponding to the maximum of each cross-correlogram window reflects the best suitable coupling delay between the two areas. This delay was used to compute a normalized peak density of the sliding window cross-correlogram. The result represents the probability of finding the best coupling between different areas occurring at a given time delay.

Following this procedure, we compared the simulated and experimental data for the two behavioral states. A wider and less precise phase locking in the passive condition was observed in both cases. Results in the active state appeared to be more coherent, with higher values in the cross-correlograms (Fig. 6.4). In particular, the two cortical areas were mostly synchronized at zero-lag whereas the hippocampus was typically delayed by 15-30 ms in the active state, and by 15-45 ms in the passive state. The maximum correlation with zero-lag occurred with a probability 45% larger in the active state than in the passive state, the latter showing a larger variability in its activity pattern (Churchland et al., 2010). Synchronization levels between the hippocampus and the cortical areas were also more consistent during active exploration when compared to motor quiescence. Simulations were in remarkably good agreement with our experimental LFP recordings. However, cross-correlograms between the hippocampus and the cortical areas peaked at the same delay value in the model due to the symmetry assumed in the conduction delays between these areas. We obtained even closer results to the experimental ones in the simulations when considering asymmetric

conduction delays (of the order of few ms) between the hippocampus and the cortical areas (Fig. 6.5).

6.2 Discussion

Although a large body of studies has evaluated the hippocampal-neocortical circuitry underlying theta oscillations (Young and McNaughton, 2009; Siapas et al., 2005; Jones and Wilson, 2005a,b; Hyman et al., 2005; Cantero et al., 2003; Paz et al., 2008; Doyère et al., 1993; Hasselmo, 2005; Koene et al., 2003; McIntosh, 1999; Ranganath and d'Esposito, 2005; Vertes, 2006; Wall and Messier, 2001; Wang et al., 2010a; Hyman et al., 2010), the mechanisms responsible for inducing coherent activity in these regions remain elusive to date (Hyman et al., 2010). The present study gives a step further by suggesting that these interactions may facilitate communication between distant cortical regions. By borrowing concepts from the dynamical relaying framework, we have studied the impact of hippocampal theta oscillations on cortico-cortical functional coupling in mice during motor quiescent, and while actively exploring the environment. Modeling results showed that zero-lag synchronization between distant cortical regions increased simultaneously with hippocampal theta oscillations in both behavioral states, although cortico-cortical coherence was mainly enhanced during motor exploratory behavior. LFPs recorded from the same brain regions and during the same behavioral states qualitatively confirmed these results. Overall, these findings suggest that the observed zero-lag cortico-cortical synchronization is likely modulated by the hippocampus in lower mammals as a function of cognitive demands and motor acts.

6.2.1 The role of hippocampal theta oscillations in long-range synchronization

The numerical results obtained from the simple model suggest that theta oscillations are critical for a long-range integration between the hippocampus and the cortical areas, especially when the animal is exploring the environment. We speculate, based on the dynamical relaying mechanism, that theta oscillations should participate if the hippocampus acts as the relay station

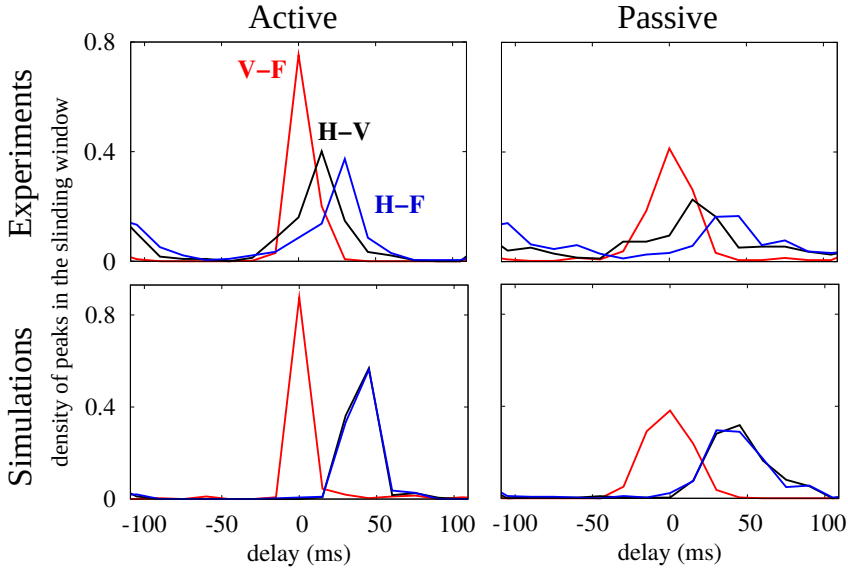

Figure 6.4: Spatio-temporal synchronization obtained from the experimental and numerical data. We plot here the density of spikes in the sliding window of filtered time series cross-correlation (see Materials and Methods section). The window has 300 ms length and is shifted by 50 ms steps and analyzed over the 60-s of continuous artifact-free LFP recordings for each behavioral state and animal (n = 4), separately. Results are normalized in a frame of -110 to 110 ms. Experimental data correspond, in this example, to an individual mouse, although other mice presented qualitatively similar results. Simulations show high agreement with experimental results for both active and passive behavioral states.

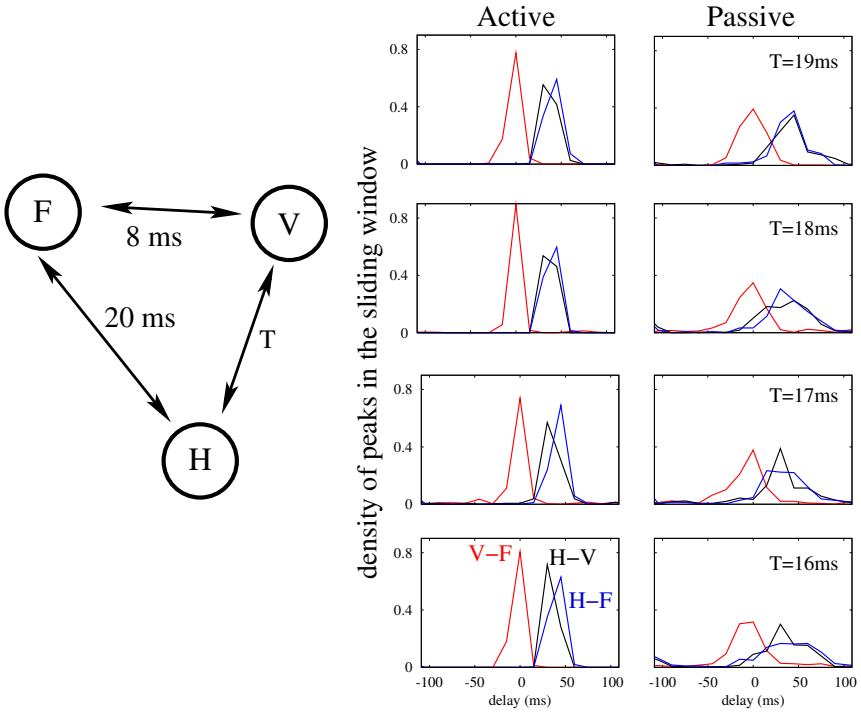

Figure 6.5: Effects of an asymmetric delay time in the inter-population couplings. If the delay time between the hippocampus and the visual area (T in the figure) is slightly different from that between the hippocampus and the frontal area (20 ms), the maxima of the cross-correlations between the hippocampus and the cortical areas become different, as shown in the experiments (Fig. 6.4, upper panels).

that putatively facilitates zero-lag synchrony between distant cortical areas. Interestingly, our results suggest the possible coexistence of dynamical relaying in different frequency bands, for example in a gamma range (Vicente et al., 2008b), which could be mediated by the thalamus (Gollo et al., 2010) or other cortical areas (Chawla et al., 2001). A better understanding of the synchronization in distinct frequency bands is however necessary.

6.2.2 Dynamical relaying and phase relation

A typical fingerprint of the dynamical relaying mechanism in neuronal systems connected via significant delays is the zero-lag synchrony coexisting with the out of phase synchrony between the relay element and the other two areas (Fischer et al., 2006; Vicente et al., 2008b; Gollo et al., 2010). The novelty of our study with respect to others lies in the inclusion of the occipital cortex in addition to the frontal cortex and the hippocampus. The occipital cortex represents the major source of visual inputs to the hippocampus, and is a key cerebral structure for the formation of spatial memories. Evidence shows that theta-burst stimulation of the thalamocortical pathways leads to a long-term enhancement of granule cell excitability in the hippocampus, preceded by a concurrent potentiation of the visual cortex response. The theta power in the dentate gyrus increases after tetanization-driven high-frequency rhythms in V1. This sequence of events has been suggested to facilitate synaptic plasticity in the hippocampus of the freely behaving rat (Tsanov and Manahan-Vaughan, 2009). Theta oscillations recorded over posterior neocortical regions during wakefulness have been further postulated as reliable markers of the homeostatic process of sleep regulation in the rat, suggesting that theta waves might have independent cortical generators over the parieto-occipital regions (Vyazovskiy and Tobler, 2005).

It is broadly accepted that hippocampal theta oscillations play a crucial role in sensorimotor integration (Bland and Oddie, 2001) and memory formation (Crespo-Garcia et al., 2010; Yamaguchi et al., 2004). For this endeavor, a precise spiking time is needed. In the context of theta rhythms, the oscillatory phase coupling has recently been proposed to enhance the efficiency of spike-time dependent plasticity (Masquelier et al., 2009). The coordination of neuronal assemblies over distant regions could be critically dependent on the increased oscillatory phase coupling (Canolty et al., 2010), playing a role in the cortico-hippocampal circuit for memory formation. For both sensorimotor integration and memory formation, the hippocampus requires inputs

from other regions typically involved in the automatic and voluntary control of attention. Accordingly, memory recollection has been supported by a distributed synchronous theta network including the prefrontal, mediotemporal and visual areas (Guderian and Duzel, 2005). Based on our findings, we speculate that an enhancement of long-range cortico-cortical synchronization patterns mediated by the hippocampus might facilitate the integration of these top-down and bottom-up control mechanisms of attention.

6.2.3 Local field potentials recorded from hippocampus and neocortex: the role of volume conduction

Zero-lag synchronization between cortical regions simultaneously with hippocampal theta oscillations could be due to hippocampal-volume conducted theta. Although concerns about volume conduction are significant in our study, converging evidence also points against this possibility. For instance, Katzner and colleagues (Katzner et al., 2009) found that the major part of the LFP recorded signal (>95%) spreads within 250 μm from the recording electrode, suggesting that the origin of LFPs is more local than often recognized. Moreover, as recently reviewed by Pesaran (2010), simultaneous LFP recordings have been extensively used to evaluate the relationship between distant areas including, for instance, the prefrontal and visual cortices (Gregoriou et al., 2009), the prefrontal and parietal cortices (Buschman and Miller, 2007) or the hippocampus and the prefrontal cortex (Siapas et al., 2005).

Theta waves recorded in the frontal cortex could be volume-conducted from the olfactory bulb rather than intrinsically generated in the frontal region. Although this hypothesis is conceivable, previous studies have provided strong evidence of theta synchronization patterns between the frontal cortex and the hippocampus (Siapas et al., 2005). Due to the course-grained nature of our experimental data, we do not have access to the individual neuronal spikes. However, after a filtering procedure, the data indicate that the hippocampus is delayed with respect to the cortical areas.

6.2.4 Final remarks

We have studied the occurrence of zero-lag synchronization between distant cortical regions. Using a simple model where two cortical areas are both directly connected and indirectly through the hippocampal relay, we

find that the activities in these regions become synchronized in the theta range in freely behaving mice. Our results suggest that the hippocampus might act as a dynamical-relaying element that mediates zero-lag synchronization between the cortico-cortical regions, during active and passive behavioral states. Simulated and experimental data showed that this zero-lag synchronization between two distant remote cortical regions occurs simultaneously with prominent theta oscillations in the hippocampus in both behavioral states, but it is significantly enhanced during exploratory motor behavior. These findings could provide an alternative explanation to the observed zero-lag relationship between distant cortical regions mediated by hippocampal theta oscillations.

6.3 Materials and Methods

6.3.1 Modeling theta synchronization in large-scale systems

We aimed at modeling theta synchronization patterns of the hippocampus, and the frontal and visual cortices supporting the emergent coherent behavior associated to spontaneous exploratory motor behavior and motor quiescence, separately. To this end, we considered three neuronal populations composed of 500 randomly connected neurons, 80% excitatory and 20% inhibitory, with excitatory innervating monosynaptic pathways linking any two of the three regions. We modeled excitatory and inhibitory neurons of the two cortical areas with the following set of equations (Izhikevich, 2003, 2007):

$$\begin{aligned} \frac{dv}{dt} &= 0.04v^2 + 5v + 140 - u + I_{syn}\,, \\ \frac{du}{dt} &= a(bv - u)\,, \end{aligned} \tag{6.1}$$

where v is the neuron's membrane potential, u is the recovery variable that accounts for the K+ and Na+ ionic currents and I_syn the total synaptic current. When the membrane potential reached the 30 mV value, v is reset to c and u to u+d. For excitatory neurons, we take the parameters (a,b) = (0.02,

0.2) and (c,d) = (-65,8)+(15,-6) σ^2, where σ is a uniformly distributed random variable within the interval (0,1). According to this distribution, cortical excitatory neurons operate in the regular spiking, in the intrinsically bursting, or in the chattering modes (Izhikevich et al., 2004). For inhibitory neurons, we assume the parameters (a,b) = (0.02, 0.25)+(0.08,-0.05) σ and (c,d) = (-65,2). These parameter values correspond to fast spiking and low-threshold spiking firing modes. With similar computational costs, excitatory neurons of the hippocampus are described with a slightly modified set of equations, specifically calibrated to reproduce the hippocampal CA1 pyramidal neurons dynamics (Izhikevich, 2007):

$$\begin{aligned} \frac{dv}{dt} &= 0.01v^2 + 105v + 27 - 0.02u + I_{syn}\,, \\ \frac{du}{dt} &= 0.02[0.5(v+60) - u)]\,. \end{aligned} \tag{6.2}$$

In this case, when v reached the value 40 mV, v and u are reset as described previously, the parameters are (c,d) = (-50,50)+(15,10)σ. This choice favors the bursting mode rather than the regular spiking regime (Izhikevich et al., 2004; Su et al., 2001). Inhibitory neurons of the hippocampus are also modeled with the set of equations (1), using identical parameters as for inhibitory neurons of the cortical regions. Nevertheless, we have checked that different distributions of parameters yielded similar results. Each neuron receives the same number of synapses from randomly selected neighbors of the same population (50 for the cortical populations which means a 10% connectivity, and 35 for the hippocampus, i.e., with a 7% of connectivity), and three long-range excitatory synapses from excitatory neurons randomly selected from the other populations. The local connectivity is composed of both excitatory and inhibitory synapses depending on the neuron type. Excitatory neurons project excitatory synapses and inhibitory neurons project inhibitory synapses. Each region corresponds to a coursed grained brain region, which is recurrently connected. Such connectivity (depicted in Fig. 6.2 A) composes a bidirectional triangular motif of the three regions of interest. The simple motif connection is satisfied only on the large scale. At the neuronal level, the connectivity is different.

The synaptic current is given by:

$$I_{syn} = -v g_{AMPA}(t) - (65+v) g_{GABA}(t)\,, \tag{6.3}$$

and the synaptic dynamics are described by:

$$\begin{aligned} \tau_{AMPA}\frac{dg_{AMPA}}{dt} &= -g_{AMPA} + 0.5\sum_{k}\delta(t - t_k - \tau_k)\,, \\ \tau_{GABA}\frac{dg_{GABA}}{dt} &= -g_{GABA} + 0.5\sum_{l}\delta(t - t_l)\,. \end{aligned} \tag{6.4}$$

where δ stands for the Dirac delta function. The summation over k (l) stands for excitatory (inhibitory) neighbor contributions. $t_k(t_l)$ is the time at which excitatory (inhibitory) firings occur in the presynaptic neurons. Conduction delays τ_k, associated to excitatory long-range connections, are assumed to be 8 ms for cortico-cortical connections and 20 ms for the connections between the cortical regions and the hippocampus. Synapses are modeled by exponential decay functions (Dayan and Abbott, 2001) with time constants $\tau_{AMPA} = 5.26$ ms for excitatory and $\tau_{GABA} = 5.6$ ms for inhibitory synapses (other decay times produced qualitatively similar results). Each population is subject to an external driving given by independent Poisson spike trains, resulting from 100 excitatory neurons, at rate r = 15.4 Hz on each neuron in the passive state, and 16.3 Hz in the active state. The equations were integrated using a fixed-step first-order Euler method with time steps of 0.05 ms.

When modeling neuronal dynamics, it is always desirable to use simple, but biologically realistic, models. The non-linear equations used in this study are rather simple but allow at the same time for some flexibility. They were derived and adjusted to fit certain behaviors: regular spiking, intrinsically bursting, chattering modes, fast spiking or low-threshold spiking. The population of spiking neurons approach gives rise to a robust dynamic and the possibility to compare with experiments at different spatial scales. It has been shown to be suitable for studying general dynamical patterns (Zhou et al., 2006; Izhikevich and Edelman, 2008) and zero-lag synchronization (Vicente et al., 2008b; Gollo et al., 2010). Utilizing the same neuronal model with a different set of parameters, arbitrary but specifically calibrated to reproduce the diverse dynamics of existing neurons, the isolated hippocampus generates theta rhythms as experimentally observed (Goutagny et al., 2009). In contrast, isolated cortical areas do not develop prominent theta oscillations, however, the emergence of these oscillations witnessed by the presence of the hippocampal relay. Parameters responsible for population and inter-population couplings were chosen to reproduce the dynamical

regimes observed in the experiments. This set of parameters is not considered unique. Canonical models are also expected to be useful to study the dynamical relaying mechanisms with the advantage of being more comprehensible although less biologically plausible.

6.3.2 Modeling theta synchronization in different behavioral states

In our model, differences between active and passive states are attributed to the rate of the uncorrelated external drives. We assume that when the animal is performing the exploratory task, not only the regions of interest are active but also many other regions contribute. On the contrary, during motor quiescence, we assume that a smaller number of regions are involved, and consequently the total external driving is considerably weaker. The possibility that an increased background activity accounts for a model transition is sustained by the increased scale-free activity found in the cortex during cognition (Miller et al., 2009), and is also consistent with the proposal that the external driving over the thalamus is a key element to control the engaging and disengaging of a zero-lag cortical synchronization (Gollo et al., 2010). The dynamical relaying mechanism is remarkably robust to reproduce the observed patterns, although similar results could also be obtained in other ways. We have checked, for instance, that using a correlated external driving or by changing the coupling strength among neurons (either for intra-population connectivity, for inter-population synapses, or for both of them) yielded qualitatively similar results (data not shown).

6.3.3 Synchronization measurements from correlation function

Our results described theta synchronization patterns between the cortical areas and the hippocampus during different behavioral states in the alert animal. We used correlation analyses to determine the level of synchrony of the hippocampus-neocortical and cortico-cortical networks, separately. Data were analyzed from the time series using both ensemble average voltage and spike time coincidences. The mean voltage of the time series is filtered in the dominant frequencies of the spectrum corresponding to the theta band (from 6.5 to 7.5 Hz), and the cross-correlation function is com-

puted via a sliding window of 300 ms width, displaced 50 ms from each other over the 60-s of continuous artifact-free LFP recordings for each behavioral state and mouse, separately. The cross-correlation between two areas A1-A2 as a function of the delay d is defined as:

$$R_{A1A2}(d) = \frac{\langle [a_1(t) - \langle a_1 \rangle][a_2(t-d) - \langle a_2 \rangle] \rangle}{\sqrt{[\langle a_1(t)^2 \rangle - \langle a_1 \rangle^2][\langle a_2(t-d)^2 \rangle - \langle a_2 \rangle^2]}}, \tag{6.5}$$

where a1 and a2 correspond to the LFP time series (ensemble average membrane potential over a population) in the experiments (simulations), and the brackets $\langle \cdot \rangle$ stand for the time average computed for each window. The delays corresponding to the maximum peak of the cross-correlation in each window are displayed in a normalized histogram window with times ranging from -110 to 110 ms. Furthermore, in the simulations, the number of spike coincidences is measured from the activity of neurons belonging to the same population (auto-correlation) within a 2 s time interval. The cross-correlation function is calculated in bins of 2 ms for a sample of 50,000 pairs of randomly chosen neurons.

6.3.4 Experimental protocol

All the experiments were carried out according to EU (2003/65/CE) and Spanish (BOE 252/34367-91, 2005) guidelines for the care and use of laboratory animals for chronic experiments. The experimental protocols were previously approved by the Ethics Committee of the University Pablo de Olavide (permit number 07/2). Mice (n = 4, 5 months old) were implanted with electrodes in the CA1 subfield of the hippocampal formation, and in two distant neocortical regions (frontal and occipital cortex) under stereotaxic guidance. The reference electrode was located above the cerebellum (1 mm posterior to lambda on midline). Following experiments, mice were deeply anesthetized with a lethal dose of Nembutal. To verify the electrode placement, sections were mounted on gelatin-coated slides, stained with the Nissl method, dehydrated, and studied with light microscopy.

LFPs were recorded in the animal's home cage with a sampling rate of 200 Hz. 60-s of continuous artifact-free LFP recordings, selected both during exploratory motor behavior (active state) and motor quiescence (passive state) in each animal. The running speed was similar in both groups of mice. The averaged spectral power was estimated by applying the Welch's modified

periodogram method (4-s segments, 1 Hz resolution, 50% overlapping, and Hanning windowing) to selected LFP recordings in each LFP derivation. The theta (5-11 Hz) peak frequency was identified as the maximum spectral power value for each cerebral site and animal, separately, by using custom scripts written for Matlab v. 7.4 (The MathWorks Inc., Natick, MA).

Chapter 7

Resonance-Induced Synchronization

The study of large-scale brain dynamics, and the cortical networks on which they unfold, is a very active research area, providing new insights into the mechanisms of functional integration and complementing the traditional focus on functional specialization in the brain (Friston, 2011). Whilst progress towards understanding the underlying network structure has been impressive (Bullmore and Sporns, 2009; Sporns, 2010), the emergent network dynamics and the constraints exerted on these dynamics by the network structure remain poorly understood. The problem is certainly not straightforward, as the dynamics between just a pair of neural regions already depends critically on the nature of the local dynamics and the connections between them: Although non-trivial, a complete description of nonlinear dynamics between a pair of nodes is nonetheless typically possible. However, aggregating such duplets into larger arrays and introducing noise and time delays leads to further challenges and prohibits an exact description of the precise functional repertoire, motivating recourse to the broader objective of finding unifying and simplifying principles. Structural and functional motifs - small subnetworks of larger complex systems - represent such a principle (Milo et al., 2002). They characterize an intermediate scale of organization between individual nodes and large-scale networks, that may play a crucial role as elementary building blocks of many biological systems. Motif distribution in cortical networks has also been shown to be

highly non-random, with a small set of motifs that appear to be significantly enriched in brain networks (Sporns and Kotter, 2004). These motifs play distinct roles in supporting various computational processes. In this report we examine the types of neuronal dynamics that emerge on small motifs and consider their putative role in neuronal function.

The mechanisms supporting zero-lag synchrony between spatially remote cortical regions can be considered paradigmatic of those mediating between structure and function. Since first reported in cat visual cortex (Roelfsema et al., 1997), zero-lag synchrony has been widely documented in empirical data and ascribed a range of crucial neuronal functions, from perceptual integration to the execution of coordinated motor behaviors (Singer, 1999; Varela et al., 2001; Uhlhaas et al., 2009). In particular, zero-lag synchrony between populations of neurons (through synchrony between the local field potentials) may play a crucial role in aligning packets of spikes into critical windows to maximize the reliability of information transmission at the neuronal level, and to bring mis-aligned spikes into the time window of spike-time-dependent plasticity. The situation is particularly pertinent in sensory systems, where very slight differences in input timing, between left and right cortex for example, may carry crucial information concerning the spatial location of the perceptual source. However, a significant problem arises because two oscillators interacting through a time-delayed connection do not, in general, exhibit zero-lag synchrony. In particular, the presence of a reciprocal delay introduces a *frustration* into the system such that zero-lag synchrony is unstable and anti-phase synchrony is instead the preferred dynamic relationship. More formally, anti-phase synchrony has a lower minimum in the variational energy landscape than zero-lag synchrony in oscillator pairs coupled through a time-delayed connection. When the coupling is unidirectional, zero-lag synchrony is not a dynamical solution at all.

Complex dynamics in spatially extended systems arise in a broad variety of other physical and biological contexts. Because of their extraordinary internal speed, even the small time delays due to the finite speed of light are non-negligible in arrays of coupled lasers. Unlike the brain, laser arrays allow almost complete experimental manipulation, hence permitting mechanistic - and not just observational - inferences to be drawn. Detailed analysis of delay-coupled laser systems has suggested that an intermediate and reciprocally coupled relay node in a motif of three nodes could represent a general mechanism for promoting zero-lag synchrony in delay-

coupled systems (Fischer et al., 2006). In previous chapters, we showed that such motif arrangements also represent a candidate mechanism for zero-lag synchrony in delay-coupled neuronal systems (Fischer et al., 2006; Vicente et al., 2007, 2008b, 2009; Gollo et al., 2010, 2011). This is encouraging because there exist several candidate neuronal circuits in the mammalian brain which are characterized by reciprocal coupling between an intermediate delay node, including corticothalamic loops (Vicente et al., 2008b, 2009; Gollo et al., 2010) and the hippocampal-cortical circuit (Gollo et al., 2011). There also exist strong reciprocal connections in the visual system, such as the heavily myelinated connections between primary visual cortex and the frontal eye fields. Indeed, the corresponding motif occurs disproportionally in mammalian cortex, hence being embedded in many cortical subsystems.

Here we undertake a systematic study of the patterns of neuronal synchrony that arise on delay-coupled structural motifs. We find that common driving - a coupling arrangement that is widely invoked in the literature - is in fact an inefficient means of inducing zero-lag synchrony at the weak-coupling regime. However, when present in a larger structural motif the existence of a single resonant pair, a reciprocal coupling arrangement - which causes anti-phase synchrony - is found to be a novel and efficient way of promoting zero-lag synchrony amongst other members of the subnetwork. This effect, which we term resonance-induced synchrony consistently arises in computational models at the neuronal, population and mesoscopic spatial scales and is robust to mismatches in system parameters, to stochastic input, for a surprisingly large range of coupling strength, and even to meaningful time delays. Remarkably, we show that the resonance effects of an anti-phase synchronized pair are not necessarily localized, but may instead propagate throughout the network. Hence, based on our results in neuronal systems, we propose the resonance-induced synchrony as a generalized and unifying mechanism of facilitating zero-lag synchrony.

7.1 Common driving versus other motifs

In thought experiments, common driving was consider as a trivial means to entail neuronal synchronization, say, for example, by shared input through bifurcating axons (Singer, 1999). Certainly, point-process input of sufficient

intensity can generate virtually perfect synchronization. Apart from such extreme conditions, however, the intuitive transparency fades. Far from being as trivial as presumably assumed, the common drive scenario spurred numerous recent studies (de la Rocha et al., 2007; Shea-Brown et al., 2008; Renart et al., 2010; Barreiro et al., 2010; Tchumatchenko et al., 2010). Here, in turn, instead of focusing on the statistical properties of the input signal to synchronize the commonly driven elements, we followed a network approach to address: How the connectivity between the elements affects the efficacy to synchronize the commonly driven elements.

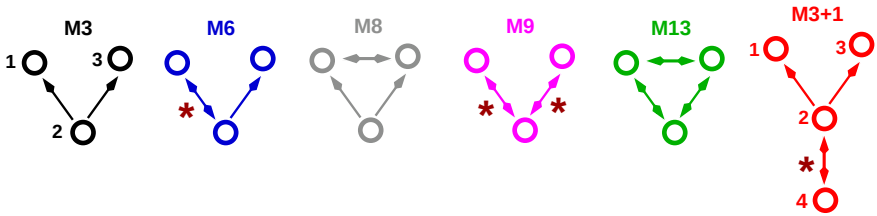

Figure 7.1: Different types of common-driving motifs. Bidirectional connections in the presence of delay generate potential resonant pairs, a pair nodes synchronized in anti-phase. The red stars indicate active resonant pairs that play a role of a resonance source to promote zero-lag synchronization between nodes 1 and 3.

As an artifice to isolate the particular behavior of interest, we explored several reduced common-driving motifs that are found abundantly in large-scale networks, including the brain. Figure 7.1 depicts the motifs comprised of three nodes, whose notation (M3, M6, M8, M9, M13) was adopted analogously to (Sporns and Kotter, 2004), and an additional motif of four nodes (M3+1), which, as we shall show, was proven specially suitable to illustrate the resonance-induced synchronization. For the sake of clarity, we assumed homogeneous delays in the motifs, i.e., all connections had the same delay. Moreover, for these motifs, we considered node 2 as the driver node, and nodes 1 and 3 as the driven nodes. The genuine common-driving motif was designated M3, whereas the other motifs represented minute structural variations of the M3. In particular, M9 is the prototypal motif of the dynamical-relaying motif (Fischer et al., 2006). This was also one of the prime structures studied in chapters 4, and 5. M13 was one of the prime structures studied in chapters 5 and 6. However, in both chapters a mis-

match of the driver node was enough to guarantee the symmetry breaking necessary to avoid the frustrated dynamics (see section 3.2.4). M8 was one structure utilized in chapters 5 and 6 to illustrate the importance of the feedback connection to the driver node since the zero-lag synchronization in this case showed highly impaired, like shown in Figs. 5.5 and 6.3.

7.2 Pair of anti-phase synchronized nodes

The novel and most important concept introduced in Fig. 7.1 corresponds to the resonant pair of nodes, which induces zero-lag synchronization of the driven nodes. The resonant pair of nodes are highlighted by the red star whenever present in the motifs.

We have previously described the dynamics of two Hodgkin-Huxley neurons delayed-connected to each other (see Fig. 3.3). A similar behavior also occurred for other systems. Figure 7.2, for example, illustrates the dynamics of two neural mass models (described in section 7.7.3) for distinct types of connectivity: bidirectional connection (top panel), unidirectional connection (middle panel), disconnection (bottom panel). As it will be shown in the following sections, when a certain node A drives other two nodes - not shown (say, besides node B), then solely the bidirectional connectivity (Fig. 7.2 a-c) would lead to a synchronized dynamics of the driven nodes. This reciprocal coupling constitutes a potential resonant pair.

Furthermore, to obtain a resonant pair, some conditions in the connectivity of the motif are required: Two nodes must be mutually connected to each other, one of which can be also a driven node, but not the two of them simultaneously; a mutual connection between the driven nodes introduces frustration in the system, which destroys the synchronizing effect of the resonant pairs.

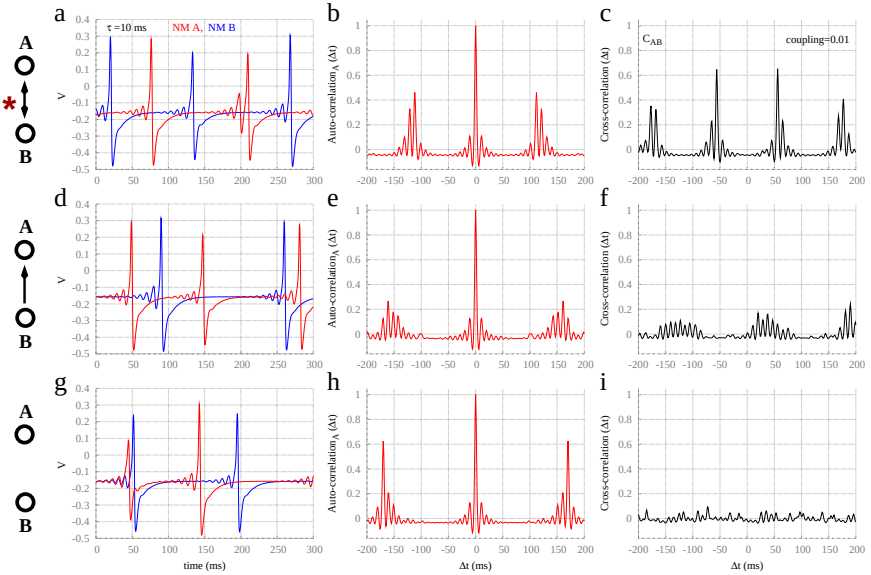

Figure 7.2: Dynamics of pairs of neural mass models. (a), (d) and (g) show the time traces; (b), (e) and (h) show the auto-correlation function of node A; (c), (f) and (i) show the cross-correlation function between nodes A and B; respectively for a pair bidirectionally connected, unidirectionally connected, and disconnected.

7.3 Common-driving motif versus different common-driving motifs enhanced with resonance-induce sources

This section illustrates the effect of a resonant pair to induce synchronization. We systematically compared the common-driving motif with other types of common-driving motifs that additionally owned at least a single active resonant pair. The presence of an active resonant pair in the motifs promoted the synchronization of the commonly driven nodes. Therefore, an active resonant pair constituted a source of resonance-induced synchronization.

7.3. COMMON-DRIVING MOTIF VERSUS DIFFERENT COMMON-DRIVING MOTIFS ENHANCED WITH RESONANCE-INDUCE SOURCES

This section mainly concentrated in four of the motifs depicted in Fig. 7.1. The common driving (M3) in which node 2 drives the dynamics of nodes 1 and 3 was contrasted with other three variations of common driving (M6, M9 and M3+1), in which resonance-induce sources have been added. In the particular case of M3, the delay between nodes if any, plays no role neither in the dynamics nor in the synchronization between nodes 1 and 3. M6 has node 2 driving nodes 1 and 3, and receiving a feedback of node 1, and owns a resonant pair: the reciprocal connection 1-2. M9 has node 2 reciprocally connected with nodes 1 and 3, and owns two resonant pairs: the reciprocal connections 1-2, and 2-3. M3+1 is given by M3 plus an extra node (4) reciprocally connected to node 2, which comprises the resonant pair.

Our study was based on extensive numerical simulations that included different types of dynamics for the nodes. We started by simply considering one neuron at each node, described by the Hodgkin-Huxley model. We next considered each node as a population of Izhikevich neuron, mimicking a cortical region. However, it was also convenient and more intuitive to work with reduced system. Finally, following this rationale, we modeled each cortical region by a neural mass model. Taking advantage of this reduction, we performed a deeper analysis, discussed in the following sections. Details about the models and parameter values are given in section 7.7.

7.3.1 Hodgkin-Huxley neurons

Nodes were chemically coupled via excitatory synapses with delay $\tau = 6$ ms. We concentrated in time traces and cross correlation functions between the different nodes. Figure. 7.3 shows results for the motifs of Hodgkin-Huxley cells. Each neuron received independent train of spikes distributed according to a Poisson distribution (see the section 7.7.1 for details). The neurons exhibited an oscillatory behavior with an average period of about 15 ms. The results showed that, in contrast to the genuine common-driving motif (M3) (which did not lead to synchronization), the other three motifs of common driving with active resonant pairs (M6, M9, M3+1) presented node 1 and 3 synchronized at zero lag. Node 2, on the other hand, was also synchronized, but in anti-phase with respect to nodes 1 and 3.

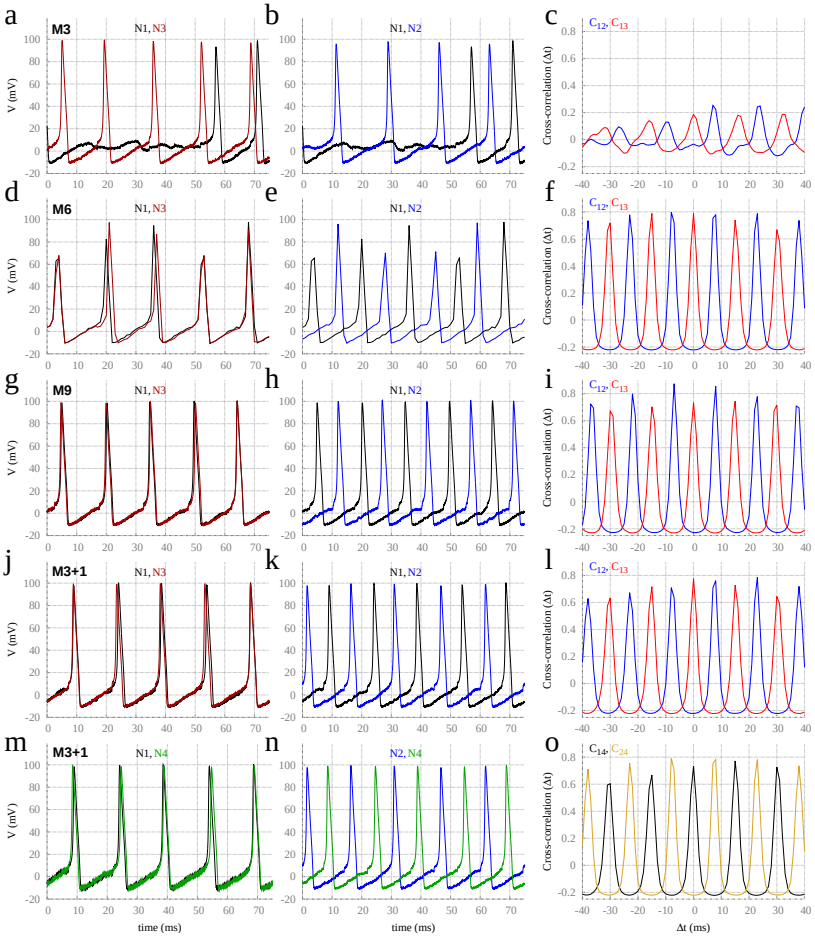

Figure 7.3: Dynamics of common driving motif (M3) versus common driving motifs with resonance-induced sources (M6, M9 and M3+1) in motifs of delayed-coupled Hodgkin-Huxley cells with delay $\tau = 6$ ms. First and second columns correspond to the time traces of neurons, whereas third column corresponds to the cross-correlation functions of the respective time series. Please refer to the section 7.7.1 for details about the Hodgkin-Huxley model.

7.3.2 Populations of Izhikevich neurons

As a straightforward model to assess the large-scale brain dynamics, we utilized an approach similar to the one presented in the previous chapter. Each population comprised (400) excitatory and (100) inhibitory Izhikevich neurons (section 7.7.2), each neuron receiving an independent Poisson spike train. Neurons were chemically coupled with no delay for the intra-population connections and with a latency of 15 ms for (exclusively excitatory) inter-population connectivity, to account for the finite propagation time. We considered $\langle V \rangle$ the average of the membrane potential v of all neurons within each population. Please refer to section 7.7.2 for details about the model. The oscillatory activity of each population was prevalently at a low frequency, with average of ~3 Hz. The oscillatory period, in this case, was much larger than the delay in the connection. Despite the discrepancies in the systems, the results also consistently showed that M3 did not render synchronization in contrast to the other three motifs M6, M9, M3+1, in which nodes 1 and 3 synchronized at zero lag. The anti-phase relation between node 2 with respect to nodes 1 and 3 appeared solely at a faster time scale, similar (but not exactly equal) to the delay period.

7.3.3 Neural mass models

Once more, we aimed at illustrating the robustness regarding to the synchronization pattern with respect to the dynamical systems utilizing a reduced model of cortical dynamics. We followed the steps of Honey et al. (2007, 2009), who successfully unveiled important features of the large-scale brain dynamics with the neural mass model. Instead of dealing with thousands of equations for each population of neuron, the model presented only three nonlinear equations to represent the spontaneous cortical dynamics of a limited region (see details in the section 7.7.3).

The dynamics of the delayed-coupled neural masses showed intrinsic oscillations with an average period of about 100 ms. As shown in Fig. 7.5, once again, the common driving with resonance-induce sources (M6, M9, M3+1) synchronized nodes 1 and 3, but not the genuine common driving (M3). Node 2 was in anti-phase with respect to nodes 1 and 3. Remarkably, however, the anti-phase relation occurred at a much slower time scale (100 ms) than the coupling delay (10 ms). The correlations in this system were most

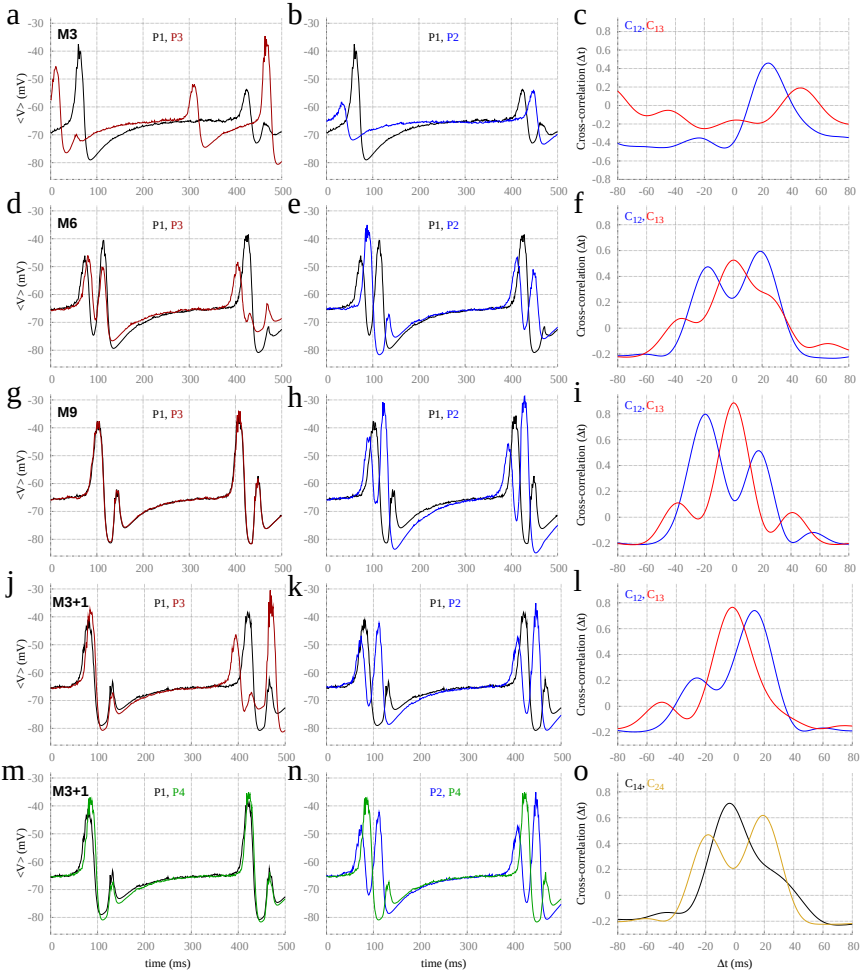

Figure 7.4: Same as figure 7.3, but for populations of Izhikevich neurons and delay $\tau = 15$ ms. Please refer to the section 7.7.2 for details about the model.

pronounced than in the other models presumably ascribed to the absence of stochastic synaptic input.

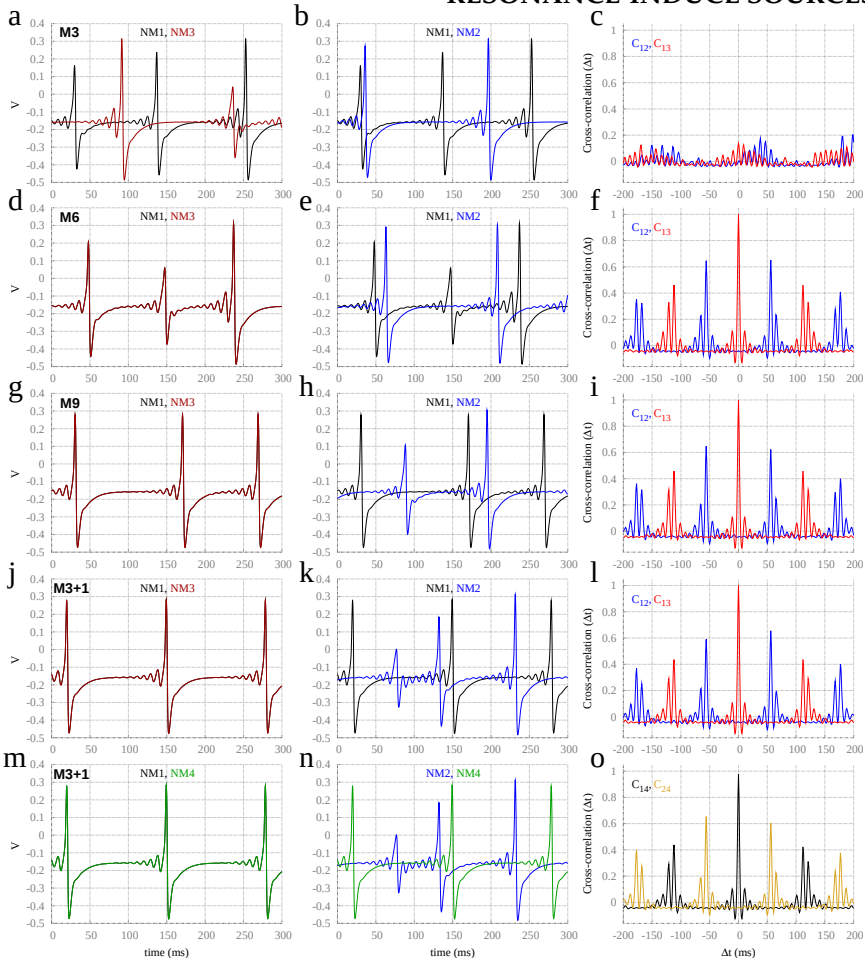

Figure 7.5: Same as figure 7.3, but for neural mass models with coupling strength $c = 0.01$, and delay $\tau = 10$ ms. Please refer to the section 7.7.3 for details about the model.

7.4 Characterizing the dynamics of the motifs

From now on we restrict ourselves exclusively to motifs of neural mass models. Such systems are clear and malleable, enabling a thorough analysis. In particular we deeply study the robustness of our findings with respect to the most key parameters of the system: the coupling strength and the delay.

Contrarily to the previous analysis, which illustrated a single trial of the dynamics, in the remainder we aimed at studying the dynamics by averaging over numerous independent runs with different initial conditions to acquire more quantitative information. Figure 7.6 shows the mean over 40 trials of the cross-correlation function between the driven nodes at zero-lag, where the error bars are given by the corresponding standard deviation. The increase in the synchronization as a function of the coupling was an expected feature of the model. There were, however, some regions of complex dynamics (considerable error bars) in which there was not a unique dominating basin of attraction, thereby entailing significant trial-to-trial variability. Moreover, the results were remarkably robust with respect to delays (restricted to the physiologically plausible range).

From Fig. 7.6, it was possible to split the different types of common-driving motifs in three distinct families:

Motif of genuine common driving (M3). It is completely independent of the delay and cannot accomplish synchronization in the weak-coupling regime;

Motifs of common driving with direct coupling between the driven nodes (e.g., M8, M13). They simultaneously require a relative strong coupling, and a negligible delay in order to promote synchronization;

Motifs of common driving enhanced by active resonant pairs (e.g., M6, M9, M3+1). They remarkably accomplished for synchronization even for very slight coupling, and irrespectively of the delay.

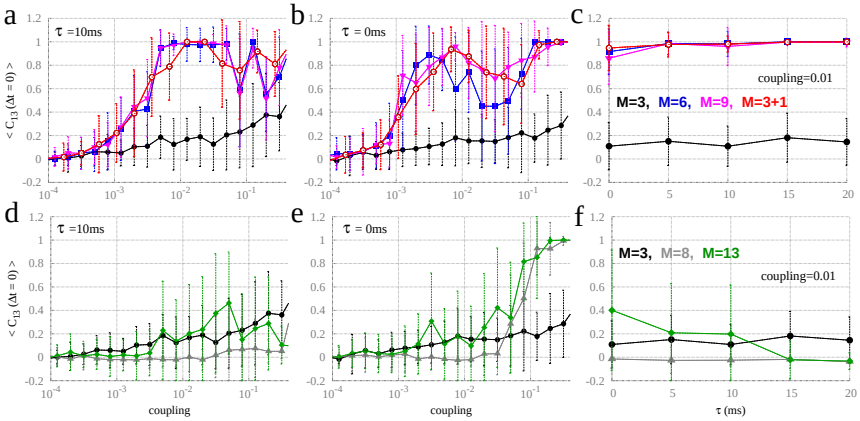

Figure 7.6: Zero-lag cross-correlation between neural masses 1 and 3 for the motifs corresponding to the different types of common driving. Top row compares common driving (M3) to common driving with a resonance-induced source (M6, M9 and M3+1) for varying coupling (panels a and b) and varying delay (panel c). Bottom panels compares common driving (M3) to common driving with a resonance-induced source disturbed (M13), and to common driving plus a bidirectional connection between 1 and 3 (M8) for varying coupling (panels d and e) and varying delay (panel f).

7.5 Propagation of the resonant effect

Next we investigated further the propagation properties of the resonant signal from a resonant pair. For this endeavor, we designed arbitrarily larger structures in which the resonant pair was the most distant from the driver node (2). This procedure is shown in Fig. 7.7 a, and exemplified in Fig. 7.7 b for a particular network of N=7 nodes. We were especially interested in the zero-lag synchronization of nodes 1 and 3 to determine whether the effects of the resonant pair were strictly local, and, additionally, on how the polysynaptic distance of the resonant pair influenced the dynamics and synchronization in such networks.

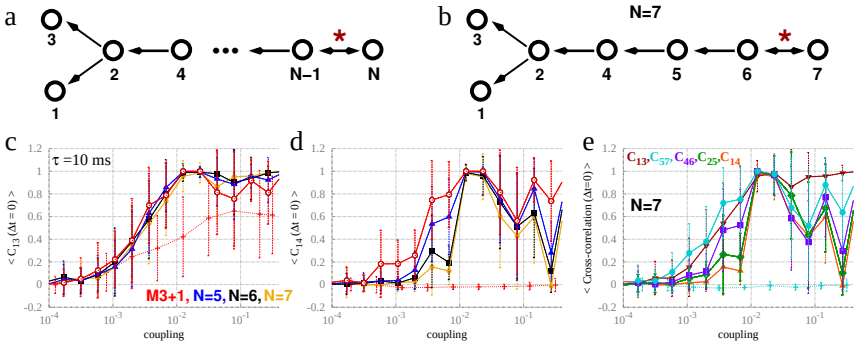

Figure 7.7: Effects of a resonant source propagates along a chain. (a) depicts a resonance source (nodes N and N-1) arbitrarily distant from a pair of commonly driven neural masses (1 and 3). (b) illustrates a chain with 7 nodes. Zero-lag cross-correlation functions between nodes 1 and 3 (c), and between 1 and 4 (d) for different chain sizes as illustrated in panel (a) are shown in solid lines. Thin dashed line represents the chain of panel (a) without the feedback connection from node N-1 to node N. (e) Zero-lag cross-correlation functions between every other node in the chain depicted in panel (b) are shown in solid lines. Thin dashed line represents the chain of panel (b) without the feedback connection from node 6 to node 7.

In Figs. 7.7 c, d we compare the zero-lag synchronization of node pairs for the motif M3+1 (which is equivalent to N=4) with other larger structures (N= 5,6,7). The results showed that the zero-lag synchronization between the driven nodes 1 and 3 remained almost unaltered with the distance to the resonant pair. The zero-lag synchronization of nodes 1 and 4 had a specific range of couplings with a perfect synchronization. Apart from this specific parameter region, synchronization decreased with structure size, or polysynaptic distance from the resonant pair. The reduction was expected because, the flux of information, for $N \geq 5$, must follow a strict direction: from node 4 to node 1. Therefore, high zero-lag synchronization required periodic time traces.

For a fixed network (N=7), we also characterized the zero-lag synchronization of different pairs of nodes that did not interact directly, but interacted indirectly through a common neighboring mediator (see Fig. 7.7 e). With

the exception of the pairs 5-7 and 1-3, the other pairs depicted a strict flux of information. Thereby, synchronization decreased with distance from the node 7, unless the system was set with a specific coupling that gave rise to a periodic dynamics.

Next, to highlight the influence of the resonant pair in the dynamics, we removed the feedback connection to node N (thin dashed lines in Figs. 7.7 c-e). By means of this control experiment, we found that:

- The zero-lag synchronization between 1-3 was consistently reduced (Fig. 7.7c);

- The zero-lag synchronization between 1-4 (Fig. 7.7 d), and between 5-7 (Fig. 7.7 e) disappeared completely.

7.5.1 Effects of common driving at higher orders

Another sort of propagation considered the synchronization of commonly driven nodes at higher polysynaptic orders as shown in Figs. 7.8 a- c. We analyzed the synchronization of indirect commonly driven nodes up to the n-th order, thus polysynaptically connected by a chain of n-1 synapses. In particular, we compared the synchronization of the symmetrically located nodes n-n' for the different connectivity states of the driver node A:

(i) A was part of a resonant pair together with node B (Fig. 7.8 a);

(ii) A received a unidirectional input from B (Fig. 7.8 b);

(iii) A did not receive any input from neighboring regions (Fig. 7.8 c).

Figures 7.8 d- g show the zero-lag synchronization from first to fourth order for the distinct states of the driver node (represented in Figs. 7.8 a- c) as a function of the coupling strength. For a fixed coupling value, Fig. 7.8 h shows how the synchronization between the symmetrical nodes (n,n') decayed with distance. In this case, for a sufficient high order (e.g., $n \geq 4$) nodes n-n' could not synchronize in the absence of a resonant pair. Similarly occurred for the maximum cross-correlation between A and node n; a resonant pair was required for the propagation of synchronous activity.

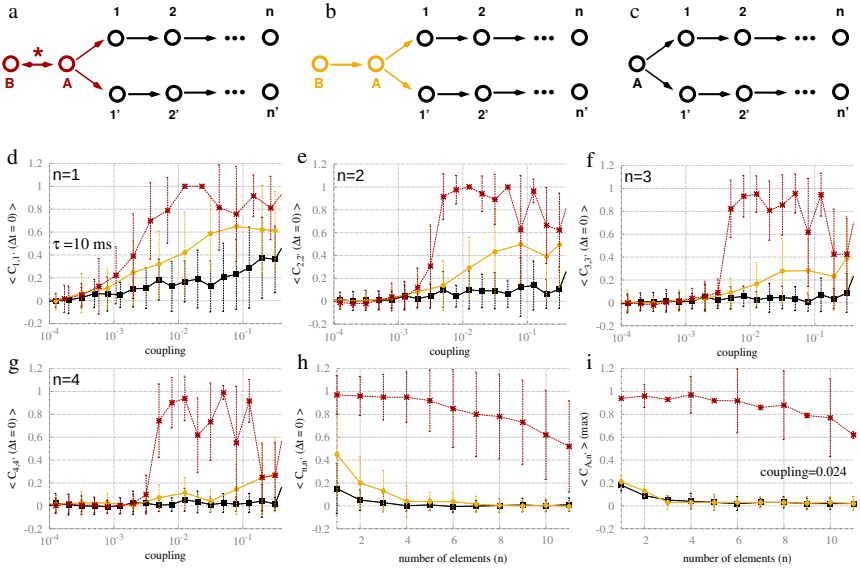

Figure 7.8: Propagation of synchrony to higher orders of pairs. Common driving to first (1,1′), second (2,2′) and n−*th* (n,n′) order for the resonance-induced pair (a), a unidirectional input (b), and simple common driving (c). (d) to (g): zero-lag cross-correlation functions for the different types of common driving from the first to the forth order. (h) The zero-lag cross-correlation functions between pairs of nodes (n,n′). (i) The maximum cross-correlation functions versus the distance from the driver node A.

7.6 Discussion

Historically, a large phenomenology pertaining to isochronous synchronization has been ascribed to common driving. Our results cast doubts on the efficacy of the genuine common driving motif to promote synchronization. Supported by extensive numerical simulations, our findings suggest that, in the weak-coupling regime, the importance of the genuine common driving to synchronize spontaneous neuronal activity has been prevalently overestimated (see Figs. 7.3, 7.4, 7.5, 7.6). Apart from the genuine common driving

(which completely disregards the effects of the delay in the coupling), a common driving enhanced with a reciprocal connection between the driven nodes could indeed improve the synchronization for a sufficiently strong coupling. However, due to frustration, this scenario prevalently fades in the presence of any non-negligible delay in the coupling (see Fig. 7.6).

Notably, in the presence of delay, regardless of its value, there is an entire family of common-driving motifs enhanced by resonant pairs with outstanding capability to promote synchronization. As a consequence of such an enhancement, the driver node receives synchronized input that sculpts its dynamics and optimizes its effectivity to synchronize the commonly driven nodes. The criteria to belong to this distinguished family is to own (or to be under the influence of) at least one active resonant pair. An active resonant pair intrinsically endows these motifs with the ability to promote correlated activity by means of resonance-induced synchronization. In other words, the resonant pair plays the role of a resonant source when active, meaning not disturbed or frustrated. Furthermore, a single resonant pair is important because it is the simplest way to send a synchronized input to the driver node.

Probably, the most especial specimen of motif in this family is the motif M9 (see Fig. 7.1), also known as the dynamical relaying (Fischer et al., 2006; Vicente et al., 2008a; Gollo et al., 2010). This motif possesses two active resonant pairs (Fig. 7.1). Therefore, one feedback connection to the driver node can be removed (i.e., transforming the motif into a M6) without compromising the synchronization. Thereby, we propose that the *essence* to promote zero-lag synchronization of the dynamical relaying relies on a resonant pair. The resonant pair is the source of resonance-induced synchronization, which, in turn, constitutes the functional basis of the dynamical relaying.

The clearest way to illustrate the effects of a resonant pair is probably with motif M3+1 (Fig. 7.1). Motif M3 has rather poor capabilities to induce synchronization. However, the addition of merely one extra node mutually connected to the driver node (and thereby comprising a resonant pair) completely changes the picture, and optimally promotes zero-lag synchronization of the driven nodes.

Some other motifs have also been studied under the dynamical-relaying framework (Vicente et al., 2008a; Gollo et al., 2010, 2011). But they have been typically considered as robustness studies, say by introducing variations in the structure to examine to what extent the synchronization remains

undisturbed. Moreover, some of these studies have also taken advantage of the mismatch in the driver node, which, as has been recently shown, enhances its capabilities to promote zero-lag synchronization (Banerjee et al., 2012). Such mismatch can be important to break the symmetry, thereby fading the frustration effects.

We argue that the dynamical relaying can be thought as a particular case of the resonance-induced synchronization, has indeed proven great robustness since its first proposal (Fischer et al., 2006). Analogously, the resonance-induced synchronization also depicts promising robustness. We have presented consistent examples covering different models (Hodgkin-Huxley neurons, populations of Izhikevich neurons, and neural mass models) and scales: motifs of neurons and motifs of cortical regions. The results also showed impressive robustness with respect to the delay and the coupling strength. In particular, surprisingly weak couplings already lead to synchronous solutions. Therefore, we expect that the resonance-induced synchronization to be also important for other scales in brain systems, say dendritic oscillations in single-neuron dynamics (Remme et al., 2009), or other physical and biological systems of any domain whenever delay and weak-coupling interactions coexist.

The effects of a resonant pair are remarkable: Such a pair not only induces synchronization, but its effects can also propagate throughout the network, resonating at distant neighbors of neighbors. Surprisingly, our results suggest that the propagation could even be almost deterministically, and decay rather slowly with the polysynaptic distance (see Fig. 7.7). Moreover, in a sufficient sparse network, like the brain, the number of neurons grows roughly exponentially with the neighboring distance. Such capacity to strongly affect the neighbors of the neighbors via polysynaptic interactions allied to the fast grow in the number of elements with distance could potentially lead to deep entailments. The coexistence of such slow correlation decay with a fast grow in the number of affected elements with the synaptic distance could provide the substrate for the unfolding of rich dynamical branching processes: The recruitment of elements to joint the blatant unison. The propagation of synchrony is considered an important problem in theoretical neuroscience (Kumar et al., 2010), which can be accomplished by the delay-coupled networks via resonance-induced synchronization.

Despite the consistency regarding different sorts of models, and the robustness with respect to the most important parameters of the model, some

boundaries remain obscure. It will be fundamental to elucidate to what extent our results could be translated to other physical and biological systems, perhaps including canonical models that are amenable to mathematical analysis.

We have identified and characterized a dynamical building block, which is the resonant pair. The insights from the resonant pair provide intuition to comprehend the dynamics of structures comprising three or more nodes. We expect that this successful approach will encourage further investigations searching for additional dynamical building blocks lurking behind the complex spatiotemporal dynamics of the networks.

We have found that a single node or connection can drastically alter the dynamics of the system. This plain fact suggests that it could be rather challenging to unravel the interplay between structure and dynamics, similarly to what have been recently reported (Adachi et al., 2011). However, this exciting field could also be reserving many pleasant surprises.

7.7 Methods

We have used three different perspectives to simulate motifs of neuronal tissue of small and large scales. First, representing the small scale, each node was taken as a single neuron. For this endeavor we utilized Hodgkin-Huxley cell. The other two perspectives aimed at the study of the neuronal dynamics at a large scale. Second, as a direct extension of the motif of single neurons, we took each node as a large population of spiking neurons. Third, we considered a simplified coarse-grained version, in which each population was taken as a neural mass model.

7.7.1 Motifs of Hodgkin Huxley neuronal model

Following the Hodgkin and Huxley original formulation (Hodgkin and Huxley, 1952), each node was modeled by the Hodgkin-Huxley equations, with three (sodium, potassium and leak) currents components as:

$$\begin{aligned} C\frac{dV}{dt} &= -g_{Na}m^3h(V-E_{Na}) - g_K n^4(V-E_k) \\ &- g_L(V-E_L) + I_{syn} + I_{ext}\ , \end{aligned} \tag{7.1}$$

where $C = 1\ \mu\text{F/cm}^2$ is the membrane capacitance The maximal conductances of the channels occur for completely open channels, for which the conductances are given by $g_{Na} = 120\ \text{mS/cm}^2$, $g_K = 36\ \text{mS/cm}^2$, and $g_L = 0.3\ \text{mS/cm}^2$, and $E_{Na} = 115$ mV, $E_K = -12$ mV, and $E_L = 10.6$ mV stand for the corresponding reversal potentials. Generally, the voltage-gated ionic channels are not fully opened. The probability of finding them open depend on the gating variables. The Na^+ channel depends on the combined effect of $m(t)$ and $h(t)$, whereas K^+ depends on $n(t)$. They evolve according to the equations:

$$\frac{dm}{dt} = \alpha_m(V)(1-m) - \beta_m(V)m\ , \tag{7.2}$$

$$\frac{dh}{dt} = \alpha_h(V)(1-h) - \beta_h(V)h\ , \tag{7.3}$$

$$\frac{dn}{dt} = \alpha_n(V)(1-n) - \beta_n(V)n\ , \tag{7.4}$$

Hodgkin and Huxley set the empirical functions α and β to fit the experimental data of the giant axon of the squid as:

$$\alpha_m(V) = \frac{2.5 - V/10}{\exp(2.5 - V/10) - 1}\ , \tag{7.5}$$

$$\beta_m(V) = 4\exp(-V/18)\ , \tag{7.6}$$

$$\alpha_h(V) = 0.07\exp(-V/20)\ , \tag{7.7}$$

$$\beta_h(V) = \frac{1}{\exp(3 - V/10) + 1}\ , \tag{7.8}$$

$$\alpha_n(V) = \frac{0.1 - V/100}{\exp(1 - V/10) - 1}\ , \tag{7.9}$$

$$\beta_n(V) = 0.125\exp(-V/80)\ . \tag{7.10}$$

The synaptic current due to the interactions between neurons of the motifs are given by:

$$\tau_{syn}\frac{dI_{syn}}{dt} = -I_{syn} + 50\sum_{k}\delta(t - t_k - \tau_k)\,, \tag{7.11}$$

where $\tau_{syn} = 0.4\ ms$, and δ stands for the Dirac delta function. The summation over k stands for the spikes of the neurons (all excitatory). t_k is the time at which the $k-th$ spike occurred. We assumed the conduction delay $\tau_k = 6$ ms.

The external current incoming to each neuron is:

$$I_{syn} = 20\sum_{j}\delta(t - t_j)\,, \tag{7.12}$$

where j are 1000 external neurons, and t_j corresponds to the spike times, modeled by a Poisson process with rate $r = 40$ Hz. The equations were integrated by the Runge-Kutta method of fourth order, with time steps of 0.01 ms.

7.7.2 Motifs of populations of Izhikevich neurons

At this comprehensive large-scale model, each node is represented by populations of 500 Izhikevich neurons randomly connected, 400 neurons are excitatory and 100 neurons are inhibitory. The Izhikevich neurons are described by the following equations:

$$\begin{aligned}\frac{dv}{dt} &= 0.04v^2 + 5v + 140 - u + I_{syn}\,,\\ \frac{du}{dt} &= a(bv - u)\,,\end{aligned} \tag{7.13}$$

where v represents the membrane potential, u represents the recovery variable, accounting for the K^+ and Na^+ ionic currents, and I_{syn} is the total synaptic current. The neurons have a threshold at 30 mV. Once this value is reached, v is reset to c and u to $u + d$. Following the recipe of Izhikevich et al. (2004), also reproduced in the previous chapter for cortical populations, we have taken diversity in these four parameters (a, b, c and d) to account for

the different behavior observed by the cortical neurons. Excitatory neurons have $(a, b) = (0.02, 0.2)$, and $(c, d) = (-65, 8) + (15, -6)\ \sigma^2$, where σ is a random number drawn from a uniform distribution in the interval [0,1]. Inhibitory neurons have $(a, b) = (0.02, 0.2) + (0.08, -0.05)\ \sigma$, and $(c, d) = (-65, 2)$.

We chose this connectivity such that the populations show oscillatory activity, which is not periodic. Each neuron receives input from 80 neurons of the same population and from 25 excitatory neurons of each afferent population. The synaptic current is given by:

$$I_{syn} = -v\ g_{AMPA}(t) - (65 + v) g_{GABA}(t)\,, \tag{7.14}$$

and the dynamics of the excitatory and inhibitory synapses are described by:

$$\begin{aligned} \tau_{AMPA} \frac{dg_{AMPA}}{dt} &= -g_{AMPA} + 0.5 \sum_k \delta(t - t_k - \tau_k)\,, \\ \tau_{GABA} \frac{dg_{GABA}}{dt} &= -g_{GABA} + 0.5 \sum_l \delta(t - t_l)\,. \end{aligned} \tag{7.15}$$

δ in the equations above stands for the Dirac delta function. The summation over k (l) stands for the spikes of the presynaptic excitatory (inhibitory) neurons. t_k (t_l) is the time at which the $k-th$ excitatory (or $l-th$ inhibitory) spike occurred. Conduction delays τ_k, associated to excitatory long-range connections, are assumed to be 15 ms. We modeled short-range connections with negligible delays. Synapses are modeled by exponential decay functions (Dayan and Abbott, 2001), with time constants $\tau_{AMPA} = 5.26$ ms for excitatory and $\tau_{GABA} = 5.6$ ms for inhibitory synapses. Each neuron is subject to an external driving given by independent Poisson spike trains, resulting from 100 excitatory neurons, at rate r = 16 Hz. The equations were integrated with the Newton method with time steps of 0.05 ms.

7.7.3 Motifs of neural mass models

The previous section showed a model that included thousands of equations. It is worthwhile and instructive to work in this system, however, accompanying the large number of parameters and equations, there are pertaining intricate challenges that precludes a mature and intuitive perspective of the system. For example, it is virtually impossible to predict what changes in

the dynamics would be produced by some changes in the model parameters, and so on. We therefore find it not only suitable to illustrate the novel phenomenology in a reduced system (Breakspear and Terry, 2002), which represents the large cortical scale (in which most brain functions are carried out), but also to thoroughly study and characterize the system with respect to the most important parameters. In contrast to the previous models, the coupling is not through discrete pulses, but by means of smooth sigmoidal functions, as a consequence of the reduction approach. This also highlights the robustness of the resonance-induced synchronization regarding to the precise details of the models.

Each node represents an ensemble of neurons; the excitatory and the inhibitory subgroups are split to generate spontaneous rhythms mimicking the cortical activity. Derived from the biophysical model of Morris and Lecar (1981), the neural mass model dynamics have been first proposed by Larter et al. (1999); the coupling was first proposed to represent synaptic interactions instead of diffusive ions by Breakspear et al. (2003); and subsequently the model have been extended for large networks to model whole brain activity by Honey et al. (2007, 2009). We utilize this most recent approach developed by Honey et al. (2007, 2009) systematically varying the features of the connectivity: architecture, coupling strength, and delay.

The cortical model of spontaneous cortical dynamics comprises three state variables:

- V: The mean membrane potential of the excitatory pyramidal neurons;
- Z: The mean membrane potential of the inhibitory interneurons;
- W: The average number of open potassium ion channels.

Despite the fact that the oscillatory rhythms accompanying the dynamics are reflected by the other state variables Breakspear et al. (2003), our main focus is on the dynamics of the pyramidal neurons. Their average membrane potential V depends on the passive leak conductance, and on the conductance of voltage-gated channels of sodium, potassium and calcium ions. The flow of current across the local pyramidal cell membranes, assumed as capacitors, governs its dynamics. In turn, the local activity of the inhibitory interneurons is course-grained modeled; its dynamics is modulated by the activity of the pyramidal cell, considered with greater physiological detail.

For each ensemble i, the equations for the dynamics of the mean membrane potential of the neurons read:

$$\begin{aligned}\frac{dV^i(t)}{dt} &= -\Big(g_{Ca} + (1-c)\, r_{NMDA}\, a_{ee}\, Q_V^i(t) \\ &\quad + c\, r_{NMDA}\, a_{ee}\, \langle Q_V^j(t-\tau)\rangle\Big)\, m_{Ca}\, (V^i(t) - V_{Ca}) \\ &\quad - \Big(g_{Na}\, m_{Na} + a_{ee}\, Q_V^i(t)\Big)\, (V^i(t) - V_{Na}) \\ &\quad - g_K\, W^i(t)\, (V^i(t) - V_K) - g_L\, (V^i(t) - V_L) \\ &\quad + a_{ie}\, Z^i(t)\, Q_Z^i + a_{ne}\, I_\delta\ ; \end{aligned} \tag{7.16}$$

$$\frac{dZ^i(t)}{dt} = b\left(a_{ni}\, I_\delta + a_{ei}\, V(t)\, Q_V^i(t)\right). \tag{7.17}$$

The fraction of channels open m_{ion} are the *neural-activation function*, whose shape reflects a sigmoidal-saturating grow with V:

$$m_{ion} = 0.5\left[1 + \tanh\left(\frac{V^i(t) - T_{ion}}{\delta_{ion}}\right)\right]. \tag{7.18}$$

The third differential equation of each node i stands for the fraction of open potassium channels:

$$\frac{dW^i(t)}{dt} = \frac{\phi\,[m_K - W^i(t)]}{\tau_W}\ . \tag{7.19}$$

The neuronal firing rate (Q_V^i, and Q_Z^i) averaged over the ensemble is assumed to obey Gaussian distributions, thereby giving rise to the sigmoidal activation functions:

$$Q_V^i(t) = 0.5\, Q_{Vmax}\left[1 + \tanh\left(\frac{V^i(t) - V_T}{\delta_V}\right)\right]; \tag{7.20}$$

$$Q_Z^i(t) = 0.5\, Q_{Zmax}\left[1 + \tanh\left(\frac{Z^i(t) - Z_T}{\delta_Z}\right)\right]. \tag{7.21}$$

From the above equations, the following parameters: g_{Ca}, r_{NMDA}, a_{ee}, V_{Ca}, g_{Na}, V_{Na}, g_K, V_K, g_L, V_L, a_{ie}, a_{ne}, I_δ, b, a_{ni}, a_{ei}, T_{ion}, δ_{ion}, ϕ, τ_W, Q_{Vmax}, V_T, δ_V, Q_{Zmax}, Z_T, δ_Z were set to physiological values taken from Breakspear et al. (2003). Equation 7.16 includes the other important parameters in our analysis: $j = 1, ..., N$, the presynaptic neighboring (afferent) regions of region i; c, the coupling strength between cortical regions; τ, the synaptic delay between cortical regions. The model is simulated in Matlab at a time resolution of 0.2 milliseconds.

Chapter 8

Concluding Remarks and Further Perspectives

Brain sciences comprise a remarkable example of interdisciplinary science. Traditionally, neuroscience has been almost uniquely dominated by experimental work. However, theoretical neuroscience has gained space in this exciting field of knowledge (Abbott, 2008). Theoretical contributions from distinct areas have introduced novel perspectives, and shaped directions of neuroscience research.

This manuscript represents mostly studies of numerical simulations on systems of large dimensionality, which are of interest to neuroscience. The thesis collects a family of results primarily focusing on the mesoscale dynamics of motifs of neuronal populations. These results had been spurred by recent developments in physics and non-linear dynamics, which can be fruitfully utilized to understand the dynamics and synchronization of distant ensembles of neurons. Nevertheless, the flux of ideas represented by this thesis was not exclusively unidirectional. As presented in the previous chapter, our study on simple motifs also attempts to contribute to the elucidation of the foundations of the synchronization phenomenon in the presence of delayed interactions. Thus, the middle-ground interface between the distinct fields has proved fertile for the reciprocal exchange of knowledge.

CHAPTER 8. CONCLUDING REMARKS AND FURTHER PERSPECTIVES

Analogously to the particular interface that we explored, neuroscience comprises other numerous fertile interfaces. In particular, there are several promising theoretical opportunities to be explored at the front-line boundaries. Apart from bringing maturity to the field, theoretical frameworks are required to sculpt a solid basis towards the scientific progress. We believe that physics should play an engaged role in such an enterprise. Physics could contribute to unravel universal patters in this hallmark of complex system. Coinciding with the criteria of great success in physics, major breakthroughs in brain sciences would also unify manifold concepts and results scattered throughout discrepant subfields.

Summary and main results.

In this thesis we showed that the dynamical relaying is consistently robust to promote zero-lag synchronization in neuronal systems. Our results entail that this mechanism could take place in a variety of brain structures: in cortical networks, in thalamocortical circuits, and in hippocampal-cortical networks. Moreover, we proposed that the dynamical relaying could be unraveled even further in a minimal relation between two resonating nodes to promote synchronization. A contextualized description of our major conclusions is provided next:

Cortical Dynamical Relaying (chapter 4): Despite of being potentially powerful and depicting a broad range of validity since its first proposal, the robustness of the dynamical relaying mechanism had been still unclear. Our first effort was to change such a picture. We scrutinized this promising mechanism in a minimal neuronal motif of three Hodgkin-Huxley neurons. The dynamical relaying showed overwhelming robustness to promote zero-lag synchrony almost irrespectively of the coupling delays.

Next, we have been striven to translate this idea to a larger neuronal scale: The scale of neuronal populations, in which most motor, sensory, and cognitive functions are carried out. The first task in this endeavor was to simulate distant populations utilizing a minimal model. To mimic cortical assemblies, we considered each population as a sparse random network, which was not specially designed for any particular function; and the nodes were taken as the simplest way possible: Integrate-and-fire neurons. Thus, we compared the synchronization of the motifs comprised two or three of

these delayed-coupled generic assemblies of spiking neurons. Our finds typically showed that the nearest neighboring populations synchronized in anti-phase, whereas the outer populations synchronized at zero lag.

The results indicated that the dynamical relaying promotes isochronous synchronization of distant populations with an overwhelming robustness. Such robustness is fundamental because long-range synchronization: (i) may involve many brain areas; (ii) is found across several species, with different brain sizes and axonal lengths; (iii) is observed in any developmental stage. Therefore, the mechanisms involved ought to be analogously general; it should not depend on an exact configuration. This extrication from a precise and specific fine tuning is probably the most important feature of the dynamical relaying.

Thalamic Dynamical Relaying (chapter 5): The universal character of the dynamical relaying in generic neuronal populations also had the limitation of being unable to reproduce the behavior of an especial circuit, like, for instance, the thalamocortical circuit. The thalamus, the entry door of most sensory stimuli into the cortex, occupies a central position in the brain. Moreover, it is naturally considered a relay center of the brain because of its multiple thalamocortical radiations. Due to these characteristics (inter alia), the thalamus is considered the strongest candidate to promote cortical synchronization by mediating the dynamical-relaying mechanism. Therefore, we studied the dynamics of a minimum thalamocortical model in which the outer (cortical) regions remained generic, but the central (thalamic) region reflected some physiological particularities. In our model, the thalamus was divided into two subregions to mimic a specific relay nucleus, and the thalamic reticular nucleus. Additionally, the input to the specific relay nucleus consisted of two components: an afferent sensory stimulus, and all the remainder connections.

Our results in the thalamocortical circuit showed and confirmed the importance of the thalamus to shape the cortical dynamics. According to this thalamocortical model, the thalamus not only promoted, but also controlled the zero-lag cortico-cortical synchronization. The thalamocortical circuit provided the substrate to generate synchronization, and to control the engagement and disengagement of cortical synchrony as a function of the thalamic input in a plausible time scale. Synchronous neuronal activity is indeed found ubiquitously in the brain, and it is thought to play an

important functional role. Nevertheless, the excess of synchronization is associated with abnormal brain activity, such as seizures and epilepsy. It is thus fundamental to control both processes the generation and the vanishment of synchronization, analogously to the accomplishments of our model of the thalamocortical circuit.

In the brain, there is a recognized close inter-relationship between the thalamus and the cortex (Briggs and Usrey, 2010), which cannot be dismissed. The thalamic activity strongly depends on the sensory stimuli (Temereanca et al., 2008; McAlonan et al., 2008; Yu et al., 2009). In turn, as confirmed by recent experiments, the thalamic dynamics coordinates and sculpts the cortical activity (Wolfart et al., 2005; Wang et al., 2010a; Poulet et al., 2012; Olsen et al., 2012).

Hippocampal Dynamical Relaying (chapter 6): Another circuit of particular interest involves the cortex and the hippocampus, which closely interact during some motor and cognitive tasks. The interactions, however, prominently take place at much slower rhythms (theta band). Therefore, to play the role of the dynamical-relaying center, a first challenge was to propose a hippocampal model of spiking neurons, whose activity was mainly generated at the theta band. This barrier was overcome by utilizing Izhikevich neurons prioritizing the spikes in the bursting mode. Moreover, the distant cortical areas were merely modeled as generic populations of Izhikevich neurons prioritizing the spikes in the tonic mode.

Our results in this large-scale model indicated that the dynamical relaying might also occur at slow frequencies. This highlighted the importance of the hippocampus in coordinating the cortical activity in those rhythms. We thus found, for the first time, the signature of the dynamical relaying in experimental data on behaving mice. The signature consists on the preferred phase relation between pairs of areas. The cortical regions (prefrontal and visual cortex) tended to synchronize at zero-lag, whereas the relation between the hippocampus and the cortical areas was phase-locked, but not in phase. On top of that, another consistent relationship observed in the experimental data was that such phase-relation signature was enhanced during a moving state compared to a quiet state. This suggested that the dynamical relaying of the motif comprised by the hippocampus, prefrontal, and visual cortex played a functional role in the retrieval of spatial memory strongly associated with the active motor state.

The phase locking between the prefrontal cortex and the hippocampus had been already reported (Siapas et al., 2005), however, it had been interpreted uniquely as an empirical fact. In this context, the dynamical relay is remarkably suitable because it provides a solid framework in which the phenomenon can be distinctly elucidated.

Banerjee et al. (2012) have recently shown that the mismatch in the mediator element enhances the zero-lag synchronization of the outer nodes in the dynamical relaying. Both the thalamocortical circuit and the hippocampo-cortical system took advantage of such mismatch in the mediator element. In particular, even in the presence of a direct cortico-cortical connection of moderated strength, the zero-lag sync was robustly found. Moreover, the mismatch played an important dynamical role in each system. The mismatch enabled: (i) the thalamus to control the synchronizing dynamics of the cortex in the thalamocortical circuit; and (ii) the hippocampus to generate prominent theta oscillations that was embedded by the hippocampo-cortical circuit.

We started with a generic and robust mechanism to promote zero-lag synchronization, and adapted the concept to especial large-scale motifs. Although each of these studies can be improved in several ways, our last endeavor was on a completely different direction.

Resonance-Induced Synchronization (chapter 7): We revisited the structure, the very starting point of the thesis, to systematically study other potentially interesting motifs. All different sorts of motifs appear in neuronal systems. Some motifs seem more important than others, showing up with a disproportional probability compared to what can be expected by chance (Sporns and Kotter, 2004). A particular configuration that has gained a lot of attention in the literature is the common driving, probably because intuition tells us that the common driving is the major factor to give rise to synchronous behavior. Utilizing different types of neuronal models, we studied various motifs in which the central node commonly drives two nodes. First of all, our results showed that the intuition about the capacity of the common driving to promote synchronization was indeed erroneous for weakly coupled systems. Moreover, we found that the minimum requirement to promote synchronization of the driven nodes, and to circumvent the limitation of the common driving motif was the presence of a resonant pair, which by definition is comprised of two mutually connected nodes.

If the central node belonged to (or was under the influence of) a resonant pair, the synchronization was efficiently induced. The effects of a resonant pair were not restrictedly localized; they could also propagate throughout monosynaptic and polysynaptic pathways to influence the driver element and consequently the synchronization pattern.

Our results were not only consistent in different systems, but they also showed a remarkable robustness with respect to delay, and coupling strength. However, despite of the robustness of the resonance-induced synchronization, the addition or removal of a single connection or node on the structure could provoke drastic changes in the dynamics.

On the other hand, for a fixed structure in which the effects of a resonant pair were not disturbed, our results suggested that the resonance-induced synchronization constitutes the basic interaction underlying the dynamical relaying. Such fundamental interaction putatively endows the intrinsic capacity of the dynamical relaying to promote synchronization of delay-coupled elements.

Perspectives.

Improvements of our work can be accomplished in many (if not all) directions. A prolific and voluble avenue is the study of more realistic models. It is a good and recommendable strategy to start with a simple version of the model. An intuitive understanding of the model is better acquired in this way. Nevertheless, further developments can be interesting and frequently give rise to new dynamical features, which may be absent in the reduced model.

For example, in our model of the thalamocortical circuit, an important dynamical distinction was not taken into account; Thalamic neurons can be found in two spiking modes: tonic or burst. The tonic mode is considered to be more reliable to transmit information to the cortex, and a neuron in the tonic mode is more excited than in the burst mode. It seems important to understand the effects of the thalamic spiking modes in the control between the states of engagement or disengagement of cortical synchronization. This study would require a more sophisticated neuronal model than the integrate-and fire neuron, which is restricted to the tonic mode.

Another limitation of our model strategy that extends beyond the neurophysiological properties of the cells refers to the absence of structure in each region. The dynamical relaying, in which the nodes are spatially extended systems, has been recently addressed (Jian-Ping et al., 2012), but its effects in neuronal systems are largely unclear. The cortical regions can be made more biologically plausible by introducing a cortical grid: comprised of overlapping horizontal layers, and vertical columns. The thalamus can be modeled in more detail by subdividing it in different nuclei, and a single nucleus can be subdivided in distinct subparts. Amongst other features, the hippocampus is also famous for exhibiting interesting spatio-temporal structure that can certainly be explored. The interactions between cortical layers and columns can be also enlightening to study. An inverse perspective of the dynamical relaying in the thalamocortical circuit can be obtained by considering different thalamic nuclei, such as one specific relay and another association nuclei (see Fig. 1.7), which do not interact directly, but indirectly (say mediated by cortical areas and the thalamic reticular). In short, the broadness of this trend seems virtually unbounded.

Those were straightforward continuations of our work. It might be perhaps more important to explore the extremely opposite direction. Our work has been almost entirely numerical because the systems were typically too complex to allow any mathematical tractability. This could be a suitable opportunity to concentrate in much simpler models in which analytical insights are made possible in the field of synchronization of delayed-coupled systems.

We expect the resonance-induced synchronization to be very general, however, its boundaries are still obscure. Analytical works in simple systems could aid to substantially delineate its frontiers. Moreover, to tackle such a basic problem, numerical solutions and a thorough analysis of the diverse systems will also be valuable means to fully characterize the phenomenon.

The resonance-induced synchronization seems to constitute a building block of the dynamics. This suggests that other dynamical building blocks with elemental properties and capacities to shape the dynamics might exist. The dynamics of complex networks presumably could be better comprehended (in a more intuitive way) when the basic dynamical elements get understood. However, even if this approach is possible, we expect this journey to be quite challenging, because just a single node can already poignantly mold the dynamics of the network. Thus, it is left as an intriguing open question: To

what extent the dynamics of a network can be dissected in such dynamical building blocks?

Though rather intricated, the interplay between structure and dynamics is absolutely important to be understood. There are innumerous questions to be answered in this topic. Why some motifs appear more often than expected? Is there a real advantage in the motif M9 (open chain of three mutually connected nodes, see Fig. 7.1), which appears most in the macaque visual cortex? Is this advantage structural or concerns the dynamics? Our results indicate that M6 (M9 without one feedback) can lead to an equivalent capacity to promote synchronization. So, which advantages does M9 offer over M6? For example, would M9 be more stable than M6? Or would the precise answer to these questions pertain to a completely different viewpoint of analysis? The puzzle does not end up there. Further strides in neuroscience will be necessary to elucidate the interplay between structure, dynamics, and function.

Bibliography

Abbott, L. 1999. Lapicque's introduction of the integrate-and-fire model neuron (1907). Brain Research Bulletin 50:303.

Abbott, L. F. 2008. Theoretical neuroscience rising. Neuron 60:489–495.

Abbott, L. F. and S. B. Nelson. 2000. Synaptic plasticity: taming the beast. Nature Neuroscience 3 Suppl:1178–83.

Abbott, L. F. and W. G. Regehr. 2004. Synaptic computation. Nature 431:796–803.

Aboitiz, F., A. Scheibel, R. Fisher, and E. Zaidel. 1992. Fiber composition of the human corpus callosum. Brain Behav. Evol. 598:143–153.

Adachi, Y., T. Osada, O. Sporns, T. Watanabe, T. Matsui, K. Miyamoto, and Y. Miyashita. 2011. Functional Connectivity between Anatomically Unconnected Areas Is Shaped by Collective Network-Level Effects in the Macaque Cortex. Cerebral Cortex .

Agmon-Snir, H., C. E. Carr, and J. Rinzel. 1998. The role of dendrites in auditory coincidence detection. Nature 393:268–272.

Aihara, I., R. Takeda, T. Mizumoto, T. Otsuka, T. Takahashi, H. G. Okuno, and K. Aihara. 2011. Complex and transitive synchronization in a frustrated system of calling frogs. Phys. Rev. E 83:031913.

BIBLIOGRAPHY

Alonso, A. and E. García-Austt. 1987. Neuronal sources of theta rhythm in the entorhinal cortex of the rat. I. Laminar distribution of theta field potentials. Experimental Brain Research 67:493–501.

Alonso, J. and Y. Chen. 2009. Receptive field. Scholarpedia 4:5393.

Anderson, P. 1956. Ordering and Antiferromagnetism in Ferrites. Physical Review 102:1008–1013.

Anderson, P. W. 1972. More Is Different. Science 177:393–396.

Antranik. 2012. http://antranik.org/detailed-features-of-epithelia/.

Appeltant, L., M. C. Soriano, G. Van Der Sande, J. Danckaert, S. Massar, J. Dambre, B. Schrauwen, C. R. Mirasso, and I. Fischer. 2011. Information processing using a single dynamical node as complex system. Nature communications 2:468.

Arieli, A., A. Sterkin, A. Grinvald, and A. Aersten. 1996. Dynamics of ongoing activity: explanation of the large variability in evoked cortical responses. Science 273:1868–1871.

Ashida, G. and C. E. Carr. 2011. Sound localization: Jeffress and beyond. Current Opinion in Neurobiology 21:745–751.

Atay, F. M. 2003. Distributed Delays Facilitate Amplitude Death of Coupled Oscillators. Phys. Rev. Lett. 91:094101.

Atay, F. M., J. Jost, and A. Wende. 2004. Delays, Connection Topology, and Synchronization of Coupled Chaotic Maps. Phys. Rev. Lett. 92:144101.

Başar, E., C. Başar-Eroglu, S. Karakaş, and M. Schürmann. 2001. Gamma, alpha, delta, and theta oscillations govern cognitive processes. International Journal of Psychophysiology 39:241–8.

Balenzuela, P. and J. García-Ojalvo. 2005. Role of chemical synapses in coupled neurons with noise. Phys. Rev. E 72:021901.

Banerjee, R., D. Ghosh, E. Padmanaban, R. Ramaswamy, L. M. Pecora, and S. K. Dana. 2012. Enhancing synchrony in chaotic oscillators by dynamic relaying. Phys. Rev. E 85:027201.

Barreiro, A. K., E. Shea-Brown, and E. L. Thilo. 2010. Time scales of spike-train correlation for neural oscillators with common drive. Phys. Rev. E 81:011916.

Bennet, Z. R., M.V.L. and. 2004. Electrical coupling and neuronal synchronization in the mammalian brain. Neuron 41:495–511.

Berger, H. 1929. Uber das elektrenkephalogramm des menschen. Arch Psychiatr Nervenkr 87:527–570.

Bi, G. Q. and M. M. Poo. 1998. Synaptic modifications in cultured hippocampal neurons: dependence on spike timing, synaptic strength, and postsynaptic cell type. Journal of Neuroscience 18:10464–10472.

Bibbig, A., R. Traub, and M. Whittington. 2002. Long-range synchronization of gamma and beta oscillations and the plasticity of excitatory and inhibitory synapses: a network model. J. Neurophysiol. 88:1634–1654.

Binder, P.-M. 2008. Frustration in Complexity. Science 320:322–323.

Bio1152. 2012. http://bio1152.nicerweb.com/Locked/media/ch49/49_02-NervousSystems-L.jpg.

Bland, B. H. and S. D. Oddie. 2001. Theta band oscillation and synchrony in the hippocampal formation and associated structures: the case for its role in sensorimotor integration. Behavioural Brain Research 127:119–136.

Bojak, I., T. F. Oostendorp, A. T. Reid, and R. Kötter. 2010. Connecting mean field models of neural activity to EEG and fMRI data. Brain Topography 23:139–149.

Bokil, H., N. Laaris, K. Blinder, M. Ennis, and A. Keller. 2001. Ephaptic Interactions in the Mammalian Olfactory System. J. Neurosci. 21:RC173.

Bonhoeffer, K. F. 1948. Activation of passive iron as a model for the excitation of nerve. The Journal of general physiology 32:69–91.

Börgers, C., S. Epstein, and N. J. Kopell. 2005. Background gamma rhythmicity and attention in cortical local circuits: A computational study. Proc. Natl. Acad. Sci. 102:7002–7007.

Börgers, C., S. Epstein, and N. J. Kopell. 2008. Gamma oscillations mediate stimulus competition and attentional selection in a cortical network model. Proc. Natl. Acad. Sci. 105:18023–18028.

BIBLIOGRAPHY

Bray, D., M. D. Levin, and C. J. Morton-Firth. 1998. Receptor clustering as a cellular mechanism to control sensitivity. Nature 393:85–88.

Breakspear, M. and C. J. Stam. 2005. Dynamics of a neural system with a multiscale architecture. Philosophical Transactions of the Royal Society of London - Series B: Biological Sciences 360:1051–1074.

Breakspear, M. and J. R. Terry. 2002. Nonlinear interdependence in neural systems: motivation, theory, and relevance. The International journal of neuroscience 112:1263–1284.

Breakspear, M., J. R. Terry, and K. J. Friston. 2003. Modulation of excitatory synaptic coupling facilitates synchronization and complex dynamics in a biophysical model of neuronal dynamics. Network: Computation in Neural Systems 14:703–732.

Bremer, F. 1958. Cerebral and cerebellar potentials. Physiological Reviews 38:357–388.

Brette, R., M. Rudolph, T. Carnevale, M. Hines, D. Beeman, J. M. Bower, M. Diesmann, A. Morrison, P. H. Goodman, F. C. Harris, Jr., M. Zirpe, T. Natschlager, D. Pecevski, B. Ermentrout, M. Djurfeldt, A. Lansner, O. Rochel, T. Vieville, E. Muller, A. P. Davison, S. El Boustani, and A. Destexhe. 2007. Simulation of networks of spiking neurons: a review of tools and strategies. Journal of Computational Neuroscience 23:349–398.

Briggman, K. L. and W. Denk. 2006. Towards neural circuit reconstruction with volume electron microscopy techniques. Current Opinion in Neurobiology 16:562–570.

Briggs, F. and W. M. Usrey. 2010. Patterned Activity within the Local Cortical Architecture. Frontiers in neuroscience 4:5.

Brock, L. G., J. S. Coombs, and J. C. Eccles. 1952. The recording of potencials from motoneurones with an intracellular electrode. J. Physiol. 117:431–460.

Brodmann, K. 1909. Vergleichende Lokalisationslehre der Grosshirnrinde in ihren Prinzipien dargestellt auf Grund des Zellenbaues. Leipzig: J.A. Barth.

Bruce, C., R. Desimone, and C. G. Gross. 1981. Visual properties of neurons in a polysensory area in superior temporal sulcus of the macaque. Journal of Neurophysiology 46:369–384.

Brunel, N. 2000. Dynamics of Sparsely Connected Networks of Excitatory and Inhibitory Spiking Neurons. Journal of Computational Neuroscience 8:183–208.

Brunel, N. and M. C. van Rossum. 2007. Lapicque's 1907 paper: from frogs to integrate-and-fire. Biol Cybern. 97:337–339.

Bruno, R. M. 2011. Synchrony in sensation. Current Opinion in Neurobiology 21:701–708.

Budd, J. M. L. 2005. Theta oscillations by synaptic excitation in a neocortical circuit model. Proceedings of the Royal Society B Biological Sciences 272:101–109.

Buia, C. I. and P. H. Tiesinga. 2008. Role of Interneuron Diversity in the Cortical Microcircuit for Attention. J Neurophysiol 99:2158–2182.

Bullmore, E. and O. Sporns. 2009. Complex brain networks: graph theoretical analysis of structural and functional systems. Nature Reviews Neuroscience 10:186–198.

Bumc. 2012. http://www.bumc.bu.edu/anatneuro/research/cellular-neurobiology/.

Buschman, T. J. and E. K. Miller. 2007. Top-down versus bottom-up control of attention in the prefrontal and posterior parietal cortices. Science 315:1860–2.

Buzsáki, G. 2002. Theta Oscillations in the Hippocampus. Neuron 33:325–340.

Buzsáki, G. 2006. Rhythms of the brain. Oxford University Press.

Buzsáki, G. 2010. Hippocampus. Scholarpedia 6:1468.

Buzsáki, G., D. L. Buhl, K. D. Harris, J. Csicsvari, B. Czeh, and A. Morozov. 2003. Hippocampal network patterns of activity in the mouse. Neuroscience 116:201–211.

BIBLIOGRAPHY

Buzsáki, G. and A. Draguhn. 2004. Neuronal oscillations in cortical networks. Science 304:1926–1929.

Campbell, A. W. 1905. Histological studies on the localisation of cerebral function. Cambridge: University Press.

Canolty, R. T., K. Ganguly, S. W. Kennerley, C. F. Cadieu, K. Koepsell, J. D. Wallis, and J. M. Carmena. 2010. Oscillatory phase coupling coordinates anatomically dispersed functional cell assemblies. Proc. Natl. Acad. Sci. 107:17356–17361.

Cantero, J. L. and M. Atienza. 2005. The role of neural synchronization in the emergence of cognition across the wake-sleep cycle. Reviews in the Neurosciences 16:69–83.

Cantero, J. L., M. Atienza, R. Stickgold, M. J. Kahana, J. R. Madsen, and B. Kocsis. 2003. Sleep-dependent theta oscillations in the human hippocampus and neocortex. Journal of Neuroscience 23:10897–10903.

Caspar, D., D. Goddenough, L. Makowski, and W. Phillips. 1977. Gap Junction Structures. The Journal of Cell Biology 74:605–628.

Castelo-Branco, M., R. Goebel, S. Neuenschwander, and W. Singer. 2000. Neuronal synchrony correlates with surface segregation rules. Nature 405:685–689.

Cell. 2012. http://www.cell.com/cell_picture_show-embryogenesis.

Chawla, D., K. J. Friston, and E. D. Lumer. 2001. Zero-lag synchronous dynamics in triplets of interconnected cortical areas. Neural Networks 14:727 – 735.

Chialvo, D. R. 1995. Generic excitable dynamics on a two-dimensional map. Chaos Solitons Fractals 5:461–479.

Chitra, R. N. and V. C. Kuriakose. 2007. Phase effects on synchronization by dynamical relaying in delay-coupled systems. Chaos Woodbury Ny 18:023129.

Churchland, M. M., B. M. Yu, J. P. Cunningham, L. P. Sugrue, M. R. Cohen, G. S. Corrado, W. T. Newsome, A. M. Clark, P. Hosseini, B. B. Scott, and et al. 2010. Stimulus onset quenches neural variability: a widespread cortical phenomenon. Nature Neuroscience 13:369–378.

Cohen, D. 1968. Magnetoencephalography: evidence of magnetic fields produced by alpha-rhythm currents. Science 161:784–786.

Contreras, D., A. Destexhe, T. Sejnowski, and M. Steriade. 1996. Control of spatiotemporal coherence of a thalamic oscillation by corticothalamic feedback. Science 274:771–774.

Crespo-Garcia, M., J. L. Cantero, A. Pomyalov, S. Boccaletti, and M. Atienza. 2010. Functional neural networks underlying semantic encoding of associative memories. NeuroImage 50:1258–1270.

Dale, H. H. 1934. Pharmacology and Nerve Endings. British medical journal 2:1161–1163.

Dayan, P. and L. F. Abbott. 2001. Theoretical Neuroscience: Computational and Mathematical Modeling of Neural Systems vol. 39. MIT Press.

de la Rocha, J., B. Doiron, E. Shea-Brown, K. Josić, and A. Reyes. 2007. Correlation between neural spike trains increases with firing rate. Nature 448:802–806.

de Sousa Vieira, M. 2010. Properties of zero-lag long-range synchronization via dynamical relaying. Chaos: An Interdisciplinary Journal of Nonlinear Science 20:013131.

Deco, G., V. K. Jirsa, and A. R. McIntosh. 2011. Emerging concepts for the dynamical organization of resting-state activity in the brain. Nature Reviews Neuroscience 12:43–56.

Deco, G., V. K. Jirsa, P. A. Robinson, M. Breakspear, and K. Friston. 2008. The Dynamic Brain: From Spiking Neurons to Neural Masses and Cortical Fields. PLoS Comput Biol 4:e1000092.

Desbordes, G., J. Jin, C. Weng, N. A. Lesica, G. B. Stanley, and J.-M. Alonso. 2008. Timing Precision in Population Coding of Natural Scenes in the Early Visual System. PLoS Biol 6:e324.

Desimone, R., T. D. Albright, C. G. Gross, and C. Bruce. 1984. Stimulus-selective properties of inferior temporal neurons in the macaque. Journal of Neuroscience 4:2051–2062.

Dhamala, M., V. K. Jirsa, and M. Ding. 2004. Enhancement of Neural Synchrony by Time Delay. Phys. Rev. Lett. 92:074104.

D'Huys, O., I. Fischer, J. Danckaert, and R. Vicente. 2011. Role of delay for the symmetry in the dynamics of networks. Phys. Rev. E 83:046223.

D'Huys, O., R. Vicente, T. Erneux, J. Danckaert, and I. Fischer. 2008. Synchronization properties of network motifs: Influence of coupling delay and symmetry. Chaos 18:037116.

Dickson, C., G. Biella, and M. de Curtis. 2003. Slow periodic events and their transition to gamma oscillations in the entorhinal cortex of the isolated guinea pig brain. Journal of Neurophysiology 900:39–46.

Doiron, B., M. J. Chacron, L. Maler, A. Longtin, and J. Bastian. 2003. Inhibitory feedback required for network oscillatory responses to communication but not prey stimuli. Nature 421:539–543.

Doiron, B., B. Lindner, A. Longtin, L. Maler, and J. Bastian. 2004. Oscillatory Activity in Electrosensory Neurons Increases with the Spatial Correlation of the Stochastic Input Stimulus. Phys. Rev. Lett. 93:048101.

Douglas, R. and K. Martin. 2004. Neuronal Circuits of the Neocortex. Annu. Rev. Neurosci. 27:419–451.

Doyère, V., F. Burette, C. R. Negro, and S. Laroche. 1993. Long-term potentiation of hippocampal afferents and efferents to prefrontal cortex: implications for associative learning. Neuropsychologia 31:1031–1053.

Draghun, A., R. Traub, D. Schmitz, and J. Jefferys. 1998. Electrical coupling underlies high-frequency oscillations in the hippocampus in vitro. Nature 394:189–192.

Duchamp-Viret, P. and A. Duchamp. 1993. GABAergic control of odour-induced activity in the frog olfactory bulb: Possible GABAergic modulation of granule cell inhibitory action. Neuroscience 56:905–914.

Eneurosurgery. 2012. http://www.eneurosurgery.com/thalamus.html.

Engel, A., Kreiter, A.K., P. Konig, and W. Singer. 1991. Synchronization of oscillatory neuronal responses between striate and extrastriate visual cortical areas of the cat. Proc. Natl. Acad. Sci. 88:6048–6052.

Eppler, J. M., M. Helias, E. Muller, M. Diesmann, and M. Gewaltig. 2009. PyNEST: a convenient interface to the NEST simulator. Front. Neuroinform. 2:12.

Ermentrout, G. B. and L. Edelstein-Keshet. 1993. Cellular Automata Approaches to Biological Modeling. Journal of Theoretical Biology 160:97–133.

Ermentrout, G. B. and N. Kopell. 1986. Parabolic bursting in an excitable system coupled with a slow oscillation. SIAM J Applied Mathematics 46:233–253.

Ermentrout, G. B. and N. Kopell. 1998. Fine structure of neural spiking and synchronization in the presence of conduction delays. Proc. Natl. Acad. Sci. 95:1259–1264.

Ermentrout, J. 1996. Type I membranes, phase resetting curves, and synchrony. Neural Comp. 8:979–1001.

Ernst, U., K. Pawelzik, and T. Geisel. 1995. Synchronization Induced by Temporal Delays in Pulse-Coupled Oscillators. Phys. Rev. Lett. 74:1570–1573.

Falkenburger, B. H., K. L. Barstow, and I. M. Mintz. 2001. Dendrodendritic inhibition through reversal of dopamine transport. Science 293:2465–2470.

Fatt, P. 1957. Sequence of events in synaptic activation of a motoneurone. J. Neurophysiol. 20:61–80.

Felleman, D. J. and D. C. Van Essen. 1991. Distributed hierarchical processing in the primate cerebral cortex. Cerebral Cortex 1:1–47.

Feng, J., V. K. Jirsa, and M. Ding. 2006. Synchronization in networks with random interactions: Theory and applications. Chaos 16:015109.

ffytche, D. H. and M. Catani. 2005. Beyond localization: from hodology to function. Philosophical Transactions of the Royal Society B: Biological Sciences 360:767–779.

Fischer, I., R. Vicente, J. M. Buldú, M. Peil, C. R. Mirasso, M. C. Torrent, and J. García-Ojalvo. 2006. Zero-lag Long-range Synchronization Via Dynamical Relaying. Physical Review Letters 97:123902.

FitzHugh, R. 1961. Impulses and physiological states in theoretical models of nerve membrane. Biophysical J. 1:445–466.

Frien, A., R. Eckhorn, R. Bauer, T. Woelbern, and H. Kehr. 1994. Stimulus-specific fast oscillations at zero phase between visual areas V1 and V2 of awake monkey. NeuroReport 5:2273–2277.

Fries, P. 2005. A mechanism for cognitive dynamics: neuronal communication through neuronal coherence. Trends in Cognitive Sciences 9:474–480.

Fries, P., D. Nikolić, and W. Singer. 2007. The gamma cycle. Trends Neurosci. 30:309–316.

Fries, P., J. H. Reynolds, A. E. Rorie, and R. Desimone. 2001. Modulation of Oscillatory Neuronal Synchronization by Selective Visual Attention. Science 291:1560 – 1563.

Fries, P., P. Roelfsema, A. Engel, P. Konig, and W. Singer. 1997. Synchronization of oscillatory responses in visual cortex correlates with perception in interocular rivalry. Proc. Natl. Acad. Sci. 94:12699–12704.

Friston, K. J. 2011. Functional and effective connectivity: a review. Brain Connectivity 1:13–36.

Furtado, L. S. and M. Copelli. 2006. Response of electrically coupled spiking neurons: a cellular automaton approach. Phys. Rev. E 73:011907.

Gerstner, W. and W. Kistler. 2002. Spiking Neuron Models: Single Neurons, Populations, Plasticity. Cambridge University Press.

Golding, N. L., N. P. Staff, and N. Spruston. 2002. Dendritic Spikes as a Mechanism for Cooperative Long-Term Potentiantion. Nature 418:326–331.

Golgi, C. 1906. The neuron doctrine - theory and facts. Nobel Lecture 1921:190–217.

Gollo, L. L., O. Kinouchi, and M. Copelli. 2009. Active Dendrites Enhance Neuronal Dynamic Range. PLoS Comput Biol 5:e1000402.

Gollo, L. L., O. Kinouchi, and M. Copelli. 2012a. Statistical physics approach to dendritic computation: The excitable-wave mean-field approximation. Phys. Rev. E 85:011911.

Gollo, L. L., C. Mirasso, and V. M. Eguíluz. 2012b. Signal integration enhances the dynamic range in neuronal systems. Phys. Rev. E 85:040902.

Gollo, L. L., C. Mirasso, and A. E. P. Villa. 2010. Dynamic control for synchronization of separated cortical areas through thalamic relay. NeuroImage 52:947–955.

Gollo, L. L., C. R. Mirasso, M. Atienza, M. Crespo-Garcia, and J. L. Cantero. 2011. Theta Band Zero-Lag Long-Range Cortical Synchronization via Hippocampal Dynamical Relaying. PLoS ONE 6:e17756.

Gomes, I., J. M. Buldú, C. Mirasso, and J. García-Ojalvo. 2006. Synchronization by dynamical relaying in electronic circuit arrays. Chaos 16:043113.

Goutagny, R., J. Jackson, and S. Williams. 2009. Self-generated theta oscillations in the hippocampus. Nature Neuroscience 12:1491–1493.

Gray, C. 1999. The temporal correlation hypothesis of visual feature integration. Neuron 24:31–47.

Gray, C. M., P. König, A. K. Engel, and W. Singer. 1989. Oscillatory responses in cat visual cortex exhibit inter-columnar synchronization which reflects global stimulus properties. Nature 338:334–337.

Greedan, J. E. 2001. Geometrically frustrated magnetic materials. J. Mater. Chem. 11:37–53.

Greenberg, J. M. and S. P. Hastings. 1978. Spatial Patterns for Discrete Models of Diffusion in Excitable Media. SIAM J. Appl. Math. 34:515–523.

Gregoriou, G. G., S. J. Gotts, H. Zhou, and R. Desimone. 2009. High-frequency, long-range coupling between prefrontal and visual cortex during attention. Science 324:1207–10.

Groh, A., C. P. J. de Kock, V. C. Wimmer, B. Sakmann, and T. Kuner. 2008. Driver or Coincidence Detector: Modal Switch of a Corticothalamic Giant Synapse Controlled by Spontaneous Activity and Short-Term Depression. Journal of Neuroscience 8:9652–9663.

Grossberg, S. 1976. Adaptive pattern classification and universal recoding: I. Parallel development and coding of neural feature detectors. Biological Cybernetics 23:121–134.

Guderian, S. and E. Duzel. 2005. Induced theta oscillations mediate large-scale synchrony with mediotemporal areas during recollection in humans. Hippocampus 15:901–912.

Gutierrez, R., S. A. Simon, and M. A. L. Nicolelis. 2010. Licking-induced synchrony in the taste-reward circuit improves cue discrimination during learning. Journal of Neuroscience 30:287–303.

Hagmann, P., L. Cammoun, X. Gigandet, R. Meuli, C. J. Honey, V. J. Wedeen, and O. Sporns. 2008. Mapping the Structural Core of Human Cerebral Cortex. PLoS Biol 6:e159.

Hansen, C. H., R. G. Endres, and N. S. Wingreen. 2008. Chemotaxis in *Escherichia coli*: A Molecular Model for Robust Precise Adaptation. PLoS Comput Biol 4:e1.

Hasselmo, M. E. 2005. What is the function of hippocampal theta rhythm?–Linking behavioral data to phasic properties of field potential and unit recording data. Hippocampus 15:936–949.

Häusser, M. and B. Mel. 2003. Dendrites: bug or feature? Curr. Opinion in Neurobiology 13:372–383.

Hayon, G., M. Abeles, and D. Lehmann. 2005. A model for representing the dynamics of a system of synfire chains. J. Comp. Neurosci. 18:41–53.

Herz, A. V. M., T. Gollisch, C. K. Machens, and D. Jaeger. 2006. Modeling Single-Neuron Dynamics and Computations: A Balance of Detail and Abstraction. Science 314:80–85.

Hindmarsh, J. L. and R. M. Rose. 1984. A Model of Neuronal Bursting Using Three Coupled First Order Differential Equations. Proc. Roy. Soc. London B 221:87–102.

Hodgkin, A. and A. Huxley. 1952. A quantitative description of the membrane current and its application to conduction and excitation in nerve. Journal of Physiology 117:500–544.

Hodgkin, A. L. 1948. The local electric changes associated with repetitive action in a non-medullated axon. The Journal of Physiology 107:165–181.

Hodgkin, A. L. and A. F. Huxley. 1939. Action potentials recorded from inside a nerve fiber. Nature 144:710–711.

Honey, C., R. Kotter, M. Breakspear, and O. Sporns. 2007. Network structure of cerebral cortex shapes functional connectivity on multiple time scales. Proc. Natl. Acad. Sci. 104:10240–10245.

Honey, C. J., O. Sporns, L. Cammoun, X. Gigandet, J. P. Thiran, R. Meuli, and P. Hagmann. 2009. Predicting human resting-state functional connectivity from structural connectivity. Proc. Natl. Acad. Sci. 106:2035–2040.

Hrsbstaff. 2012. http://hrsbstaff.ednet.ns.ca/holmesdl/Biology%2012/Chemical-Messengers.jpg.

Huguenard, J. R. and D. A. McCormick. 2007. Thalamic synchrony and dynamic regulation of global forebrain oscillations. Trends in Neurosciences 30:350–356.

Hyman, J. M., E. A. Zilli, A. M. Paley, and M. E. Hasselmo. 2005. Medial prefrontal cortex cells show dynamic modulation with the hippocampal theta rhythm dependent on behavior. Hippocampus 15:739–749.

Hyman, J. M., E. A. Zilli, A. M. Paley, and M. E. Hasselmo. 2010. Working Memory Performance Correlates with Prefrontal-Hippocampal Theta Interactions but not with Prefrontal Neuron Firing Rates. Frontiers in integrative neuroscience 4:13.

Izhikevich, E. 2006. Polychronization: computation with spikes. Neural computation 18:245–282.

Izhikevich, E. M. 2000. Neural Excitability, Spiking and Bursting. Int. J. Bifurcat. Chaos 10:1171–1266.

Izhikevich, E. M. 2003. Simple model of spiking neurons. IEEE Transactions on Neural Networks 14:1569–72.

Izhikevich, E. M. 2004. Which model to use for cortical spiking neurons? IEEE Transactions on Neural Networks 15:1063–1070.

Izhikevich, E. M. 2007. Dynamical Systems in Neuroscience. The MIT press.

Izhikevich, E. M. and G. M. Edelman. 2008. Large-scale model of mammalian thalamocortical systems. Proc. Natl. Acad. Sci. 105:3593–3598.

Izhikevich, E. M., J. A. Gally, and G. M. Edelman. 2004. Spike-timing dynamics of neuronal groups. Cerebral Cortex 14:933–944.

Izhikevich, E. M. and F. Hoppensteadt. 2004a. Classification of bursting mappings. International Journal 14:3847–3854.

Izhikevich, E. M. and F. Hoppensteadt. 2004b. Classification of Bursting Mappings. Int. J. Bifurcat. Chaos 14:3847–3854.

Jeffress, L. A. 1948. A place theory of sound localization. Journal of Comparative and Physiological Psychology 41:35–39.

Jian-Ping, L., Y. Lian-Chun, Y. Mei-Chen, and C. Yong. 2012. Zero-Lag Synchronization in Spatiotemporal Chaotic Systems with Long Range Delay Couplings. Chinese Physics Letters 29:050501.

Johnston, D., J. Magee, C. Colbert, and B. Christie. 1996. Active Properties of Neuronal Dendrites. Annu. Rev. Neurosci. 19:165–186.

Jones, E. 2002. Thalamic circuitry and thalamocortical synchrony. Phil. Trans. R. Soc. Lond. B 357:1659–1673.

Jones, E. G. 1985. The Thalamus. Plenum Press, New York.

Jones, M. W. and M. A. Wilson. 2005a. Phase precession of medial prefrontal cortical activity relative to the hippocampal theta rhythm. Hippocampus 15:867–873.

Jones, M. W. and M. A. Wilson. 2005b. Theta Rhythms Coordinate Hippocampal-Prefrontal Interactions in a Spatial Memory Task. PLoS Biology 3:e402.

Joris, P. X., P. H. Smith, and T. C. Yin. 1998. Coincidence detection in the auditory system: 50 years after Jeffress. Neuron 21:1235–1238.

Kahana, M. J. 2006. The cognitive correlates of human brain oscillations. Journal of Neuroscience 26:1669–1672.

Kahana, M. J., D. Seelig, and J. Madsen. 2001. Theta returns. Current Opinion in Neurobiology 11:739–744.

Kandel, E. R., J. H. Schwartz, and T. M. Jessell, eds. 2000. Principles of Neural Science. 4th ed. McGraw-Hill Medical, New York.

Katz, B. and R. Miledi. 1965. The measurement of synaptic delay, and the time course of acetylcholine release at the neuromuscular junction. Proceedings of the Royal Society of London. Series B, Biological Sciences 161:483–495.

Katzner, S., I. Nauhaus, A. Benucci, V. Bonin, D. L. Ringach, and M. Carandini. 2009. Local Origin of Field Potentials in Visual Cortex. Neuron 61:35–41.

Kay, L. M. and S. M. Sherman. 2007. An argument for an olfactory thalamus. Trends in Neurosciences 30:47–53.

Kinouchi, O. and M. Copelli. 2006. Optimal dynamical range of excitable networks at criticality. Nat. Phys. 2:348–352.

Kinouchi, O. and M. H. R. Tragtenberg. 1996. Modeling Neurons by Simple Maps. Int. J. Bifurcat. Chaos 6:2343–3460.

Knight, B. W. 1972. Dynamics of encoding in a population of neurons. J. Gen. Physiol. 59:734–766.

Knoblauch, A. and F. Sommer. 2003. Synaptic plasticity, conduction delays, and inter-areal phase relations of spike activity in a model of reciprocally connected areas. Neurocomputing 52-54:301–306.

Knoblauch, A. and F. Sommer. 2004. Spike-timing-dependent synaptic plasticity can form "zero lag links" for cortical oscillations. Neurocomputing 58-60:185–190.

Knudsen, E. I. 1982. Auditory and visual maps of space in the optic tectum of the owl. Journal of Neuroscience 2:1177–1194.

Knudsen, E. I. and M. Konishi. 1978. Center-surround organization of auditory receptive fields in the owl. Science 202:778–780.

Koch, C. 1999. Biophysics of Computation. Oxford University Press, New York.

Koene, R. A., A. Gorchetchnikov, R. C. Cannon, and M. E. Hasselmo. 2003. Modeling Modeling goal-directed spatial navigation in the rat based on physiological data from the hippocampal formation. Neural Networks 16:577–584.

Kolb, B. and I. Q. Whishaw. 1990. Fundamentals of Human Neuropsychology. Freeman, New York.

König, P., A. Engel, and W. Singer. 1995. Relation between oscillatory activity and long-range synchronization in cat visual cortex. Proc. Natl. Acad. Sci. USA 92:290–294.

Kopell, N. and G. Ermentrout. 2004. Chemical and electrical synapses perform complementary roles in the synchronization of interneuronal networks. Proc. Natl. Acad. Sci. 101:15482–15487.

Kopell, N., G. B. Ermentrout, M. A. Whittington, and R. D. Traub. 2000. Gamma rhythms and beta rhythms have different synchronization properties. Proc. Natl. Acad. Sci. 97:1867–1872.

Kötter, R. 2004. Online retrieval, processing, and visualization of primate connectivity data from the CoCoMac database. Neuroinformatics 2:127–144.

Krahe, R. and F. Gabbiani. 2004. Burst firing in sensory systems. Nat Rev Neurosci. 5:13–23.

Kumar, A., S. Rotter, and A. Aertsen. 2010. Spiking activity propagation in neuronal networks: reconciling different perspectives on neural coding. Nature Reviews Neuroscience 11:615–627.

Landsman, A. S. and I. B. Schwartz. 2007. Complete chaotic synchronization in mutually coupled time-delay systems. Phys. Rev. E 75:026201.

Lapicque, L. 1907. Recherches quantitatives sur l'excitation électrique des nerfs traiteé comme une polarization. J. Physiol. Pathol. Gen. 9:620–635.

Larter, R., B. Speelman, and R. M. Worth. 1999. A coupled ordinary differential equation lattice model for the simulation of epileptic seizures. Chaos: An Interdisciplinary Journal of Nonlinear Science 9:795–804.

Lee, A. K. and M. A. Wilson. 2002. Memory of sequential experience in the hippocampus during slow wave sleep. Neuron 36:1183–1194.

Lehmann-Horn, F. and K. Jurkat-Rott. 2003. Nanotechnology for neuronal ion channels. Journal of Neurology, Neurosurgery & Psychiatry 74:1466–1475.

Leung, L. S. 1998. Generation of theta and gamma rhythms in the hippocampus. Neuroscience and Biobehavioral Reviews 22:275–290.

Leung, L. W. and J. G. Borst. 1987. Electrical activity of the cingulate cortex. I. Generating mechanisms and relations to behavior. Brain Research 407:68–80.

Lindner, B., J. García-Ojalvo, A. Neiman, and L. Schimansky-Geier. 2004. Effects of noise in excitable systems. Physics Reports 392:321–424.

Lisman, J. and G. Buzsáki. 2008. A neural coding scheme formed by the combined function of gamma and theta oscillations. Schizophrenia Bulletin 34:974–980.

Liu, Z. 2008. Multimodal Neuroimaging Integrating Functional Magnetic Resonance Imaging and Electroencephalography. Ph.D. thesis University of Minnesota.

Llinás, R. 1988. The intrinsic electrophysiological properties of mammalian neurons: insights into central nervous system function. Science 242:1654–1664.

Llinás, R. and D. Pare. 1997. Thalamus chap. Coherent oscillations in specific and nonspecific thalamocortical networks and their role in cognition. Pergamon, New York.

Llinás, R. and U. Ribary. 1993. Coherent 40-Hz oscillation characterizes dream state in humans. Proc. Natl. Acad. Sci. 90:2078–2081.

Llinás, R., U. Ribary, D. Contreras, and C. Pedroarena. 98. The neuronal basis for conciousness. Phil. Trans. R. Soc. Lond. B 353:1841–1849.

Llinás, R. R., U. Ribary, D. Jeanmonod, E. Kronberg, and P. P. Mitra. 1999. Thalamocortical dysrhythmia: A neurological and neuropsychiatric syndrome characterized by magnetoencephalography. Proc. Natl. Acad. Sci. 96:15222–15227.

Lowe, G. 2003. Electrical Signaling in the Olfactory Bulb. Curr. Opin. Neurobiol. 13:476–481.

Lowel, S. and W. Singer. 1992. Selection of intrinsic horizontal connections in the visual cortex by correlated neuronal activity. Science 255:209–212.

Mann, E. and O. Paulsen. 2007. Role of GABAergic inhibition in hippocampal network oscillations. Trends in Neurosciences 30:343–349.

Marinazzo, D., H. J. Kappen, and S. C. A. M. Gielen. 2007. Input-Driven Oscillations in Networks with Excitatory and Inhibitory Neurons with Dynamic Synapses. Neural Computation 19:1739–1765.

Masquelier, T., E. Hugues, G. Deco, and S. J. Thorpe. 2009. Oscillations, phase-of-firing coding, and spike timing-dependent plasticity: an efficient learning scheme. Journal of Neuroscience 29:13484–13493.

Maunsell, J. H. and D. C. Van Essen. 1983. The connections of the middle temporal visual area (MT) and their relationship to a cortical hierarchy in the macaque monkey. Journal of Neuroscience 3:2563–2586.

McAlonan, K., J. Cavanaugh, and R. H. Wurtz. 2008. Guarding the gateway to cortex with attention in visual thalamus. Nature 456:391–394.

McCormick, D. and T. Bal. 1994. Sensory gating mechanisms of the thalamus. Current Opinion in Neurobiology 4:550–556.

McIntosh, A. R. 1999. Mapping cognition to the brain through neural interactions. Memory Hove England 7:523–548.

Mel, B. W. 1993. Synaptic integration in an excitable dendritic tree. J. Neurophysiol. 70:1086–1101.

Mesulam, M. M. 1998. From sensation to cognition. Brain 121):1013–1052.

Michel, C. M., M. M. Murray, G. Lantz, S. Gonzalez, L. Spinelli, and R. Grave De Peralta. 2004. EEG source imaging. Clinical Neurophysiology 115:2195–2222.

Migliore, M., M. L. Hines, and S. G. M. 2005. The role of distal dendritic gap juncions in synchronization of mitral cell axonal output. J. Comp. Neurosc. 18:151–161.

Miller, K. J., L. B. Sorensen, J. G. Ojemann, and M. Den Nijs. 2009. Power-Law Scaling in the Brain Surface Electric Potential. PLoS Computational Biology 5:10.

Miller, R. 1996. Axonal conduction time and human cerebal laterality: a psychobiological theory. Harwood Academics Publisher, Amsterdam.

Miller, R. 2000. Time and the brain. Harwood Press.

Milner, P. M. 1974. A model for visual shape recognition. Psychological Review 81:521–535.

Milo, R., S. Shen-Orr, S. Itzkovitz, N. Kashtan, D. Chklovskii, and U. Alon. 2002. Simple Building Blocks of Complex Networks. Science 298:824 – 827.

Mima, T., T. Oluwatimilehin, and M. Hiraoka, T. nad Hallett. 2001. Transient Interhemispheric Neuronal Synchrony Correlates with Object Recognition. The Journal of Neuroscience 21:3942–3948.

Mitchell, S. J. and J. B. Ranck. 1980. Generation of theta rhythm in medial entorhinal cortex of freely moving rats. Brain Research 189:49–66.

Mori, K., H. Nagao, and Y. Yoshihara. 1999. The olfactory bulb: coding and processing of odor molecule information. Science 286:711–5.

Morris, C. and H. Lecar. 1981. Voltage Oscillations in the Barnacle Giant Muscle Fiber. Biophys. J. 35:193–213.

Mountcastle, V. B. 1957. Modality and topographic properties of single neurons of catÊijs somatic sensory cortex. Journal of Neurophysiology 20:408–434.

Mountcastle, V. B. 1997. The columnar organization of the neocortex. Brain: A journal of neurology 120 (Pt 4):701–722.

Mountcastle, V. B., P. W. Davies, and A. L. Berman. 1957. Response properties of neurons of catÊijs somatic sensory cortex to peripheral stimuli. Journal of Neurophysiology 20:374–407.

Murre, J. M. and D. P. Sturdy. 1995. The connectivity of the brain: multi-level quantitative analysis. Biological Cybernetics 73:529–545.

Murthy, V. N. and E. E. Fetz. 1992. Coherent 25- to 35-Hz oscillations in the sensorimotor cortex of awake behaving monkeys. Proc. Natl. Acad. Sci. 89:5670–5674.

Nagumo, J., S. Arimoto, and S. Yoshizawa. 1962. An active pulse transmission line simulating nerve axon. Proc IRE. 50:2061–2070.

Nicolelis, M. and S. Ribeiro. 2002. Multielectrode recordings: the next steps. Current Opinion in Neurobiology 12:602–606.

Niebur, E. 2008. Neuronal cable theory. Scholarpedia 3:2674.

Niebur, E., H. G. Schuster, and D. M. Kammen. 1991. Collective frequencies and metastability in networks of limit-cycle oscillators with time delay. Phys. Rev. Lett. 67:2753–2756.

Nikolić, D. 2009. Model this! Seven empirical phenomena missing in the models of cortical oscillatory dynamics. *in* Proceedings of the International Joint Conference on Neural Networks, IJCNN.

O'Keefe, J. and L. Nadel. 1978. The Hippocampus as a Cognitive Map vol. 3. Oxford University Press.

Olsen, S. R., D. S. Bortone, H. Adesnik, and M. Scanziani. 2012. Gain control by layer six in cortical circuits of vision. Nature 483.

Pare, D., E. Shink, H. Gaudreau, A. Destexhe, and E. Lang. 1998. Impact of spontaneous synaptic activity on the resting properties of cat neocortical pyramidal neurons in vivo. J. Neurophysiol. 78:1450–1460.

Parker, G. H. 1919. The elementary nervous system. Lippincott, Philadelphia.

Paz, R., E. P. Bauer, and D. Paré. 2008. Theta synchronizes the activity of medial prefrontal neurons during learning. Learning Memory 15:524–531.

Peil, M., L. Larger, and I. Fischer. 2007. Versatile and robust chaos synchronization phenomena imposed by delayed shared feedback coupling. Phys. Rev. E 76:045201.

Pérez, T., G. C. García, V. M. Eguíluz, R. Vicente, G. Pipa, and C. Mirasso. 2011. Effect of the Topology and Delayed Interactions in Neuronal Networks Synchronization. PLoS ONE 6:e19900.

Pesaran, B. 2010. Neural correlations, decisions, and actions. Current Opinion in Neurobiology 20:166–171.

Pikovsky, A., M. Rosemblum, and J. Kurths. 2002. Synchronization: A universal Concept in Nonlinear Science. Cambridge University Press.

Pinsky, F. P. and J. Rinzel. 1994. Intrinsic and network rhythmogenesis in a reduced traub model for CA3 neurons. J. Comput. Neurosci. 1:39–60.

Poirazi, P. and B. W. Mel. 2001. Impact of active dendrites and structural plasticity on the memory capacity of neural tissue. Neuron 29:779–796.

Pons, A. J., J. L. Cantero, M. Atienza, and J. García-Ojalvo. 2010. Relating structural and functional anomalous connectivity in the aging brain via neural mass modeling. NeuroImage 52:848–861.

Ponten, S. C., A. Daffertshofer, A. Hillebrand, and C. J. Stam. 2010. The relationship between structural and functional connectivity: graph theoretical analysis of an EEG neural mass model. NeuroImage 52:985–994.

Poulet, J. F. A., L. M. J. Fernandez, S. Crochet, and C. C. H. Petersen. 2012. Thalamic control of cortical states. Nature Neuroscience 15:1–3.

Quiroga, Q., L. Reddy, G. Kreiman, C. Koch, and I. Fried. 2005. Invariant visual representation by single neurons in the human brain. Nature 435:1102–1107.

Rall, W. 1959. Branching dendrites tree and motoneuron membrane resistivity. Exp. Neurol. 1:491–527.

Rall, W. 1964. Theoretical significance of dendritic trees for neuronal input-output relations Pages 73–97. 4 Stanford University Press.

Ramana Reddy, D. V., A. Sen, and G. L. Johnston. 1998. Time Delay Induced Death in Coupled Limit Cycle Oscillators. Phys. Rev. Lett. 80:5109–5112.

Ranganath, C. and M. d'Esposito. 2005. Directing the mindÊijs eye: prefrontal, inferior and medial temporal mechanisms for visual working memory. Current Opinion in Neurobiology 15:175–182.

Remme, M. W. H., M. Lengyel, and B. S. Gutkin. 2009. The Role of Ongoing Dendritic Oscillations in Single-Neuron Dynamics. PLoS Comput Biol 5:e1000493.

Renart, A., J. De La Rocha, P. Bartho, L. Hollender, N. Parga, A. Reyes, and K. D. Harris. 2010. The asynchronous state in cortical circuits. Science 327:587–90.

Reyes, A. and E. Fetz. 1993. Two modes of interspike interval shortening by brief transient depolarizations in cat neocortical neurons. J. Neurophysiol. 69:1661–1672.

Ribary, U., A. Ioannides, K. Singh, R. Hasson, J. Bolton, F. Lado, A. Mogilner, and R. Llinas. 1991. (1991) Magnetic field tomography of coherent thalamocortical 40-Hz oscillations in humans. Proc. Natl. Acad. Sci. 88:11037–11041.

Rikenresearch. 2012. http://www.rikenresearch.riken.jp/eng/hom/6236.

Ringo, J. L., R. W. Doty, S. Demeter, and P. Y. Simard. 1994. Time is the essence: A conjecture that hemispheric specialization arises from interhemispheric conduction delay. Cerebral Cortex 4:331–343.

Rinzel, J. and G. B. Ermentrout. 1998. Analysis of neural excitability and oscillations. Methods in neuronal modeling 2:135–169.

Rinzel, J., D. Terman, X.-J. Wang, and B. Ermentrout. 1998. Propagating Activity Patterns in Large-Scale Inhibitory Neuronal Networks. Science 279:1351–1355.

Rizzuto, D., J. Madsen, E. Bromfield, A. Schulze-Bonhage, D. Seelig, R. Aschenbrenner-Scheibe, and M. Kahana. 2003. Reset of human neocortical oscillations during a working memory task. Proc. Natl. Acad. Sci. 100:7931–7936.

Robles, L. and M. A. Ruggero. 2001. Mechanics of the mammalian cochlea. Physiological Reviews 81:1305–52.

Rodriguez, E., N. George, J. Lachaux, J. Martinerie, B. Renault, and F. Varela. 1999. Perception's shadow: long-distance synchronization of human brain activity. Nature 397:430–433.

Roelfsema, P., A. Engel, P. Konig, and W. Singer. 1997. Visuomotor integration is associated with zero time-lag synchronization among cortical areas. Nature 385:157–161.

Root, C. M., J. L. Semmelhack, W. A. M., J. Flores, and J. W. Wang. 2007. Propagation of olfactory information in Drosophila. Proc. Natl. Acad. Sci. 104:11826–11831.

Rose, R. M. and J. L. Hindmarsh. 1989. The assembly of ionic currents in a thalamic neuron. I. The three-dimensional model. Proceedings of the Royal Society of London Series B Containing papers of a Biological character Royal Society Great Britain 237:267–288.

Roskies, A. L. 1999. The binding problem. Neuron 24:7–9.

Rossoni, E., Y. Chen, M. Ding, and J. Feng. 2005. Stability of synchronous oscillations in a system of Hodgkin-Huxley neurons with delayed diffusive and pulsed coupling. Phys. Rev. E 71:061904.

Rouiller, E. M. and E. Welker. 2000. A comparative analysis of the morphology of corticothalamic projections in mammals. Brain Research Bulletin 53:727–741.

Roxin, A., N. Brunel, and D. Hansel. 2005. Role of Delays in Shaping Spatiotemporal Dynamics of Neuronal Activity in Large Networks. Phys. Rev. Lett. 94:238103.

Rumsey, C. C. and L. F. Abbott. 2006. Synaptic Democracy in Active Dendrites. J. Neurophysiol. 96:2307–2318.

Ruppin, E., E. L. Schwartz, and Y. Yeshurun. 1993. Examining the volume efficiency of the cortical architecture in a multi-processor network model. Biological Cybernetics 70:89–94.

Salami, M., C. Itami, T. Tsumoto, and F. Kimura. 2003. Change of conduction velocity by regional myelination yields to constant latency irrespective of distance between thalamus to cortex. Proc. Natl. Acad. Sci. 100:6174–6179.

Salinas, E. and T. Sejnowski. 2000. Impact of correlated synaptic input on output firing rate and variability in simple neuronal models. J. Neurosci. 20:6193–6209.

Salinas, E. and T. Sejnowski. 2001. Correlated neuronal activity and the flow of neuronal information. Nat. Rev. Neurosci. 2:539–550.

Sarnthein J, R. P. S. G. v. S. A., Petsche H. 1998. Synchronization between prefrontal and posterior association cortex during human working memory. Proc. Natl. Acad. Sci. 95:7092–7096.

Scannell, J. W., G. A. P. C. Burns, C. C. Hilgetag, M. A. OÊijNeil, and M. P. Young. 1999. The Connectional Organization of the Cortico-thalamic System of the Cat. Cerebral Cortex 9:277–299.

Scheller, B., M. Daunderer, and G. Pipa. 2009. General Anesthesia Increases Temporal Precision and Decreases Power of the Brainstem Auditory-evoked Response-related Segments of the Electroencephalogram. Anesthesiology 111:340–355.

Segev, I. and W. Rall. 1988. Computational study of an excitable dendritic spine. J. Neurophysiol. 60:499–523.

Sethia, G. C., A. Sen, and F. M. Atay. 2008. Clustered Chimera States in Delay-Coupled Oscillator Systems. Phys. Rev. Lett. 100:144102.

Shea-Brown, E., K. Josić, J. de la Rocha, and B. Doiron. 2008. Correlation and Synchrony Transfer in Integrate-and-Fire Neurons: Basic Properties and Consequences for Coding. Phys. Rev. Lett. 100:108102.

Shepherd, G. M., ed. 1991. Foundations of the neuron doctrine. Oxford University Press.

Shepherd, G. M., ed. 1998. The Synaptic Organization of the Brain. Oxford University Press.

Sherman, S. and R. Guillery. 2002. The role of the thalamus in the flow of information to the cortex. Phil. Trans. R. Soc. Lond. B 357:1695–1708.

Sherman, S. M. 2001. Tonic and burst firing: dual modes of thalamocortical relay. Trends Neurosci. 24:122–126.

Sherman, S. M. 2005. Thalamic relays and cortical functioning. Prog Brain Res. 149:107–126.

Shipp, S. 2003. The functional logic of cortico-pulvinar connections. Philosophical Transactions of the Royal Society of London. Series B: Biological Sciences 358:1605–1624.

Siapas, A. G., E. V. Lubenov, and M. A. Wilson. 2005. Prefrontal phase locking to hippocampal theta oscillations. Neuron 46:141–51.

Singer, W. 1999. Neuronal Synchrony: A Versatile Code for the Definition of Relations. Neuron 24:49–65.

Singer, W. 2007. Binding by synchrony. Scholarpedia 2:1657.

Singer, W., A. Engel, A. Kreiter, M. Munk, S. Neuenschwander, and P. Roelfsema. 1997. Neuronal assemblies: necessity, signature and detectability. Trends in Cognitive Sciences 1:252–260.

Skoge, M., Y. Meir, and N. S. Wingreen. 2011. Dynamics of Cooperativity in Chemical Sensing among Cell-Surface Receptors. Phys. Rev. Lett. 107:178101.

Smith, D. G., C. L. Cox, S. M. Sherman, and J. Rinzel. 2000. Fourier Analysis of Sinusoidally Driven Thalamocortical Relay Neurons and a Minimal Integrate-and-Fire-or-Burst Model. J Neurophysiol 83:588–610.

Soleng, A., M. Raastad, and P. Andersen. 1998. Conduction latency along CA3 hippocampal axons from the rat. Hippocampus 13:953–961.

Sotero, R. C., N. J. Trujillo-Barreto, Y. Iturria-Medina, F. Carbonell, and J. C. Jimenez. 2007. Realistically coupled neural mass models can generate EEG rhythms. Neural Computation 19:478–512.

Soteropoulus, D. and S. Baker. 2006. Cortico-cerebellar coherence during a precision grip task in the monkey. J. Neurophysiol. 95:1194–1206.

Sourjik, V. and H. C. Berg. 2002. Receptor sensitivity in bacterial chemotaxis. Proc. Natl. Acad. Sci. 99:123–127.

Sporns, O. 2010. Networks of the Brain vol. 1. MIT Press.

Sporns, O., D. Chialvo, M. Kaiser, and C. Hiltetag. 2004. Organization, development and function of complex brain networks. Trends in Cognitive Sciences 8:418–425.

Sporns, O. and R. Kotter. 2004. Motifs in brain networks. PLoS Biology 2:e369.

Squire, L. R., F. E. Bloom, S. K. McConnell, J. L. Roberts, N. C. Spitzer, and M. J. Zigmound. 2003. Fundamental Neuroscience. Elsevier Science.

Steriade, M. and R. R. Llinas. 1988. The functional states of the thalamus and the associated neuronal interplay. Physiological Review 68:649–742.

Steriade, M., A. Nuñez, and F. Amzica. 1993. A novel slow (< 1 Hz) oscillation of neocortical neurons in vivo: Depolarizing and hyperpolarizing components. Journal of Neuroscience 13:3252–3265.

Strogatz, S. H. 2003. Sync: The Emerging Science of Spontaneous Order. Hyperion.

Stuart, G., N. Spruston, and M. Häusser. 1999. Dendrites. Oxford University Press, New York.

Stuart, G. J. and B. Sakmann. 1994. Active Propagation of Somatic Action Potentials into Neocortical Pyramidal Cell Dendrites. Nature 367:6–72.

Su, H., G. Alroy, E. D. Kirson, and Y. Yaari. 2001. Extracellular calcium modulates persistent sodium current-dependent burst-firing in hippocampal pyramidal neurons. Journal of Neuroscience 21:4173–4182.

Swadlow, H. 1985. Physiological properties of individual cerebral axons studied in vivo for as long as one year. Journal of Neurophysiology 54:1346–1362.

Swadlow, H. 1994. Efferent neurons and suspected interneurons in motor cortex of the awake rabbit: axonal properties, sensory receptive fields, and subthreshold synaptic inputs. Journal of Neurophysiology 71:437–453.

Swadlow, H. 2000. Information flow along neocortical axons. chap. 4, Pages 131–155 *in* Time and the Brain (R. Miller, ed.) Conceptual Advances in Brain Research. Harwood Academic Publishers, Amsterdam.

Swadlow, H., D. Rosene, and S. Waxman. 1978. Characteristics of interhemispheric impulse conduction between the prelunate gyri of the rhesus monkey. Experimental Brain Research 33:455–467.

Swadlow, H. and S. Waxman. 1975. Observations on impulse conduction along central axons. Proc. Natl. Acad. Sci. 72:5156–5159.

Swanson, L. W. 1995. Mapping the human brain: past, present, and future. Trends in Neurosciences 18:471–474.

Swanson, L. W. 1998. Brain maps : structure of the rat brain. New York: Elsevier.

Swindale, N. 2003. Neural synchrony, axonal path lengths, and general anesthesia: a hipothesis. The Neuroscientist 9:440–445.

Takayanagi, M. and H. Ojima. 2006. Microtopography of the dual corticothalamic projections originating from domains along the frequency axis of the cat primary auditory cortex. Neuroscience 142:769–780.

Tchumatchenko, T., A. Malyshev, T. Geisel, M. Volgushev, and F. Wolf. 2010. Correlations and Synchrony in Threshold Neuron Models. Phys. Rev. Lett. 104:058102.

Tejada, S., J. J. González, R. V. Rial, A. M. L. Coenen, A. Gamundí, and S. Esteban. 2010. Electroencephalogram functional connectivity between rat hippocampus and cortex after pilocarpine treatment. Neuroscience 165:621–31.

Temereanca, S., E. N. Brown, and D. J. Simons. 2008. Rapid changes in thalamic firing synchrony during repetitive whisker stimulation. Journal of Neuroscience 28:11153–11164.

Terry, J. R., K. S. Thornburg, D. J. DeShazer, G. D. VanWiggeren, Z. S. Q., A. P., and R. Roy. 1999. Synchronization of chaos in an array of three lasers. Phys. Rev. E 59:4036 – 4043.

Tetko, I. V. and A. E. P. Villa. 1997. Efficient partition of learning datasets for neural network training. Neural Networks 10:1361–1374.

Tiana-Alsina, J., K. Hicke, X. Porte, M. C. Soriano, M. C. Torrent, J. García-Ojalvo, and I. Fischer. 2012. Zero-lag synchronization and bubbling in delay-coupled lasers. Phys. Rev. E 85:026209.

Tiesinga, P., J. Fellows, and T. Sejnowski. 2008. Regulation of spike timing in visual cortical circuits. Nature Rev. Neuroscience 9:97–109.

Toro, R., M. Perron, B. Pike, L. Richer, S. Veillette, Z. Pausova, and T. Paus. 2008. Brain size and folding of the human cerebral cortex. Cerebral Cortex 18:2352–7.

Toulouse, G. 1977. Theory of the frustration effect in spin glasses: I. Communications on Physics 2:115–119.

Traub, R., N. Kopell, A. Bibbig, E. Buhl, F. Lebeau, and M. Whittington. 2001. Gap junctions between interneuron dendrites can enhance synchrony of gamma oscillations in distributed networks. The Journal of Neuroscience 21:9478–9486.

Traub, R., R. Wong, R. Miles, and H. Michelson. 1991. A model of a CA3 hippocampal pyramidal neuron incorporating voltage-clamp data on intrinsic conductances. J. Neurophysiol. 66:635–649.

Traub, R. D., M. A. Whittington, I. M. Stanford, and J. G. R. Jefferys. 1996. A mechanism for generation of long-range synchronous fast oscillations in the cortex. Nature 383:621–624.

Trimble. 2012. http://www.trimble.k12.ky.us/tchsweb/teachers/dgriffin/Anatomy%20and%20Physiology/Chapter%2012/HAP7_12-a_files/frame.htm.

Tsanov, M. and D. Manahan-Vaughan. 2009. Visual Cortex Plasticity Evokes Excitatory Alterations in the Hippocampus. Frontiers in integrative neuroscience 3:13.

Tsao, D. Y. and M. S. Livingstone. 2008. Mechanisms of face perception. Annual Review of Neuroscience 31:411–37.

Uhlhaas, P., D. Linden, W. Singer, C. Haenschel, M. Lindner, K. Maurer, and E. Rodriguez. 2006. Dysfunctional long-range coordination of neural activity during Gestalt perception in schizofrenia. J. Neurosci. 26:8168–8175.

Uhlhaas, P., G. Pipa, B. Lima, L. Melloni, S. Neuenschwander, D. Nikolić, and W. Singer. 2009. Neural synchrony in cortical networks: history, concept and current status. Front. Integr. Neurosci. 3.

Umm. 2012. http://www.umm.edu/patiented/articles/what_epilepsy_000044_1.htm.

Ursino, M., F. Cona, and M. Zavaglia. 2010. The generation of rhythms within a cortical region: analysis of a neural mass model. NeuroImage 52:1080–1094.

Vannimenus, J. and G. Toulouse. 1977. Theory of the frustration effect. II. Ising spins on a square lattice. Journal of Physics C Solid State Physics 10:L537–L542.

Varela, F., J. Lachaux, E. Rodriguez, and J. Martinerie. 2001. The brainweb: phase synchronization and large-scale integration. Nat. Rev. Neurosci. 2:229–239.

Vasilkov, V. A. and R. A. Tikidji-Hamburyan. 2012. Accurate Detection of Interaural Time Differences by a Population of Slowly Integrating Neurons. Phys. Rev. Lett. 108:138104.

Vertes, R. P. 2006. Interactions among the medial prefrontal cortex, hippocampus and midline thalamus in emotional and cognitive processing in the rat. Neuroscience 142:1–20.

Vicente, R. 2006. Nonlinear Dynamics and Synchronization of Bidirectionally Coupled Semiconductor Lasers. Ph.D. thesis UIB.

Vicente, R., I. Fischer, and C. R. Mirasso. 2008a. Synchronization properties of three delay-coupled semiconductor lasers. Phys. Rev. E 78:066202.

Vicente, R., L. L. Gollo, C. Mirasso, I. Fischer, and G. Pipa. 2009. Coherent Behavior in Neuronal Networks chap. Far in space and yet in synchrony: neuronal mechanisms for zero-lag long-range synchronization, Pages 143–167. Springer New York.

Vicente, R., L. L. Gollo, C. R. Mirasso, I. Fischer, and G. Pipa. 2008b. Dynamical relaying can yield zero time lag neuronal synchrony despite long conduction delays. Proc. Natl. Acad. Sci. 105:17157–17162.

Vicente, R., G. Pipa, I. Fischer, and C. R. Mirasso. 2007. Zero-Lag Long Range Synchronization of Neurons Is Enhanced by Dynamical Relaying. Lecture Notes in Computer Science 4688:904–913.

Vicente, R., S. Tang, J. Mulet, C. R. Mirasso, and J. M. Liu. 2006. Synchronization properties of two self-oscillating semiconductor lasers subject to delayed optoelectronic mutual coupling. Phys. Rev. E 73:047201.

Villa, A. E. P. 2002. Cortical Modulation of Auditory processing in the Thalamus. chap. 4, Pages 83–119 *in* Virtual lesions: Examining Cortical Function with reversible Deactivation (S. G. Lomber and R. A. W. Galuske, eds.). Oxford University Press, Oxford, UK.

Villa, A. E. P., V. M. Bajo, and G. Vantini. 1996. Nerve Growth Factor (NGF) modulates information processing in the auditory thalamus. Brain Research Bulletin 39:139–147.

Villa, A. E. P., E. M. Rouiller, G. M. Simm, P. Zurita, Y. de Ribaupierre, and F. de Ribaupierre. 1991. Corticofugal modulation of information processing in the auditory thalamus of the cat. Exp. Brain Res. 86:506–517.

Villa, A. E. P., I. V. Tetko, P. Dutoit, Y. De Ribaupierre, and F. De Ribaupierre. 1999a. Corticofugal modulation of functional connectivity within the auditory thalamus of rat. J. Neurosci. Meth. 86:161–178.

Villa, A. E. P., I. V. Tetko, B. Hyland, and A. Najem. 1999b. Spatiotemporal activity patterns of rat cortical neurons predict responses in a conditioned task. Proc. Natl. Acad. Sci. 96:1006–1011.

Villain, J. 1977. Spin glass with non-random interactions. Journal of Physics C Solid State Physics 10:1717–1734.

Volgushev, M., M. Chistiakova, and W. Singer. 1998. Modification of discharge patterns of neocortical neurons by induced oscillations of the membrane potential. Neuroscience 83:15–25 83:15–25.

von der Malsburg, C. 1981. The correlation theory of brain function. *in* Internal Report 81-2. Dept. of Neurobiology, Max-Planck-Institute for Biophysical Chemistry, Gottingen, Germany.

von der Marlsburg, C. 1973. Self-organization of orientation selective cells in the striate cortex. 14:85–100. Kybernetic 14:85–100.

von Kriegstein, K., R. D. Patterson, and T. D. Griffiths. 2008. Task-Dependent Modulation of Medial Geniculate Body Is Behaviorally Relevant for Speech Recognition. Curr. Biol. 18:1855–1859.

Vyazovskiy, V. V. and I. Tobler. 2005. Theta activity in the waking EEG is a marker of sleep propensity in the rat. Brain Research 1050:64–71.

Wagemakers, A., J. M. Buldu, and M. A. F. Sanjuan. 2007. Isochronous synchronization in mutually coupled chaotic circuits. Chaos: An Interdisciplinary Journal of Nonlinear Science 17:023128.

Wall, P. and C. Messier. 2001. The hippocampal formation - orbitomedial prefrontal cortex circuit in the attentional control of active memory. Behavioural Brain Research 127:99 – 117.

Wang, H.-P., D. Spencer, J.-M. Fellous, and T. J. Sejnowski. 2010a. Synchrony of thalamocortical inputs maximizes cortical reliability. Science 328:106–109.

Wang, Q., G. Chen, and M. Perc. 2011. Synchronous Bursts on Scale-Free Neuronal Networks with Attractive and Repulsive Coupling. PLoS ONE 6:e15851.

Wang, Q., Z. Duan, M. Perc, and G. Chen. 2008. Synchronization transitions on small-world neuronal networks: Effects of information transmission delay and rewiring probability. Europhysics Letters 83:50008.

Wang, Q., M. Perc, Z. Duan, and G. Chen. 2009. Synchronization transitions on scale-free neuronal networks due to finite information transmission delays. Phys. Rev. E 80:026206.

Wang, Q., R. M. Webber, and G. B. Stanley. 2010b. Thalamic synchrony and the adaptive gating of information flow to cortex. Nature Neuroscience 13:1534–1541.

Wang, X.-J. 2010. Neurophysiological and Computational Principles of Cortical Rhythms in Cognition. Physiological Reviews 90:1195–1268.

Ward, L. M. 2011. The thalamic dynamic core theory of conscious experience. Consciousness and Cognition 20:464–486.

Wen, Q. and D. Chkolvskii. 2005. Seggregation of the brain into Gray and White matter: a design minimiying conduction delays. PLoS Computational Biology 1:e78.

White, J. G., E. Southgate, J. N. Thomson, and S. Brenner. 1986. The Structure of the Nervous System of the Nematode Caenorhabditis elegans. Philosophical Transactions of the Royal Society B Biological Sciences 314:1–340.

Whittington, M., H. Doheny, R. Traub, F. LeBeau, and E. Buhl. 2001. Differential expression of synaptic and nonsynaptic mechanisms underlying stimulus-induced gamma oscillations in vitro. The Journal of Neuroscience 21:1727–1738.

Wikipedia. 2012a. http://en.wikipedia.org/wiki/Hippocampus.

Wikipedia. 2012b. http://en.wikipedia.org/wiki/Neuron.

Williams, R. W. and K. Herrup. 1988. The control of neuron number. Annual Review of Neuroscience 11:423–453.

Wilson, D. A. 2001. Receptive fields in the rat piriform cortex. Chemical Senses 26:577–584.

Wilson, D. A. and R. J. Stevenson. 2003. The fundamental role of memory in olfactory perception. Trends in Neurosciences 26:243–247.

Wilson, H. R. and J. D. Cowan. 1972. Excitatory and Inhibitory Interactions in Localized Populations of Model Neurons. Biophys. J. 12:1–23.

Wilson, H. R. and J. D. Cowan. 1973. A mathematical theory of the functional dynamics of cortical and thalamic nervous tissue. Kybernetik 13:55–80.

Winful, H. G. and L. Rahman. 1990. Synchronized chaos and spatiotemporal chaos in arrays of coupled lasers. Phys. Rev. Lett. 65:1575.

Witham, C., M. Wang, and S. Baker. 2007. Cells in somatosensory areas show synchrony with beta oscillations in monkey motor cortex. European Journal of Neuroscience. 26:2677–2686.

Wolfart, J., D. Debay, G. Masson, A. Destexhe, and T. Bal. 2005. Synaptic background activity controls spike transfer from thalamus to cortex. Nature Neuroscience 8:1760–1767.

Womelsdorf, T. and P. Fries. 2007. The role of neuronal synchronization in selective attention. Curr Opin Neurobiol 17:154–160.

Womelsdorf, T., J.-M. Schoffelen, R. Oostenveld, W. Singer, R. Desimone, A. K. Engel, and P. Fries. 2007. Modulation of neuronal interactions through neuronal synchronization. Science 316:1609–1612.

Wyss, R., P. König, and P. F. M. J. Verschure. 2006. A Model of the Ventral Visual System Based on Temporal Stability and Local Memory. PLoS Biol 4:e120.

Yamaguchi, Y., Y. Aota, N. Sato, H. Wagatsuma, and Z. Wu. 2004. Synchronization of neural oscillations as a possible mechanism underlying episodic memory: a study of theta rhythm in the hippocampus. Journal of Integrative Neuroscience 3:143–157.

Yeung, M. K. S. and S. H. Strogatz. 1999. Time Delay in the Kuramoto Model of Coupled Oscillators. Phys. Rev. Lett. 82:648–651.

Young, C. K. and N. McNaughton. 2009. Coupling of theta oscillations between anterior and posterior midline cortex and with the hippocampus in freely behaving rats. Cerebral Cortex 19:24–40.

Yu, X., X. Xu, S. He, and J. He. 2009. Change detection by thalamic reticular neurons. Nat Neurosci 12:1165–1170.

Zeki, S. and S. Shipp. 1988. The functional logic of cortical connections. Nature 335:311–317.

Zemanová, L., C. Zhou, and J. Kurths. 2006. Structural and functional clusters of complex brain networks. Physica D: Nonlinear Phenomena 224:202–212.

Zhang, K. and T. J. Sejnowski. 2000. A universal scaling law between gray matter and white matter of cerebral cortex. Proc. Natl. Acad. Sci. 97:5621–5626.

Zhou, B. B. and R. Roy. 2007. Isochronal synchrony and bidirectional communication with delay-coupled nonlinear oscillators. Phys. Rev. E 75:026205.

Zhou, C., L. Zemanová, G. Zamora, C. C. Hilgetag, and J. Kurths. 2006. Hierarchical Organization Unveiled by Functional Connectivity in Complex Brain Networks. Phys. Rev. Lett. 97:238103.

Zhou, C., L. Zemanová, G. Zamora-López, C. C. Hilgetag, and J. Kurths. 2007. Structure–function relationship in complex brain networks expressed by hierarchical synchronization. New Journal of Physics 9:178–178.